

Plasma Catalysis for Hydrogen Production: A Bright Future for Decarbonization

Ni Wang,[†] Hope O. Otor,[†] Gerardo Rivera-Castro,[†] and Jason C. Hicks*



Cite This: ACS Catal. 2024, 14, 6749–6798



Read Online

ACCESS |

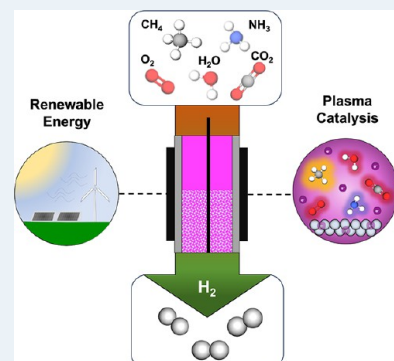
Metrics & More

Article Recommendations

Supporting Information

ABSTRACT: Thermal approaches have played a dominant role in driving chemical reactions within the chemicals and fuels industries, benefiting from ongoing enhancements in efficiency via heat integration, catalyst development, and process intensification. Nevertheless, these traditional thermal approaches remain heavily reliant on fossil fuels, and there exists an urgent demand for the implementation of renewable energy technologies to synthesize fuels, commodity chemicals, and specialty chemicals. Nonthermal plasmas have gained considerable attention in recent years as a promising solution, and the prospects of combining plasmas with suitable catalysts have become even more appealing. Moreover, the evolution of nonthermal plasma catalysis approaches for the generation of clean hydrogen could be transformative in reducing greenhouse gas emissions. This comprehensive review highlights the influential contributions in plasma catalysis for hydrogen production, discusses recent advancements, and provides future prospects for researchers aiming to advance the production of clean hydrogen.

KEYWORDS: electrification, excitation, nonthermal, chemicals, clean energy



1. INTRODUCTION

The global transition in energy production and consumption has been fueled by the unavoidable environmental impacts of fossil-based resources (e.g., greenhouse gas emissions). In recent years, decarbonization technologies based on low- or zero-carbon sources have emerged to address anthropogenic activities associated with carbon dioxide emissions. Decarbonization can be addressed by developing new, green processes or modifying existing processes that rely heavily on fossil fuels for energy via electrification. It is clear that many opportunities exist to address carbon emissions (e.g., batteries,^{1,2} electric heating,^{3,4} electrocatalysis,^{5,6} plasma, ...), and it is likely that one approach will not address all of the challenges facing greenhouse gas emissions. However, clean hydrogen production utilizes electrification strategies and serves as a carbon-free fuel in fuel cells or combustion engines.^{7–9} Further, hydrogen is an excellent energy carrier with negligible end-use emissions, and it can be derived from a wide range of resources. Hydrogen has several key benefits, including exceptional energy conversion efficiencies, CO₂-emission-free combustion, and multiple storage options (e.g., as a gas or liquid or through metal hydrides).

Currently, the annual global use of hydrogen stands at around 95 million tonnes, serving as both an energy source and a reactant in the synthesis of valuable chemicals and fuels such as gasoline, ammonia, methanol, and various other high-value products (Figure 1).¹⁰ In 2022, approximately 99% of the world's hydrogen production relied on fossil fuels, resulting in significant quantities of CO₂ (more than 900 Mt) and

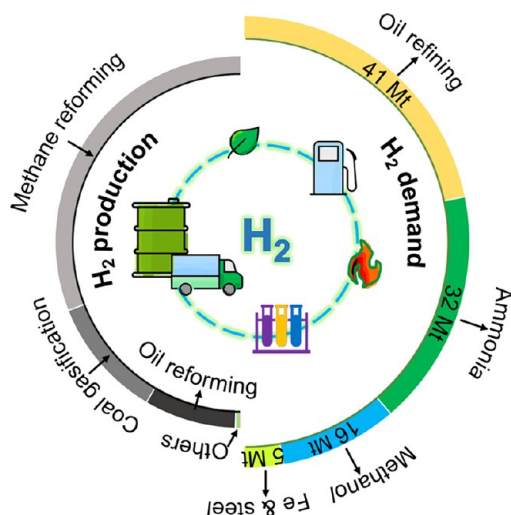


Figure 1. Global hydrogen production technologies (left) and annual industrial hydrogen demand in 2022 (right).

Received: November 10, 2023

Revised: April 2, 2024

Accepted: April 3, 2024

contributing to ~4% of the global emissions.¹⁰ H₂ production that takes advantage of renewable energy sources (e.g., solar, sea, hydro, wind, and nuclear) and/or materials (e.g., water, green ammonia, and biomass) is, therefore, vital for a carbon-free society. A possible alternative is water electrolysis, known for its low carbon emissions at 1–2 kg CO₂/kg H₂ when powered by wind, solar, or nuclear electricity. Nevertheless, the cost of electricity, restricted manufacturing capacity and high cost of electrolyzers contribute to its high production cost, in the range of \$7–12/kg H₂.¹¹ Other low-emission hydrogen approaches, such as photocatalysis, biophotolysis, and photoelectrochemical methods, exhibit the lowest greenhouse gas emissions at 0.5–1.3 kg CO₂/kg H₂.^{12,13} However, their production costs remain high (\$7–10/kg H₂),¹⁴ well above the US Department of Energy (DOE) target of \$1–1.5/kg H₂ by 2030.^{15,16} Thus, the development of an environmentally friendly method to sustainably produce clean hydrogen would be transformational.

A rapidly growing area of research and development to minimize carbon emissions and combat effects to the environment is nonthermal plasma catalysis. Generally, nonthermal plasma (NTP) can be generated by exerting an external electric field on a neutral gas via renewable electricity. The nonequilibrium characteristic in NTP allows the bulk gas to remain at room or low temperature, while the temperature of highly energetic electrons in plasma is orders of magnitude hotter. The energetic and reactive plasma species (e.g., electrons, ions, excited species, radicals, and photons) facilitate reactions that are thermodynamically unfavorable at low temperatures and atmospheric pressure, giving rise to chemical reactions on the nanosecond time scale.¹⁷ Consequently, plasma technology holds the promise of substantially addressing challenges arising from variable and occasionally unpredictable electricity generation and supply situations. Moreover, in combination with a catalyst, the selectivity can be altered to follow desired reaction pathways for plasma-assisted H₂ production.

This review article highlights the use of nonthermal plasma technology for hydrogen production, although thermal plasmas are discussed when appropriate. We acknowledge the significant advances in electrochemical^{18–20} and biomass-derived approaches^{21,22} for clean hydrogen production and point the reader to the highlighted review articles in those areas.

2. OVERVIEW OF PLASMAS AND PLASMA (DISCHARGE) TYPES FOR HYDROGEN GENERATION

2.1. Basic Principles of Plasma Technology. Plasma is an ionized gas, often referred to as the “fourth state of matter”, distinct from the conventional states of solid, liquid, and gas. It is a highly reactive system, consisting of electrons, ions (both positive and negative), atoms (ground state or excited state), molecules (ground state or excited state), and free radicals. Plasma maintains quasi-electroneutrality, indicating a balance between the total positive and negative charges, regardless of the degree of ionization.²³ Various energy sources (e.g., thermal energy, magnetic fields, and electric fields) can be used to generate plasma in the forms of discharge, photoionization, thermoelectric ionization, and X-ray irradiation.²⁴ In general, neutral gas molecules are excited, dissociated, and ionized in the plasma by applying an external electric field between two electrodes. The generated species (electrons, ions, radicals,

excited atoms, and molecules) subsequently collide with one another and/or electrode surfaces, producing new charged particles. Free electrons are accelerated by the electric field to promote additional electron–particle collisions that release additional electrons, known as the electron avalanche.²⁴ Once a balance is reached between the avalanche and annihilation of charged particles, the plasma discharge turns to a steady state.²⁵ With the exception of local short-range collisions among charged particles, the Coulomb force strongly influences their motion and aggregation, leading to various outcomes such as the development of an electric field, the induction of electric current, and the establishment of a magnetic field, as well as the emission and conduction of heat.²⁶

In general, plasma can be categorized as either an equilibrium plasma or a nonequilibrium plasma, depending on the temperatures and energies of the particles within it. In an equilibrium plasma, also known as thermal plasma or hot plasma, the temperatures of electrons, ions, and neutrals are nearly equal, resulting in a state of thermal equilibrium. Thus, thermal plasmas are usually fully ionized and have relatively high temperatures (4000–20000 K) and high electron densities (10^{21} – 10^{26} m⁻³), showing both thermal and plasma chemical effects.²⁷ Thermal plasmas can be formed at either high temperatures or high gas pressures. This technology is widely used in thermal activation, cracking, and pyrolysis processes due to its notable advantages, such as high temperatures, high-intensity nonionizing radiation, high energy density, large treatment capacity, and a relatively high conversion rate.^{28–30} However, there are many challenges that need to be addressed in thermal plasmas, such as reaction selectivity, high energy requirement, and additional capital costs for electrode cooling and/or pressure pumping units.³¹ Nonequilibrium plasma (nonthermal plasma), on the other hand, is characterized by a state where electrons are at a much higher energy level (10000–100000 K) than that of heavy species (<1000 K).³² Generally, nonthermal plasma (NTP) is generated at atmospheric or low gas pressure and has a lower average energy density (< 10^{19} m⁻³) but higher average electron energies than thermal plasmas.³³ Moreover, NTP can be further classified into warm plasma and cold plasma, depending on the overall temperature of the system. A cold plasma typically has a relatively low gas temperature (from 300 to 500 K), providing unique benefits for thermodynamically unfavorable processes.^{23,34} A warm plasma normally shows transitional properties between thermal and cold plasma, which has an intermediate gas temperature (1300–2000 K) and electron temperature (~10000 K), as well as a relatively high electron density of 10^{19} – 10^{21} m⁻³ in the system.³⁵ Over the last two decades, we have seen many advancements in nonthermal plasma (NTP) technology for chemical production, yielding substantial practical benefits for clean H₂ production. As such, this review focuses primarily on NTP processes, and the subsequent sections provide a brief overview of various NTP types applied to hydrogen generation.

2.2. Plasma Types. **2.2.1. Corona Discharge.** Corona discharge gets its name because it resembles a crown.³⁶ Corona discharge is a relatively low power electrical discharge, and it is usually nonuniform, characterized by a high electric field, a relatively low current density, and strong luminosity located close to one electrode.²³ This partial self-sustaining gas discharge can be generated in a nonhomogeneous but sufficiently high electric field powered by alternating current

(AC) or continuous/pulsed direct current (DC) at atmospheric pressure. Electrodes in these systems are commonly configured in several ways. As shown in Figure 2, one typical

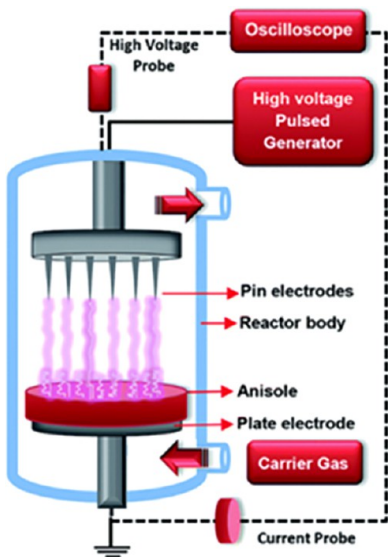


Figure 2. A typical point-to-plane pulsed corona discharge reactor. Reprinted in part with permission from ref 37. Copyright 2016 Royal Society of Chemistry.

setup involves a grounded plate outer electrode, complemented by a concentric high-voltage wire or rod acting as the inner electrode.³⁷ Alternatively, they may be arranged in point-to-point or point-to-cylindrical electrode configurations. The use of asymmetrical electrodes efficiently improves the stability of the corona discharge while reducing the plasma volume. Generally, corona discharge occurs in regions of high electric field strength near sharp points, edges, or thin wires where the radius of the curvature of the electrode is small. The formation mechanism of corona discharges differs when the polarities of the electrodes are different, which lead to various discharge forms, such as positive corona, negative corona, bipolar corona, AC corona, and high-frequency (HF) corona. DC and pulsed DC reactors offer the flexibility to be operated with either polarity, while AC reactors inherently exhibit no polarity effects.³⁶ Additionally, a positive corona can be generated when the high electric field is concentrated around the anode, which can readily transition into spark discharges due to the high applied voltage.³⁶ A negative corona is created when the high electric field is centered on the cathode, characterized by a more stable discharge behavior but a restricted operating voltage range.³⁶

2.2.2. Dielectric Barrier Discharge (DBD). Dielectric barrier discharge (DBD) plasma is the most commonly employed

method of nonthermal plasma generation in research applications. The widespread use of DBDs is attributed to the ease in setup/design, ambient conditions for operation, and ability for intermittent start-up and shutdown operations.^{38–40} DBDs are constructed with one or more layers of insulating (dielectric) material located between two electrodes that are connected to an electric power source.^{40–42} Typically, the DBD plasma is formed in either planar or coaxial configurations, as shown in Figure 3.⁴⁰ The dielectric thickness is usually on the order of a few millimeters and made of materials such as quartz, glass, polymers, or ceramics.⁴³ The electrode thickness is on the order of tens of micrometers,⁴⁴ while the discharge gaps can vary from a few millimeters to centimeters, depending on the application.⁴⁵ Upon the application of high voltage, the gas in the gap between the electrodes breaks down to form a plasma while the dielectric prevents transition to an electric arc or spark discharge.^{46,47} Consequently, DBD plasmas are often referred to as silent discharge plasmas due to the lack of complete gas breakdown.³⁸ The self-limiting nature of the DBD plasma leads to the formation of filaments with an extinction time on the order of 10^{-7} s and is characterized by high local electron densities up to 10^{15} cm^{-3} .⁴⁷ Furthermore, depending on the operating conditions (frequency, voltage, gas type, temperature), discharges in the DBD plasma could be filamentary or diffuse.⁴⁵

DBD plasma experiments are typically conducted at low temperatures and atmospheric pressures. In most cases, the DBD plasma is powered by an alternating current (AC), which typically operates in a frequency range of kHz.^{41,43} However, more recent applications have employed pulsed or radio-frequency plasma with frequency in the MHz range.⁴¹ At such high-frequency ranges, the gas breakdown voltage is decreased,⁴⁸ and the charges are stored in the gap rather than charging up the dielectric.⁴¹ DBD plasma has been mostly used for many plasma-catalysis studies.⁴⁹ Combining the DBD plasma with a catalyst can be accomplished in two general ways: (1) in-plasma catalysis (IPC) or single-stage catalysis, where the catalyst is located in the plasma zone, and (2) postplasma catalysis (PPC) or two-stage catalysis, where the catalyst is located downstream of the plasma zone.⁵⁰ For PPC operation, only long-lived plasma species or stable reaction intermediates are likely to interact (e.g., adsorb) with the catalyst surface. For IPC operation, short-lived species such as ions, radicals, and electronically excited species can interact with the catalyst surface, enabling alternative pathways for chemical transformations.⁵⁰

2.2.3. Microwave. Microwave (MW) plasma is also known as a warm plasma with properties comparable to the characteristics of thermal plasmas.⁵¹ The energy dissipation in MW plasma surpasses that observed in other plasma

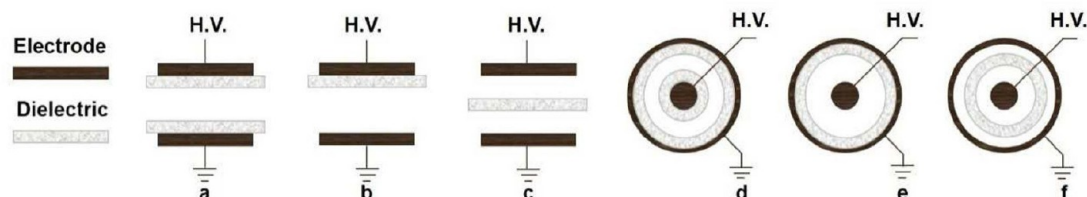


Figure 3. Different DBD plasma configurations. (a–c) Planar configuration. (d–f) Coaxial configuration. Reprinted with permission from ref 40. Copyright 2022 Elsevier.

reactors due to the high MW frequency (300 MHz to 10 GHz).⁵¹ The MW discharges show advantages such as high conversion, good product selectivity, and large gas treatment volume. Furthermore, the microwave discharge is an electrode-free process, yielding relatively pure plasma by avoiding electrode-induced reactions. Figure 4 presents a schematic

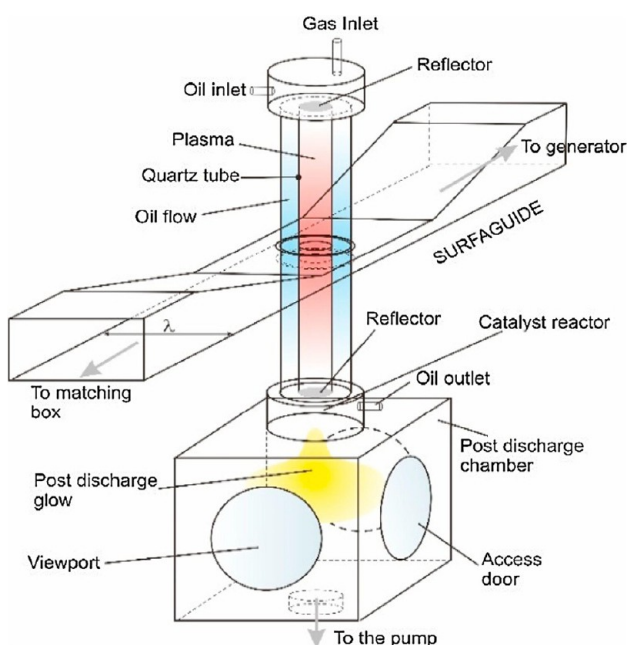


Figure 4. Schematic representation of surface-wave microwave setup at 915 MHz. Reprinted with permission from ref 52. Copyright 2016 Elsevier.

diagram of a typical microwave plasma system.⁵² Typically, MW discharge systems operate at either 2.45 GHz or 915 MHz and comprise several essential components, including a magnetron head, a circulator, a stub tuner, a waveguide, a plasma discharge tube, and a postdischarge chamber.^{52,53} In this setup, the microwaves are created by a magnetron, and these microwaves are then guided by a waveguide to the process chamber. A dielectric tube is included within the waveguide and commonly made of quartz due to its

transparency to microwave radiation. Consequently, when the processing gas inside the dielectric tube intersects with a waveguide, the electrons of the gas absorb the MW energy, thus igniting the ionization reactions.⁵⁴ The power can be concentrated into a confined region, where the interaction between the waveguide and the dielectric tube occurs, resulting in the formation of MW plasma, characterized by a high ion density of $>10^{11} \text{ cm}^{-3}$. Furthermore, depending on the level of MW power consumption, the bulk gas temperature can range from room temperature to several thousand kelvin.⁵⁵ MW plasma has various discharge modes, including surface wave discharge, electron cyclotron resonance, cavity-induced discharges, and freely expanding atmospheric plasma discharge torches.⁵⁶ However, the intricate equipment setup in MW discharges adds to considerable project costs.⁵⁷

2.4. Gliding Arc. Gliding arc (GA) discharges are a prevalent form of warm plasmas and have a higher bulk gas temperature and current density than corona discharges or DBDs. GA discharges exhibit higher energy efficiency and high gas volume treatment capacity. The most widely used GA is the quasi-two-dimensional discharge reactor, which is composed of two or more diverging metallic electrodes (see Figure 5).⁵⁸ Generally, torch-like arcs are created between knife-shaped electrodes powered by DC or AC. Specifically, the ignition of the initial arc occurs at the narrowest interelectrode gap, situated between two flat diverging electrodes. This initial arc is then driven by gas flow to a larger interelectrode distance. At the same time, with the expansion of the plasma column, the gas temperature experiences a rapid drop, while the electron temperature remains high. This leads to a quick transition (on the order of nanoseconds) from thermal to nonthermal ionization that constitutes approximately 75–80% of the discharge energy.^{59–61} As the interelectrode distance increases, the discharge extinguishes, and a new arc at the shortest interelectrode distance ignites once again. Consequently, high feed rates are necessary to maintain the arc evolution and discharge stability during the GA discharge. However, the primary challenges in conventional GA reactors involve addressing the low gas conversions caused by the short residence time of the reactants and electrode deterioration due to the carbon deposition on the electrode surface.^{62,63} Various

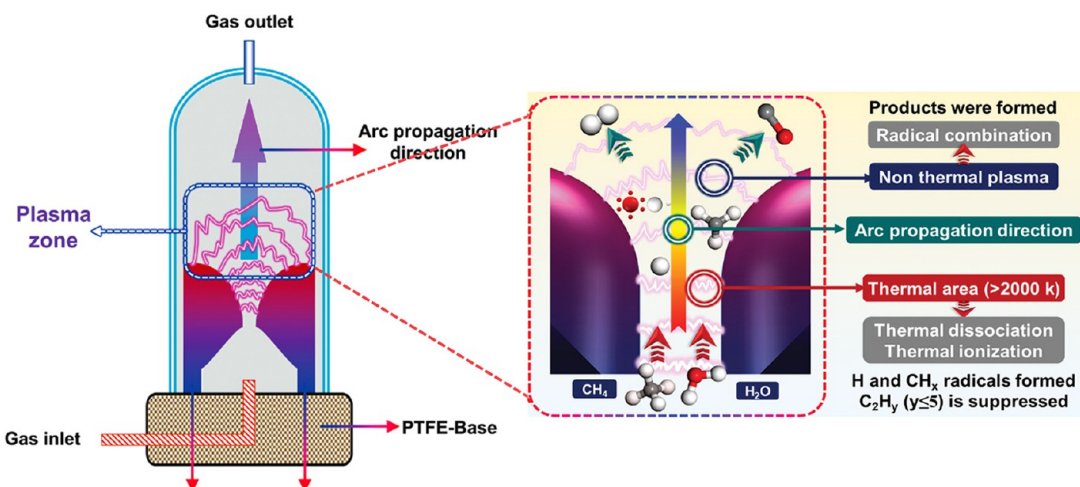


Figure 5. A typical quasi-two-dimensional gliding arc reactor configuration and arc characteristics. Adapted with permission from ref 58. Copyright 2022 Wiley-VCH GmbH.

Table 1. Key Benefits and Critical Challenges of Selected Hydrogen Production Technologies^{11,14,65–70}

technology	feedstock	energy source	energy efficiency (%) ^a	carbon release (kg CO ₂ /kg H ₂)	cost (\$/kg H ₂)	maturity	H ₂ color category	advantages	challenges
steam reforming	hydrocarbons	heat	74–85	13.2	0.8–1.8	commercial	gray	high H ₂ production rate, low cost	high CO ₂ emission
partial oxidation	hydrocarbons	heat	60–75	7.3	1.8	commercial	gray	feasible for heavier feedstock	capital intensive
coal gasification	coal	heat	65	12	1–2	commercial	brown/black	abundant reserves	unreacted solid feedstock, byproduct ash
methane pyrolysis	natural gas	heat	53	3–6.5	1.8	early stage	turquoise	low cost, valuable carbon product	H ₂ and carbon separation, membrane durability
water electrolysis	water	electricity	50	0.5–7	5–15	commercial	green/yellow/pink/purple	abundant reserves, green H ₂ production with renewable energy	low efficiency, high capital costs
thermochemical water splitting	water	electricity+ heat	20–40	0.5–2.2	1.5–8	conceptual stage	green/yellow/pink/purple	clean and sustainable, recycled chemicals	less effective and durable
chemical looping	hydrocarbons + oxygen carrier	heat	70–80	1.7/9.5 (with/ without CCUS)	2–3	conceptual stage	gray/blue	low CO ₂ capture cost, high thermal efficiency	depends heavily on the lifetime of the oxygen carrier
photoelectrochemical water splitting	water	solar	2–12	2	5–11	conceptual stage	green	low operation temperature, clean and sustainable	limited charge transport and visible light absorption efficiency
photobiological water splitting	water + algae	solar	10–14	3	1.5–2	conceptual stage	green	clean and sustainable	low H ₂ production potential, requirement of large surface area
biomass gasification	biomass	heat	55–65	4.5	2	commercial	green	abundant reserves, clean and sustainable	feedstock impurities
Plasma reforming (oxidative and nonoxidative)	hydrocarbons	electricity	1–60			conceptual stage	green/yellow/pink/purple	green H ₂ production with renewable energy sources, fast response, compact, compatible with various feedstocks	scalability, energy efficiency, stability
plasma NH ₃ decomposition	ammonia	electricity	2–46			conceptual stage	green/yellow/pink/purple	C/O-free H ₂ production, high gravimetric and volumetric H ₂ densities, ease of transportation and storage	dilution with inert gas, high temperature, scalability, energy efficiency

^aEnergy efficiencies for different H₂ production technologies are calculated based on eq 2.

studies have reported rotating gliding arcs (RGAs) to address these issues.

3. PLASMA CATALYSIS FOR HYDROGEN GENERATION

Key benefits and critical challenges in the current and emerging hydrogen production technologies are summarized in **Table 1**. Color designations for hydrogen production have been implemented to denote the various hydrogen sources (**Table 1**). Specifically, “black”, “gray”, and “brown” are terms used to refer to the production of hydrogen from coal, natural gas, and lignite, respectively, with the distinction being based on the amount of CO₂ emissions during the entire process. “Blue” is a common descriptor for hydrogen production from fossil fuels but combined with Carbon Capture, Utilization, and Storage (CCUS) technologies. Conversely, “green” designates the production of hydrogen that is carbon emission free during the production stage from renewable/clean energy sources and/or green materials. However, variation in color terminology exists, especially for low-emission hydrogen production methods like water electrolysis. This variation arises from the diverse environmental impacts, influenced by the source of electricity generation, be it renewable/nuclear or fossil fuels. As advancements are made in the expansion of hydrogen production, increasing the contribution from renewable energy sources is one of the critical components for a green hydrogen economy with a low (or net zero) carbon footprint.⁶⁴

As previously stated, nonthermal plasma technology stands out as an emerging low-emission technology for hydrogen generation when the electricity is generated by renewable methods. Given its characteristic properties, however, the impact of processing parameters on reaction kinetics differs from conventional thermal methods. Our following sections will first introduce the significance of these characteristic parameters within a plasma system. Then, the subsequent sections will discuss various plasma-assisted hydrogen production methods using different feedstocks, including conventional fossil fuels (such as CH₄), ammonia, alcohols, and renewable biomass. While some processes are well-established, like hydrocarbon reforming, others, such as ammonia decomposition, are emerging alternatives for renewable hydrogen production. The discussion covers the state-of-the-art for each method, with further emphasis on the influence of operating parameters on reactant conversion and hydrogen yield (plasma power, specific energy input, feed composition, and reaction temperature), plasma configurations, and reaction mechanisms.

3.1. Characteristic Plasma Parameters. Plasma-assisted H₂ production processes are significantly influenced by a variety of factors, including discharge parameters (voltage, frequency, power, SEI, etc.), plasma reactor configuration (type, size, material, and geometry), feed characteristics (ratio, flow rate, and dilute reactant gas), and the catalyst (e.g., nature and density of active sites, dielectric constant, morphology, work function, and packing characteristics). Consequently, variation in these parameters leads to challenges when attempting to directly compare different studies. Therefore, we first provide a general overview of these parameters and how they are applied to plasma-catalysis studies. Detailed insights into how these characteristic parameters influence hydrogen production for different chemical reactions are discussed in the subsequent sections.

Plasma discharge power is the active power dissipated in the discharge of a plasma system. It is generally smaller than the total input power for the entire plasma system, which encompasses additional power consumed by auxiliary systems (e.g., cables, power generator, and transformer). The discharge power is an important factor in influencing the efficiency in plasma systems, as it affects the electron temperature, electron density, and overall plasma characteristics. Discharge power can be controlled by adjusting either the applied voltage or frequency of the plasma system.⁷¹ Several instruments are typically used to measure, or estimate, discharge power in different plasma systems, such as impedance matching,⁷² a magnetic probe,⁷³ a Langmuir probe,⁷⁴ and a voltage probe.⁷⁵ In the case of DBDs, the charge–voltage (Q–V) diagram, known as the Lissajous figure,⁴⁷ is a common method used to calculate discharge power.

The specific energy input (SEI) plays a significant role in governing reactant conversions and energy efficiency in a plasma system. SEI is a distinctive factor that quantifies the energy deposited into a plasma per unit volume (**eq 1**), effectively integrating the discharge power and total gas flow rate (i.e., the sum of all reactants and inert gas). Consequently, at a constant discharge power, changes in the total flow rate not only influence the residence time of the reagents within the plasma but also affect the plasma chemistry, such as the density of reactive species and reaction rates. Further, the reaction performance (e.g., product yield) in the same plasma system can vary at identical SEI conditions but operated at different powers and gas flow rates.⁷⁶ In general, a higher SEI leads to a higher product yield but results in lower energy efficiencies, thus providing a trade-off between these factors.⁷⁷ Because the definition of energy efficiency varies across the literature, we apply **eq 2** to the different processes highlighted here to allow for direct comparison.

$$\text{SEI (kJ/L)} = \frac{\text{discharge power (kW)}}{\text{total gas flow rate (L/s)}} \quad (1)$$

$$\text{energy efficiency } \eta (\%) = \frac{m(\text{H}_2) \times \text{LHW}(\text{H}_2)}{E_{\text{in}}} \quad (2)$$

m(H₂) is the mass flow rate of produced hydrogen, *LHW(H₂)* is the lower heating value of hydrogen (120 MJ/kg), and *E_{in}* is the rate of energy input to the process.

$$\text{hydrogen yield (\%)} = \frac{\eta \times H_2(\text{out, mol/s})}{2 \times A(\text{in, mol/s})} \times 100 \quad (3)$$

A is the feed (i.e., C_xH_y and N_xH_y).

Feed composition not only influences the concentrations and transport of the reactants but also impacts discharge properties, consequently influencing the reaction pathway. Unlike thermal processes in which inert carrier gases typically have a minimal effect on reaction pathways, diluent gases in a plasma system can be excited, ionized, or dissociated in the plasma phase, creating additional avenues for product formation.^{78,79} Furthermore, the addition of diluent gases influences electron density, breakdown voltage, and discharge behavior.^{79,80} Consequently, production costs can be negatively influenced in a diluted plasma-assisted system because a fraction of the energy is dedicated to ionizing and exciting the diluent gas.⁸⁰

In nonthermal plasma (NTP), the temperature of the neutrals is the dominant contributor to the bulk gas temperature, due to the low mass of electrons and the low

concentration of ions.^{32,33} This temperature is typically 2–3 orders of magnitude lower than the electron temperature in the plasma. The bulk gas temperature can be manipulated by adjusting the energy input within the plasma (e.g., uncontrollably via Joule/resistive heating) or by using a temperature-controlled external furnace. Various instruments are employed to detect the bulk gas temperature in nonthermal plasmas, such as infrared cameras,⁸¹ thermocouples,⁸² and optical fiber temperature sensors,⁸³ with a thermocouple placed downstream of the plasma zone being the most common method. Changes in bulk gas temperature are accompanied by changes in plasma properties and discharge mode even at a constant discharge power.⁸⁴ For instance, variations in bulk gas temperature within a plasma reactor can influence factors such as gas density, the reduced field (E/N), and the excitation levels of energetic species, which in turn impacts the reaction dynamics and product yields.⁸⁵

Generally, plasma phase chemistry, packed-bed effects, and catalyst–surface reactions are the most important contributors to the overall reaction performance. Packed bed effects occur when solid particles or porous materials are completely or partially placed within the plasma discharge region. The packed bed can be constructed with various bed material geometries, such as pellets, powders, and foams.⁸⁶ As shown in Figure 6, the interactions between plasmas and catalysts are complicated, where catalysts affect the properties of the plasma and vice versa.⁸⁷ On one hand, packing materials change the plasma discharge properties, including the creation of microdischarges inside pores larger than the Debye length,

propagation of streamers on the surface, modifications in the discharge volume, and enhancement in the electric field. These effects have a direct impact on the electron energy distribution and rates of electron-impact collisions, consequently leading to changes in the distribution of chemical species within the plasma.⁸⁶ Alternatively, plasma may also improve the catalyst properties (e.g., surface area, oxidation–reduction state, defects, and electron extraction potential).^{88–92} Additionally, microdischarges near high-curvature regions can create hot spots on the material surface.⁹³ More importantly, reactive species, like radicals, and excited molecules may lower activation barriers for surface reactions, providing additional pathways for yielding desired products.⁸⁶

3.2. Plasma-Assisted Oxidative Methane Reforming.

Natural gas, which is primarily methane, is the predominant source for H₂ production commercially due to its abundant reserves and high H/C ratio.¹² In this section, a review of current plasma-assisted technologies is provided for the generation of hydrogen, focusing on advances in oxidative methane reforming with various oxidative sources (H₂O, O₂, and CO₂).

3.2.1. Background/Motivation. In an oxidative methane reforming process, methane and an oxidant such as H₂O, O₂, and/or CO₂ are initially cofed with or without the assistance of a catalyst to produce syngas (eqs 4–6). These processes are normally operated at high temperatures (700–1300 °C) due to the endothermic nature of the reactions (e.g., methane steam reforming and methane dry reforming with CO₂). The water-gas shift reaction (WGS, eq 7) enhances the H₂ production yield and converts CO to CO₂.

The most developed, efficient (74–85%), low-cost (<\$2/kg H₂), and extensively studied method for large-scale H₂ production is steam methane reforming (SMR, eq 8).¹² SMR is characterized by its highly endothermic nature and its thermodynamic favorability at high temperatures, low pressures, and high steam-to-methane (S/C) ratios.⁹⁴ SMR provides a high hydrogen production rate (H₂/CH₄ = 4); however, it demands precise thermal management (850–900 °C) and elevated pressure (around 30 bar) for maintaining desired purified H₂ and preventing coke formation on the catalyst surface.⁶⁶ Moreover, SMR is not universally applicable to all feedstocks, and this technology falls under the category of “gray” H₂ due to the substantial CO₂ output (5.8 and 13.2 kg CO₂/kg H₂ for SMR with and without CCUS, respectively).¹¹

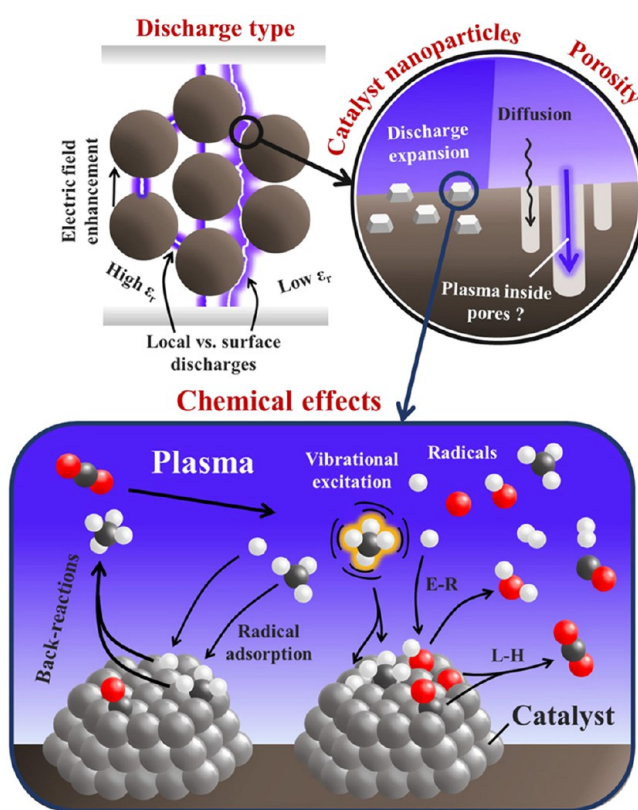
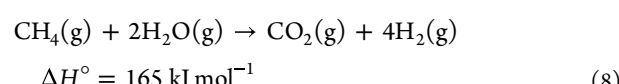
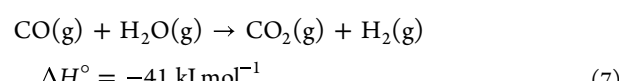
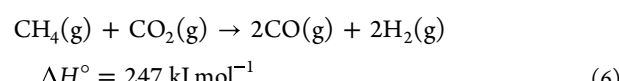
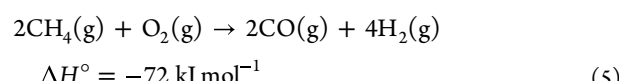
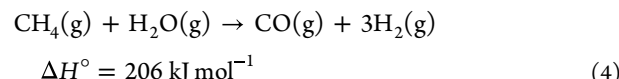
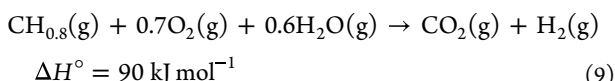


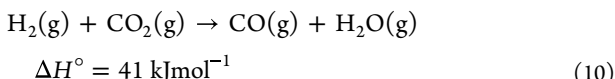
Figure 6. Plasma–catalyst synergy and reaction pathways in plasma catalysis. E-R refers to the Eley–Rideal mechanism, and L-H refers to the Langmuir–Hinshelwood mechanism. Reprinted with permission from ref 87. Copyright 2023 Elsevier.



When a small amount of O₂ or a combination of H₂O and small amount of O₂ is used as the oxidizing source, the reforming process is commonly referred to as partial oxidation (POX). Compared to SMR, POX presents a lower H₂ production rate (H₂/CH₄ = 2) but higher operating temperature (~1300 or 950 °C with the assistance of a catalyst).⁹⁵ Various hydrocarbons, such as methane, naphtha, heavy oil, and coal, can be used as the feedstock for H₂ production in the POX process. When using methane as the reactant (eq 5), the controlled CH₄ combustion provides the heat for the POX process with an overall CO₂ emission of 7.3 kg CO₂/kg H₂.¹⁴ When using heavy oil as the feedstock, POX typically operates at a pressure of 6 MPa, yielding syngas with an H₂/CO ratio of 1. Note that the steam contributes significantly to the hydrogen production (~69%) due to the relatively low hydrogen-to-carbon ratio in the heavy oil.⁹⁶ Alternatively, coal gasification is considered both economically feasible and practical, primarily because of the abundant global coal reserves.¹⁴ The coal gasification process is typically conducted under high temperatures (800–1300 °C) and pressures (30–70 bar) with the presence of steam and oxygen (eq 9).¹¹ Similar to the heavy oil POX process, a substantial portion (approximately 83%) of the produced H₂ is derived from steam during coal gasification.⁹⁶ This process typically has an energy efficiency of ~65%, but it also generates significant CO₂ emissions (12 kg CO₂/kg H₂), categorizing it as a “brown/black” H₂ production process.¹⁴ Additionally, the overall H₂ production cost of coal gasification is slightly higher than that of SMR, primarily due to the high capital costs involved in an oxygen recirculation plant, desulfurization steps, and supplementary units for managing solid unreacted fuel and ash.



Compared to SMR and POX, dry reforming of methane (DRM, eq 6) presents a viable pathway capable of achieving low-carbon H₂ initiatives.⁶² DRM can utilize CO₂ and CH₄ from a diverse slate of feedstocks like shale gas, biogas, and landfill gas to form syngas. The mixture of CO and H₂ serves as a fundamental chemical precursor enabling its direct utilization without the need for a separation unit. DRM is generally operated at high temperatures (above 700 °C). However, a side reaction, the reverse water-gas shift reaction (RWGS, eq 10), is particularly prominent at high temperatures during DRM. This phenomenon can lead to a reduction in H₂ production, thereby diminishing the viability of the DRM process in conventional applications. Further, CO₂ serves a dual role of supplying oxygen while also introducing additional carbon into the feed. Consequently, this introduction of carbon presents additional challenges, such as issues related to carbon deposition.⁹⁷



Nonthermal plasma is a promising strategy in oxidative methane reforming processes to produce low-emission H₂ by using renewable energy (Figure 7). NTP enables the activation of CH₄ at low temperatures and the generation of highly pure H₂ or H₂-enriched syngas. Furthermore, it demonstrates remarkable capability in accommodating diverse hydrocarbon feedstocks for a specific H₂ production route through either

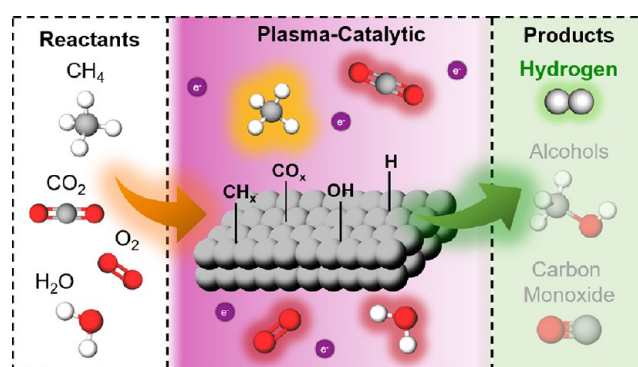


Figure 7. Schematic diagram of plasma-assisted oxidative methane reforming processes.

warm NTPs (e.g., gliding arc and microwave discharge) or cold NTPs (e.g., DBD, RF discharge, and corona discharge).

3.2.2. Advancements and State-of-the-Art in Plasma-Assisted Oxidative Methane Reforming. Early studies on plasma-assisted oxidative methane reforming can be traced back to 1897, which predates the formal definition of “plasma” by Langmuir.^{98,99} Although only CO₂ and H₂O were produced in the glow discharge at a CH₄/O₂ ratio of 1/2, Mixer proposed the role of plasma in assisting activating the reactants at low temperatures.⁹⁸ In this early study, the author excluded the possibility of heat effects from the methane combustion and ozone formation from the methane oxidation, suggesting the primary mechanism was through activated species.

In 1927, the formation of H₂ was separately reported in a methane-oxygen plasma¹⁰⁰ and a methane-air plasma¹⁰¹ in spark discharges. Approximately 10 years later, Fujimoto¹⁰² observed the production of both H₂ and liquid oxygenates in an ozonizer using a CH₄/O₂ spark discharge.¹⁰² This pioneering study proposed the existence of excitations of CH₄ and O₂ molecules in the discharge, as well as the dissociation of the C–H bonds of methane to enhance partial ionization.¹⁰² H₂O emerged as an oxygen source for methane in a thermal plasma arc in 1975,¹⁰³ while CO₂ appeared later in the late 1990s.¹⁰⁴ Since then, research in plasma-assisted oxidative methane reforming has gained interest, and the combination of a catalyst into the plasma system has been introduced to improve H₂ production.^{104–106}

Although plasma-assisted POX has a longer history compared to SMR and DRM, it holds the lowest promise for H₂ production due to difficulty in controlling the degree of oxidation, which leads to a low H₂ selectivity even in the presence of a catalyst.⁹⁴ Conversely, plasma-assisted SMR and DRM have higher potential for efficiently producing H₂ with or without the cooperation of a catalyst. For example, a high H₂ production rate of 2247 g(H₂)/h and an energy yield of 70 g(H₂)/kWh were obtained in a microwave torch SMR reactor without the need of a catalyst.⁹⁵ This H₂ energy yield is within the range of those reported for oxidative methane reforming processes but above those reported for other electrified routes such as electrolysis. Other studies have emphasized that adding a catalyst in the plasma can improve the H₂ production yield by targeting the WGS reaction (CO + H₂O → CO₂ + H₂). In one example, Geng et al.¹⁰⁷ introduced a “one-pot” cascade design for a DBD plasma-assisted catalytic SMR reactor at 300 °C. As shown in Figure 8, a Ni/CaAl₄O₇ catalyst was packed in the discharge zone with a Cu/ZnO/Al₂O₃/MgO catalyst placed downstream to facilitate the WGS reaction.¹⁰⁷

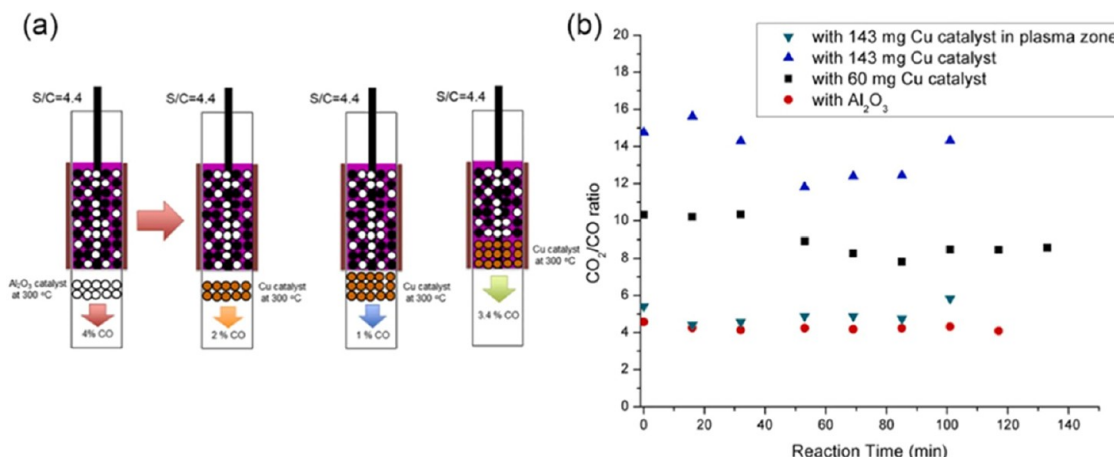


Figure 8. (a) Configuration of cascade design with Cu/ZnO/Al₂O₃/MgO catalyst placed at three regions and (b) effect of Cu catalyst on CO₂ selectivity/CO selectivity at 300 °C and S/C = 4.4. Reprinted with permission from ref 107. Copyright 2022 Elsevier.

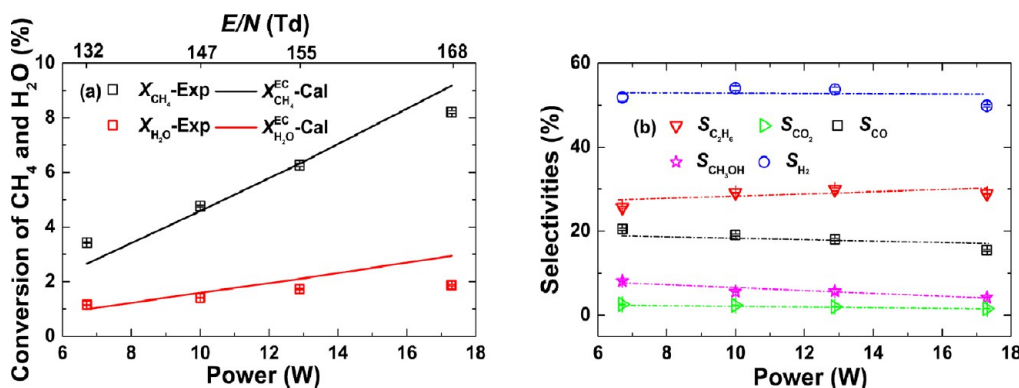


Figure 9. Effect of discharge power on (a) conversions of methane and water (data points indicate experiment and solid lines represent calculation) and (b) product selectivities (dashed lines indicate trend lines based on experiment). Reprinted with permission from ref 85. Copyright 2018, IOP Publishing Ltd.

Compared to plasma-assisted Ni/CaAl₄O₇ alone (CO₂/CO selectivity at ~4%), the hybrid two-zone configuration achieved significantly higher CO₂/CO selectivity (8–16) at 60% methane conversion.¹⁰⁷ This study highlights the ability to directly tune the catalytic SMR performance through catalyst selection and placement, providing an electrified route for enhanced hydrogen production.

Plasma-assisted DRM is the most developed process in oxidative methane reforming, with DBDs being the most studied plasma type due to their exceptional operating flexibility and promising scalability.^{38,108} DBD reactors are reported with reactant conversions ranging from 40% to 80% and H₂/CO ratios from 1 to 3 in oxidative methane reforming. However, the energy efficiency typically falls within the range of 1–20% (maximum 60%, eq 2). The synergy between the plasma and included catalyst can address many of the limitations from processes with plasma alone (e.g., low H₂ selectivity). For example, zeolites,^{109–113} γ-Al₂O₃,¹¹⁴ and Ni- and Mn-based catalysts¹¹⁵ facilitate the H₂ production via plasma-assisted surface reactions. In a recent development, Tu and co-workers¹¹⁶ reported a high CO₂ conversion of 30%, CH₄ conversion of 49%, and H₂ yield of 19% using a 10Ni3Co alloy catalyst for DRM. They attributed the exceptional H₂ production performance of 10Ni3Co to the suppression of carbon deposition and enhanced reactivity.¹¹⁶

The exceptional synergy between plasma and catalysts has led to innovative approaches to hydrogen production. Consequently, current research is aimed at disentangling the distinct roles of plasma chemistry, thermal catalysis, and plasma-assisted catalysis in this domain. Fundamental insights from mechanistic studies will help guide catalyst selection for plasma-assisted oxidative methane reforming to selectively produce H₂.

3.2.3. Process Parameters. The following sections provide a concise overview of the variation in macroscopic process parameters, including discharge power, specific energy input (SEI), CH₄/oxidant molar ratio, reaction temperature, and carrier gas on plasma-assisted oxidative methane reforming processes.

3.2.3.1. Effect of Discharge Power. Discharge power has been established as a critical component governing the reaction performance in plasma-assisted oxidative methane reforming. As a general trend, increasing the discharge power enhances the CH₄ conversion in various plasma systems (e.g., corona, MW, GA, and DBD).^{29,71,77,95,117–119} Raising discharge power at a constant frequency can yield more energetic electrons and reactive species (CO, O, OH, CH_x), along with increased temperatures, collectively amplifying the effectiveness of the plasma systems.¹²⁰ Furthermore, in a DBD reactor, increasing the discharge power generally increases the number of microdischarge filaments, thus creating additional reaction

pathways for chemical processes.^{121,122} Kim et al.¹¹⁹ found that CH₄ conversion linearly increased with the increase of discharge power in plasma-assisted SMR using DBD. Similarly, the Hicks group¹²³ reported a linear relationship in the natural log of the rate constant with reciprocal power (1/power) in plasma-assisted DRM. This dependency of plasma power on reaction rates was attributed to the increase in electron density with an increase in discharge power within the reaction controlled volume, subsequently affecting the rate of excitation of CH₄ to CH₄*.¹²³

Interestingly, the impact of discharge power on H₂ selectivity varies in different studies. For example, Liu et al.⁸⁵ found that increasing the power had a relatively minimal effect on H₂ selectivity, which remained stable at around 52% in plasma-assisted SMR using a DBD (Figure 9).⁸⁵ Similarly, Tu et al.¹²⁴ observed an invariant H₂ selectivity with a change in discharge power for plasma-assisted DRM in a DBD reactor. However, other studies reported that higher discharge power significantly enhanced H₂ selectivity. A significant increase in H₂ selectivity, rising from 47% to 63%, was observed as the discharge power was raised in a corona discharge for DRM.¹²⁵ The authors attributed the enhanced H₂ production to the enhanced presence of CO and O* radicals, along with improved CH₄ dissociation with increased discharge power.¹²⁵ Conversely, Lu et al.¹²⁶ observed a slight decrease in H₂ selectivity when they increased the power in a rotating gliding arc reactor for DRM. The authors indicated that the intensified electric field promoted the reverse water gas shift reaction, thus enhancing the production of water vapor. This water vapor then condensed and accumulated on the inner wall of the glass cover, leading to the decrease in H₂ selectivity.¹²⁶

In summary, increasing discharge power typically has a promotional effect on CH₄ conversion, while its influence on H₂ selectivity is limited, which results in an improvement in the H₂ production yield. However, the enhancement in gas conversion comes with a trade-off in energy efficiency when the discharge power increases to higher values.⁷⁷ The selection of an appropriate discharge power is crucial to achieve balance between conversion and energy efficiency in plasma-assisted processes.

3.2.3.2. Effect of Specific Energy Input (SEI). Changing the gas flow rate at a constant discharge power is a common method to manipulate the SEI for achieving an optimal energy efficiency in a plasma system. In general, lowering the gas flow rate proves advantageous for enhancing gas conversions because of the increase in the residence time of the reactants within the plasma environment. Conversely, an increase in the gas flow rate generally leads to decreased reactant conversions at a constant H₂ selectivity, thereby resulting in a reduction in H₂ yield.^{115,127}

However, altering the SEI by changing the gas flow rate in a GA reactor can occasionally exhibit a volcano curve in H₂ yield, owing to the critical role the gas flow rate plays in sustaining and propagating arcs for this discharge form. For example, Lu et al.¹²⁶ found that CH₄ conversion reached its maximum (28%) at a SEI of 1.8 kJ/L within the range of 1.38 to 2.75 kJ/L when they changed the gas flow rate from 2 to 4 L/min in a RGA reactor. However, the H₂ selectivity only slightly dropped from 49% to 41% as the gas flow rate increased. More recently, a similar volcano curve in H₂ production was observed in an atmospheric pressure microwave plasma torch for DRM (Figure 10).¹²⁸ Akande et al.¹²⁸ reported the hydrogen production rate and H₂ energy yield

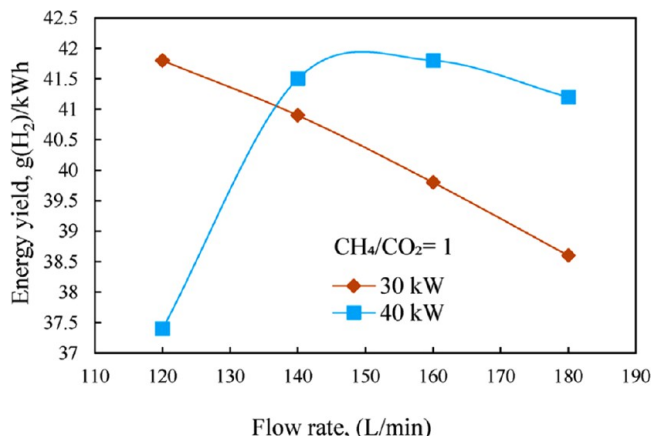


Figure 10. H₂ production energy yield as a function of flow rate at different discharge powers. Reprinted with permission from ref 128. Copyright 2023 Elsevier.

peaked at 1672 and 41.8 g (H₂)/kWh, respectively, at an optimal flow rate of 140 L/min. The authors attributed the enhanced H₂ production rate to the plasma flame elongation as the flow rate increased from 120 to 140 L/min.¹²⁸ Given this, it is worth mentioning that achieving both higher hydrogen production and enhanced energy efficiency simultaneously requires careful consideration of an appropriate SEI in the plasma system.

3.2.3.3. Effect of CH₄ Concentration. CH₄ concentration in the feed gas notably impacts both conversion and H₂ selectivity in plasma-assisted oxidative methane reforming processes. At a fixed low total gas rate, a lower CH₄ concentration generally minimizes carbon deposition and improves CH₄ conversion due to the higher concentration of active O species from electron-impact dissociation of H₂O, O₂, or CO₂.^{115,129} Akande and Lee⁹⁵ revealed that as the CH₄/H₂O ratio decreased from 1/3 to 1/6, CH₄ conversion reached nearly 100% in a microwave torch for SMR.⁹⁵ The authors attributed this improvement primarily to the increased electric field resulting from the extended plasma flame and prolonged reactant collision time. However, it is challenging to decouple the individual roles that the CH₄/H₂O ratio and the total gas flow rate play in the improvement, as these factors were changed simultaneously in this study.

Conversely, a higher CH₄ concentration is normally beneficial for improving H₂ selectivity due to the enhanced formation of H and CH_x radicals. For most plasma types, manipulating the CH₄ concentration in plasma-assisted DRM may control the H₂/CO ratio to achieve desired reaction outcomes. Recently, Tu et al.¹¹⁷ found that the H₂/CO ratio in the product linearly increased with the CH₄/CO₂ ratio in a GA reactor. A similar phenomenon was observed in a DBD reactor, as noted in the study conducted by Vakili et al.¹³⁰ The authors found that increasing the CH₄/CO₂ molar ratio from 1/2 to 3/2 resulted in a remarkable increase in the H₂/CO ratio, rising from 0.4 to 1.6.¹³⁰ The H₂ yield peaked at ~50% as the CH₄ concentration in the feed was raised to 60 vol %.¹³⁰ However, the CH₄ concentration can have different effects on plasma-assisted SMR compared to DRM, as H₂O is also a significant H source for H₂ production. For example, Wang et al.¹³¹ found that the change in CH₄/H₂O molar ratio has a minor influence on H₂ selectivity when they conducted the plasma-assisted SMR in an atmospheric-pressure microwave plasma reactor.

Moreover, Czylkowski et al.¹³² reported a high hydrogen production rate of 192 g(H₂)/h and an energy yield of 42.9 g(H₂)/kWh when they optimized the concentrations of CH₄, CO₂, and water vapor in the feed.

3.2.3.4. Effect of Reaction Temperature. Altering the reaction temperature exerts a more intricate influence on plasma-assisted oxidative methane reforming reactions compared to thermal processes. This complexity arises due to the modifications in plasma properties, such as gas density and reduced electric field (E/N), when the bulk gas temperature is manipulated.⁸⁵ Some investigations have suggested that temperature has a minor influence on the performance of plasma-assisted oxidative methane reforming. These findings were observed in studies conducted using a nanosecond pulsed discharge reactor¹³³ and a RGA reactor.¹³⁴ Martin-del-Campo et al.¹³⁴ additionally reported a decrease in the H₂/CO ratio, shifting from 0.86 to 0.77, upon raising the inlet temperature to 200 °C. More recently, Liu et al.⁸⁵ found that both CH₄ and H₂O conversions, along with H₂ selectivity, decreased as the gas temperature increased from 350 to 400 °C in plasma-assisted SMR using a DBD reactor. The authors attributed this phenomenon to the rise in dielectric loss and enhanced water formation via radical reactions (e.g., H^{*} + OH^{*} and CH₃^{*} + OH^{*}) above a certain temperature.⁸⁵ Interestingly, this study emphasized the importance of temperature in CH₄ conversion, whereas H₂O consumption was only dependent on plasma electron energy.⁸⁵

However, Li et al.¹³⁵ found that raising the DBD reactor temperature from 350 to 550 °C led to an increase in H₂ yield to 50% and a boost in energy efficiency to 18.56%. Recently, Kim et al.⁸⁴ emphasized the important role of bulk temperature in altering the chemically active plasma for DRM reaction using a temperature-controlled DBD reactor (Figure 11). The authors systematically conducted experiments that identified the role of gas-phase plasma reactions, charge confinement, plasma power at fixed temperature, and bulk gas temperature at fixed power. Plasma-driven electron impact activation and charge confinement were found to play a minor role in activating C–H bonds of CH₄ at elevated temperatures (>420 °C).⁸⁴ Furthermore, DBD plasma-driven hot Ni sites were unlikely the primary cause for the observed enhancement because the bulk gas temperature changed by <10 °C.⁸⁴ Conversely, it was demonstrated that the bulk gas temperature was a major contributor to C–H activation, yielding an 8-fold increase in CH₄ conversion and H₂ yield at high temperatures (>360 °C).⁸⁴

3.2.3.5. Effect of Carrier Gas. Generally, the most common carrier gases in plasma-assisted oxidative methane reforming are N₂, Ar, and He. The benefits of adding carrier gases into the reactant include enhanced discharge stability and enhanced methane excitation and dissociation via additional pathways facilitated by excited He/Ar/N₂ species (Figure 12).^{79,80,135} Recently, Wang et al.¹³⁶ investigated the effects of N₂ on plasma-assisted SMR using a novel liquid microwave plasma for H₂ production. While CH₄ conversion and H₂ selectivity were insensitive to N₂ addition, the total H₂ production yield was significantly enhanced by 43% when 16 vol % N₂ was introduced into the plasma region.¹³⁶ Given the lower bond dissociation energy in H₂O (4.5 eV) compared to CH₄ (5.5 eV), the excited nitrogen species (N₂^{*} and N^{*}) and N₂⁺ facilitated the consumption of liquid H₂O, rising from 0.42 to 0.63 mL/min.¹³⁶ It is important to note that the addition of N₂ could also participate in plasma phase reaction pathways. In a

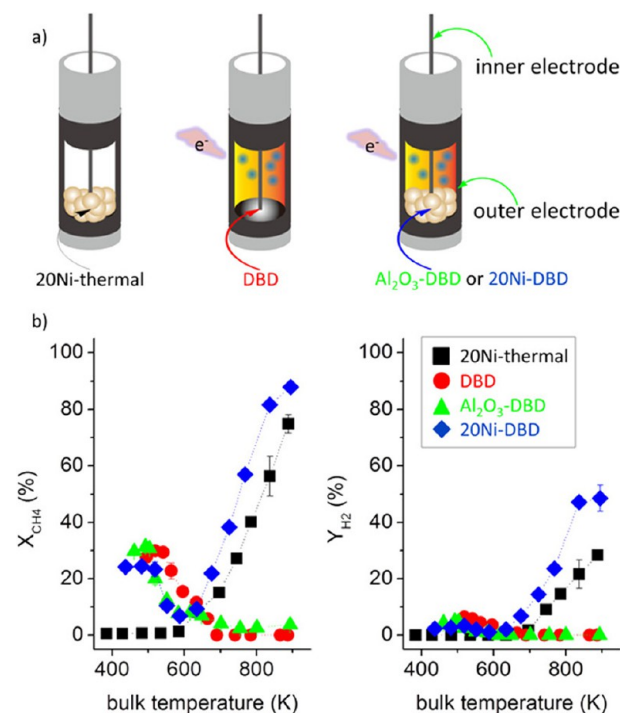


Figure 11. (a) Reaction environments for thermal DRM and plasma-assisted DRM and (b) CH₄ conversions and H₂ yields at various bulk temperatures. Reprinted with permission from ref 84. Copyright 2016 American Chemical Society.

recent study, Kok et al.¹³⁷ demonstrated the occurrence of significant C–N coupling reactions in a mixture of N₂/CH₄/CO₂, as both HCN and NH₃ were detected in a FTIR gas cell. This study provides direct evidence for the involvement of N species in the reaction pathways, indicating the possibility of one-step C–N coupling reactions and opening the door to a range of chemical syntheses. However, it is worth noting that the presence of a carrier gas creates additional challenges in gas/product separation downstream. Further, the energy efficiency is reduced because a fraction of the deposited energy is dedicated to ionizing and exciting the carrier gas.

In summary, an inherent trade-off exists within plasma-assisted oxidative methane reforming reactions. Each plasma system exhibits distinct processing parameters that necessitate optimization to achieve H₂ production and energy efficiency targets.

3.2.4. Plasma Reactor Types. Nonthermal plasmas have garnered sustained research attention for H₂ production over the past few decades.^{92,10,138–144} Using eqs 2 and 3 to calculate the energy efficiency and H₂ yield in various plasma-assisted processes, we report the aggregate data from literature sources, considering both reaction types and reactor types (Figure 13 and Tables S1–S3). In plasma-assisted oxidative methane reforming processes, DBD systems are the most commonly employed, particularly in DRM and POX reactions.³⁸ Additionally, warm plasmas, such as GA and MW systems, are becoming increasingly popular in plasma-assisted SMR due to their higher processing temperatures compared to cold plasmas and their ability to handle water vapor during the process.

3.2.4.1. Corona Discharge. Compared to plasma-assisted SMR and POX processes, corona systems are more commonly used in DRM. As shown in Figure 13 and Table S1, corona

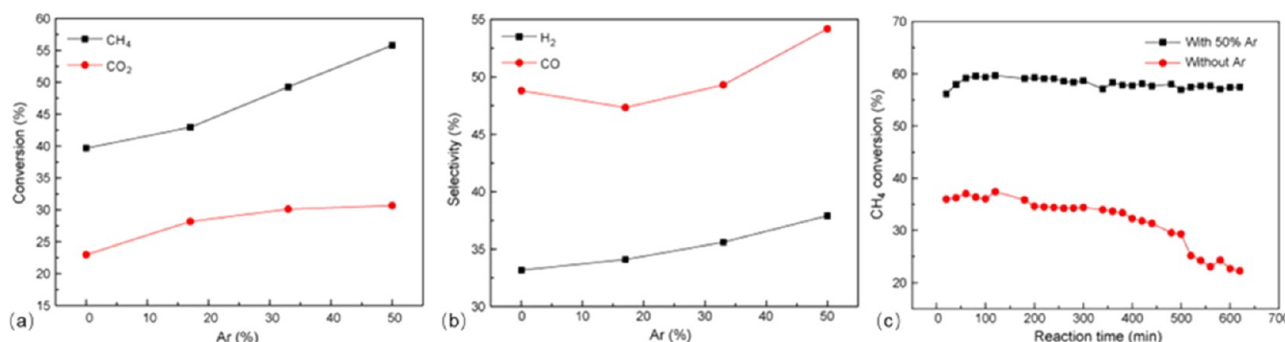


Figure 12. Influence of argon concentration in the feeds on (a) the conversions of CH₄ and CO₂, (b) the selectivities of H₂ and CO, and (c) the reaction stability. Adapted with permission from ref 80. Copyright 2010 Elsevier.

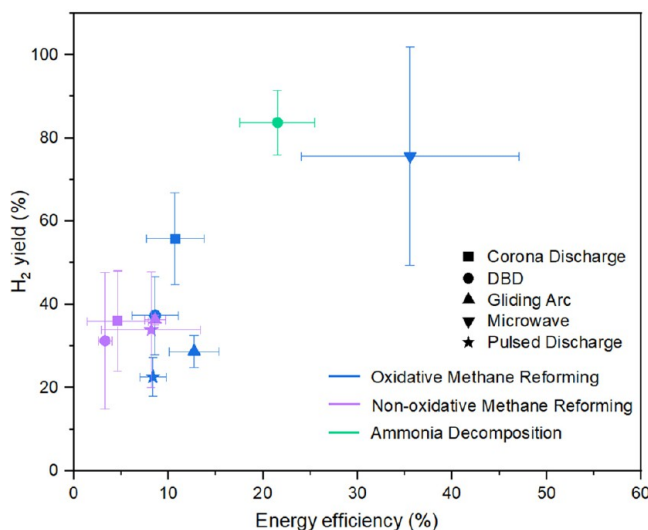


Figure 13. Energy efficiency versus H₂ yield in plasma-assisted processes from refs 30, 68, 77, 95, 97, 107, 111, 114–119, 125–129, 131–136, 140, 141, and 144–198 (details are provided in the Supporting Information).

discharges present an energy efficiency of $\sim 10.7\%$ and a H₂ yield of $\sim 56\%$. Previous research has revealed that positive

corona discharges yield enhanced gas conversions in the plasma DRM reaction compared to negative corona discharges.⁷⁷ This is attributed to the large active volume and high electron energy associated with positive corona discharges.⁷⁷ However, the utilization of negative corona discharge proves advantageous in enhancing H₂ selectivity, leading to the attainment of a H₂/CO ratio surpassing that achieved through positive corona discharge.⁷⁷ Li et al.¹⁴⁵ also observed that an increase in CH₄ conversion in different corona discharges followed the order of positive corona > AC corona > negative corona. High CH₄ conversion (70%), H₂ yield (70%), and energy efficiency (14.3%) were also achieved by using a positive corona discharge for the DRM process at a SEI of 45 kJ/L.¹⁴⁵ Notably, the authors revealed a contrasting pattern in terms of the impact of different corona discharges on the H₂/CO ratio in the syngas: negative corona > AC corona > positive corona.¹⁴⁵

3.2.4.2. Dielectric Barrier Discharge. Dielectric barrier discharge (DBD) stands out as the predominant plasma type, especially for POX and DRM processes.¹⁹⁹ DBDs have advantages such as low operating temperature, compact design, ease in construction, ease in incorporating catalysts, and ability of handling various feedstocks. The electrode type,²⁰⁰ dielectric constant of the packed material,^{151,201–203} and reactor geometry^{152,204–206} have a direct impact on plasma-assisted

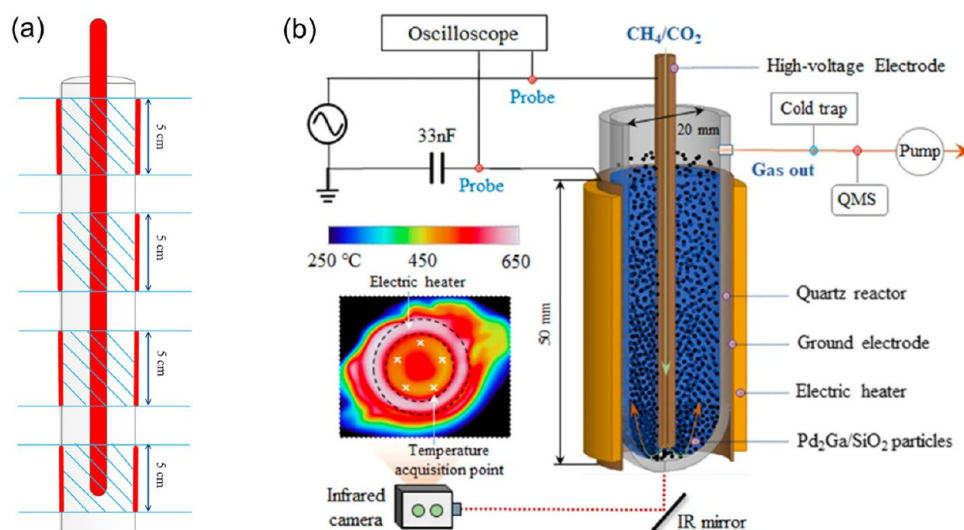


Figure 14. Schematic diagrams. (a) Multistage DBD. Adapted with permission from ref 199. Copyright 2019 Elsevier. (b) Fluidized-bed DBD. Adapted with permission from ref 207. Copyright 2023 Springer Nature.

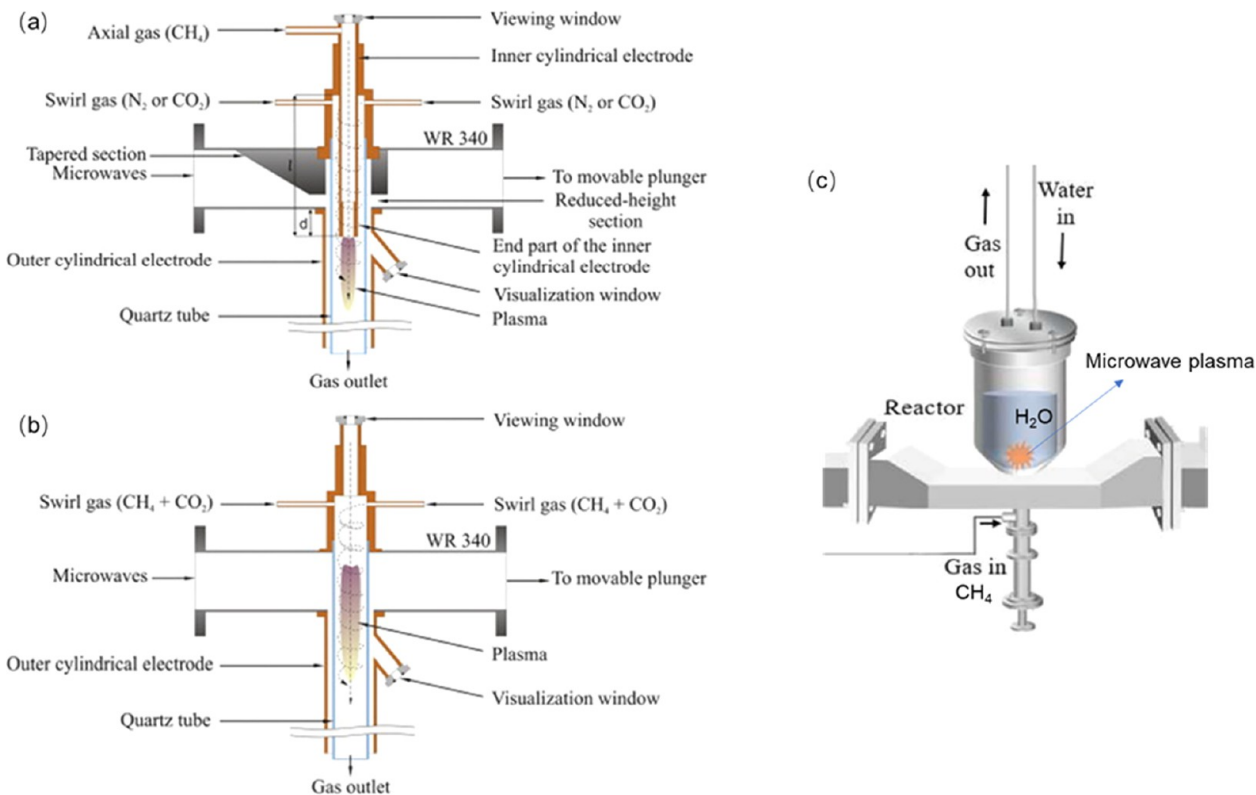


Figure 15. Schematic diagrams. (a) Nozzleless coaxial-line-based MW and (b) nozzleless metal-cylinder-based MW used for DRM. Adapted with permission from ref 209. Copyright 2013. (c) Microwave liquid plasma reactor for SMR. Adapted with permission from ref 136. Copyright 2022 Elsevier.

oxidative methane reforming. DBD-assisted H₂ production processes generally have an energy efficiency of 6–10% with a H₂ yield of 30–40% (Figure 13). Li et al.²⁰⁰ reported that a Ti electrode exhibited the highest CH₄ conversion compared to Al, Fe, and Cu, in a DBD plasma-assisted DRM. Khoja et al.²⁰⁵ found that the optimal discharge gap and discharge length were 3 and 300 mm, respectively, when the discharge gap was varied between 1 and 5 mm and the discharge length was varied between 100 and 300 mm in a cylindrical DBD reactor. Wang and co-workers^{152,199} developed a multistage DBD reactor with a series of tandem ground electrodes sharing one high-voltage electrode (see Figure 14a). The authors found that the multistage DBD reactor promoted H₂ selectivity compared to a conventional one-stage DBD reactor.¹⁵² The authors proposed that the improvement in H₂ selectivity was due to the quenching sections between the ground electrodes, limiting CO₂ recombination.¹⁵²

Recently, the Nozaki group^{153,207,208} developed a highly efficient fluidized-bed DBD reactor and highlighted its advantages for plasma-assisted DRM. As shown in Figure 14b, the feed gas flowed through the hollow of the high-voltage electrode and dispersed the catalyst particles, initiating self-sustaining fluidization motion.²⁰⁷ Compared to a conventional packed-bed DBD reactor, CH₄ conversion dramatically increased from 10–65% to 20–90% in the temperature range of 450–650 °C in the fluidized-bed DBD reactor.¹⁵³ Furthermore, H₂ selectivity increased from 60% to 80% at 450 °C, with coke formation and higher hydrocarbons being fully suppressed.¹⁵³ The authors reported that the fluidized-bed reactor enhanced heat and mass transport inside the discharge region. Given that plasma is not accessible to catalysts in the

micro/mesopores of La–Ni/Al₂O₃, the fluidized-bed reactor improved the interactions between the accessible sites in the catalyst with the vibrationally excited plasma species, thereby improving C–H bond activation.¹⁵³

3.2.4.3. Microwave (MW) Plasma. Microwave (MW) discharges have demonstrated high conversions, high H₂ selectivities, and high gas volume treatment capacity, leading to a H₂ yield of 50–100% (Figure 13). MW plasma systems are electrode-free, which effectively circumvents electrode contamination and soot formation issues. The energy efficiency of microwave plasmas in hydrogen production (24–47%) is comparable to atmospheric pressure plasma jets, spark discharges, and atmospheric pressure glow discharges. To that end, many studies highlighted the potential of atmospheric pressure microwave plasma for hydrogen production.^{131,132,161,209} In one example, Jasiński and co-workers²⁰⁹ employed a metal-cylinder-based microwave reactor for plasma-assisted DRM. As shown in Figure 15a,b, this design allows the absence of an internal electrode and eliminates axial gas flow. Compared to the coaxial-line-based MW that has an internal electrode, this metal-cylinder-based MW significantly increased the plasma volume.²⁰⁹ The authors reported that the hydrogen production rate in the metal-cylinder-based MW almost doubled (~100 g(H₂)/h) that in the traditional coaxial-line-based MW, with the energy efficiency increased to 7.34%.²⁰⁹

In early studies, microwave liquid plasma was proposed for the decomposition of methane hydrate in subsea sites for hydrogen production.²¹⁰ More recently, Wang et al.¹³⁶ made significant advancements by developing this innovative microwave liquid discharge approach for plasma-assisted SMR. As

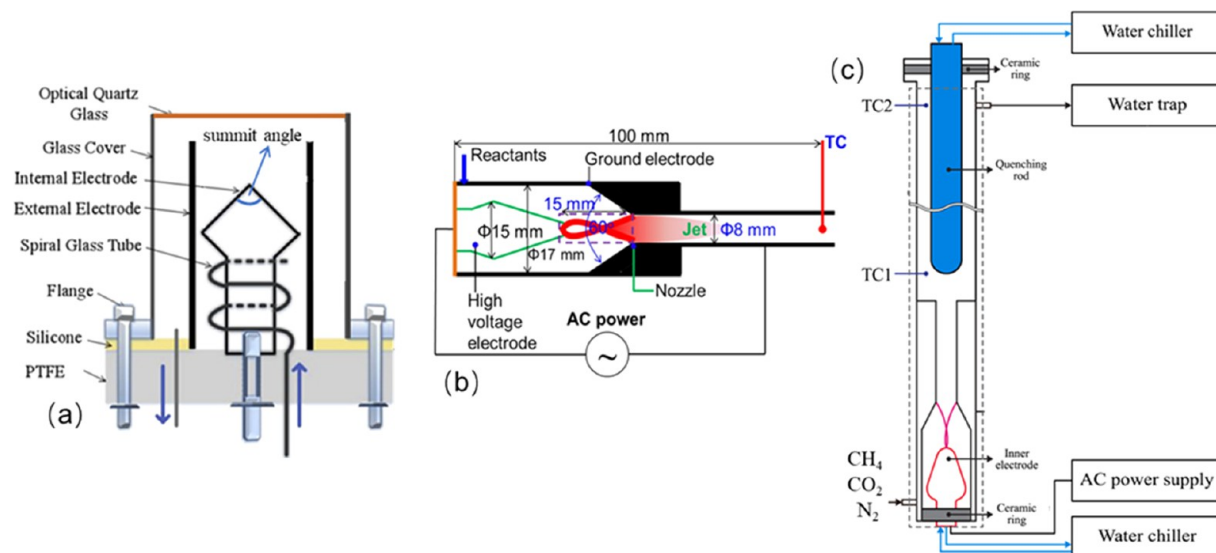


Figure 16. Schematics of rotating gliding arc plasma systems. (a) Variations in electrode structure. Adapted with permission from ref 126. Copyright 2018 Elsevier. (b) 3D nozzle. Adapted with permission from ref 155. Copyright 2020 Elsevier. (c) Water-cooled quenching rod. Adapted with permission from ref 156. Copyright 2023 Elsevier. TC refers to the thermocouple.

shown in Figure 15c, plasma-assisted SMR can occur directly in liquid water, effectively avoiding discharge instabilities due to carbon deposition.¹³⁶ This development offers a practical and viable alternative, particularly for processing the multiphasic mixture of gaseous CH₄ and liquid H₂O, without the need of vaporizing H₂O for the reaction.¹³⁶

3.2.4.4. Gliding Arc (GA). In general, gliding arc discharges have an energy efficiency of 10–16% and a H₂ yield of 25–33% (Figure 13). Recently, Cleiren et al.¹⁵⁷ developed a highly efficient GA plasmatron reactor that achieved an electron temperature ranging from 0.9 to 2.4 eV in DRM. The authors reported a H₂ selectivity of 50% and an energy efficiency of 10%.¹⁵⁷ The authors emphasized the significant contributions of vibrationally excited CO₂ molecules and H and OH radicals within the arc, as well as the thermal effects around the arc column.¹⁵⁷ However, a notable challenge with this reactor is the relatively low CO₂ and CH₄ conversions (18% and 10%, respectively).¹⁵⁷ In recent studies, advancements have been made in the development of rotating gliding arc (RGA) reactors to increase the residence time of the reactants passing through the plasma column. Zhu and co-workers¹⁵⁴ developed a novel RGA reactor codriven by a tangential gas flow and a magnetic field. With the combined effects of swirling flow and the Lorentz force, the arc can rotate rapidly and steadily around an inner cone-shaped electrode, providing a stable and large three-dimensional plasma region with an enlarged residence time of the reactants.¹⁵⁴ A CH₄ conversion of 58.5% and H₂ yield of 20.7% were achieved with a 10 wt % Ni/ γ -Al₂O₃ catalyst packed downstream of the RGA reactor.¹⁵⁴

Furthermore, Lu et al.¹²⁶ investigated the effect of electrode geometry (such as internal electrode summit angle and external electrode length) on DRM in a spiral feeding-gas RGA (Figure 16a). The authors found that a summit angle of 45° showed the highest CH₄ conversion (28%) and H₂ production yield (16%).¹²⁶ This is due to the optimal balance between the sliding space and the rotating time of the arc at the top of the electrode.¹²⁶ Additionally, a long external electrode enhanced the arc extension, increasing CH₄ conversion by 27%, compared to a short external electrode.¹²⁶

Furthermore, apart from modifying the electrode configuration, a 3D nozzle (see Figure 16b)¹⁵⁵ and a water-cooled quenching rod (see Figure 16c)¹⁵⁶ were also developed. These innovations have led to enhanced hydrogen production and increased energy efficiency. The former study attributed these improvements to reduced heat dissipation facilitated by the incorporation of flow-induced thermal insulation,¹⁵⁵ while the latter investigation highlighted the suppression of the reverse water-gas shift (RWGS) reaction, which consumes H₂, aided by the introduction of a quenching device.¹⁵⁶

3.2.5. Mechanistic Evaluation. The mechanisms in plasma catalysis are not a simple sum of plasma-phase chemistry and catalysis. Further, traditional metrics of catalytic activity, such as site-normalized turnover rates, are not applied in many plasma-assisted processes. Due to the significant contributions of NTP phase reactions and their unique nonequilibrium characteristics, the distinctive roles of plasma chemistry, thermal catalysis, and plasma-catalyst synergy are important to identify.

Equations 11–19 summarize basic electron-impact activations of the reactants in the plasma. The formation of H* and CH₃* radicals from electron impact CH₄ dissociation is the first dehydrogenation step. However, the electron-impact dehydrogenation of alkanes (e.g., C₂H₆ and C₃H₈) and CH₄ (to CH₂* and CH*) are primary routes for the production of H₂ in the plasma phase.^{211–213} In plasma-assisted SMR, H₂O provides active species such as H, OH, and O radicals that can activate CH₄ to increase the formation rate of CH₃ radicals⁸⁵ and improve the concentration of H species via the dissociation of OH radicals (eqs 20–22).²¹⁴ In plasma-assisted POX, with the exception of the contribution of O radicals, the electronegativity of O₂ facilitates the formation of negative ions through dissociative attachment.^{215,216} In plasma-assisted DRM, CO₂ offers oxidative species such as CO and O for methane reforming.¹⁹⁹ These active oxidizing species further collide and react with methane and CH_x species in the plasma phase to accelerate CH_x dehydrogenation processes, thus yielding H₂. We identify plasma modeling articles for a deeper

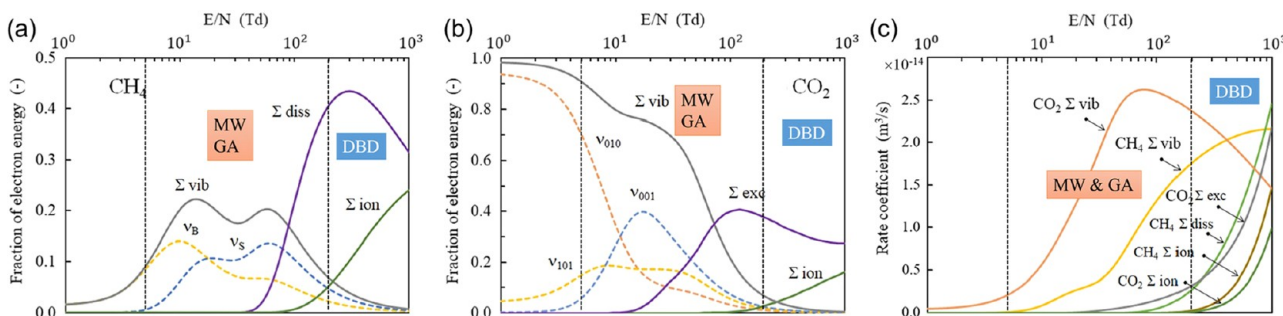


Figure 17. Fraction of electron energy to the excited states of (a) CH_4 and (b) CO_2 , respectively, in plasma-assisted DRM and (c) electron collision rate coefficients. Adapted with permission from ref 207. Copyright 2023 Springer Nature.

understanding on plasma phase chemistries in SMR,^{215,217,218} POX,^{219,220} and DRM.^{221,222}

Alkane activation:



Steam activation:



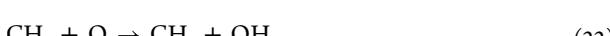
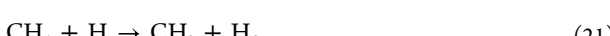
O_2 activation:



CO_2 activation:



Hydrocarbon oxidation processes:



The threshold energies required to directly dissociate CH_4 , H_2O , O_2 , and CO_2 are 9, 7, 8.4, and 7 eV, respectively.⁵⁸ However, electron-impact vibrational excitation in these molecules is capable of dissociating reactants with a much lower energy barrier.^{32,223,224} In the case of plasma-assisted DRM, the electron energy loss fractions to vibrational excitation of CH_4 and CO_2 are smaller than 10% in DBDs ($E/N > 200$ Td). However, the production of vibrationally excited CH_4 and CO_2 is the dominant reaction pathway at $E/N < 700$ Td, compared to the dissociation and ionization rates (see Figure 17).²⁰⁷

Zhu et al.²²⁵ investigated the surface-induced gas-phase redistribution in plasma-catalytic DRM using 1D plasma fluid model combined with 0D surface kinetics. The authors reported that surface reaction changes the development of electron avalanches in the plasma phase, resulting in an improved spatial inhomogeneity.²²⁵ Additionally, the catalyst surface adsorption–desorption processes significantly increased H radical amount and H_2 consumption rate near the catalyst surface (see Figure 18).²²⁵ This study highlighted that

the catalyst could affect the spatial distributions of active species, thereby influencing the plasma chemistry indirectly.²²⁵

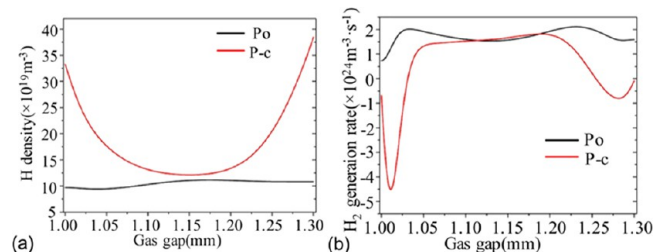


Figure 18. (a) H density and (b) H_2 generation rate in plasma only (Po) and plasma-assisted catalysis (P-c) after the discharge pulse peak. Adapted with permission from ref 225. Copyright 2022 IOP Publishing Ltd.

An experimental study from the Nozaki group^{207,226} investigated the electronic changes in $\text{Ni}/\text{Al}_2\text{O}_3$ for DRM. As shown in Figure 19, the Ni was partially oxidized to NiO up to a 20 μm depth after CO_2 plasma treatment, due to the strong oxidation ability of electron-impact excited CO_2 and NTP heating effects via a plasma-mediated Eley–Rideal mechanism.²²⁶ Consequently, the plasma-induced NiO provides the oxygen-rich surface, which efficiently oxidizes CH_4 , driving the oxidation–reduction cycle in plasma-assisted DMR for CH_4 dehydrogenation.²²⁶ Furthermore, the formation of NiO on the nickel surface inhibited the diffusion of plasma-excited species into the Ni pores, thus efficiently suppressing carbon formation inside the Ni pores (Figure 19d,e).²²⁶

Additionally, many studies have investigated the plasma–surface interaction and surface speciation.^{227–230} Vakili et al.¹⁴⁴ observed that the H_2/CO ratio in the products was promoted by 38% compared to plasma-only experiments due to the contribution of the Pt surface reactions to DRM. The authors reported that Pt nanoparticles facilitated the adsorption of the dissociated CO_2 and C_2H_4 from the plasma phase.¹⁴⁴ Recently, Sheng et al.²²⁹ investigated the thermal catalytic mechanisms and the plasma-assisted catalytic mechanisms in DRM using a $\text{La}-\text{Ni}/\text{Al}_2\text{O}_3$ catalyst by operando spectroscopy. As shown in Figure 20a, the intensities of bidentate and monodentate carbonates on La were promoted by 1.7-fold compared to the thermal process, due to the plasma-catalyst interaction.²²⁹ Moreover, additional bicarbonate and bridge carbonate were observed in plasma catalysis but not in the thermal process. The authors reported that these enhancements in CO_2 adsorption and activation on the catalyst surface were attributed to the contribution from vibrationally excited CO_2 .

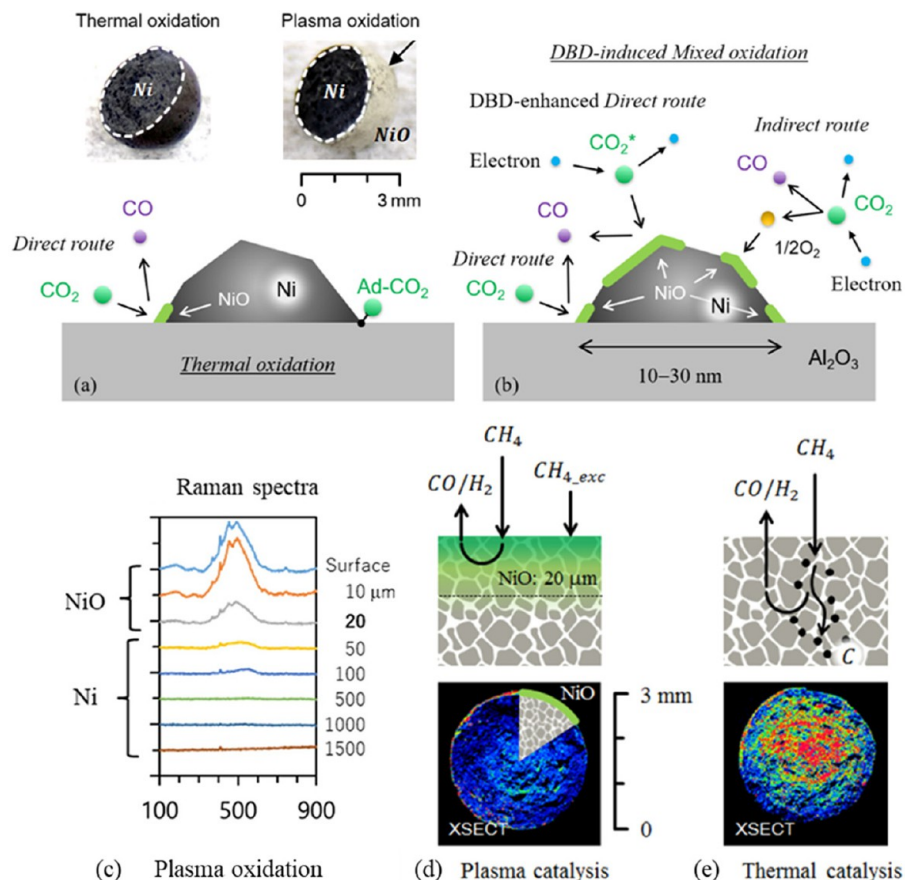


Figure 19. Oxidation pathways over the surface nickel sites in (a) thermal catalytic process and (b) plasma-assisted oxidation process. Adapted with permission from ref 226. Copyright 2018, IOP Publishing Ltd. (c) Cross-sectional Raman spectroscopy of nickel oxide distribution after plasma reaction. Adapted with permission from ref 207. Copyright 2023, Springer Nature. Carbon distribution over the pellet cross-section after (d) plasma catalysis and (e) thermal catalysis. Adapted with permission from ref 226. Copyright 2018, IOP Publishing Ltd.

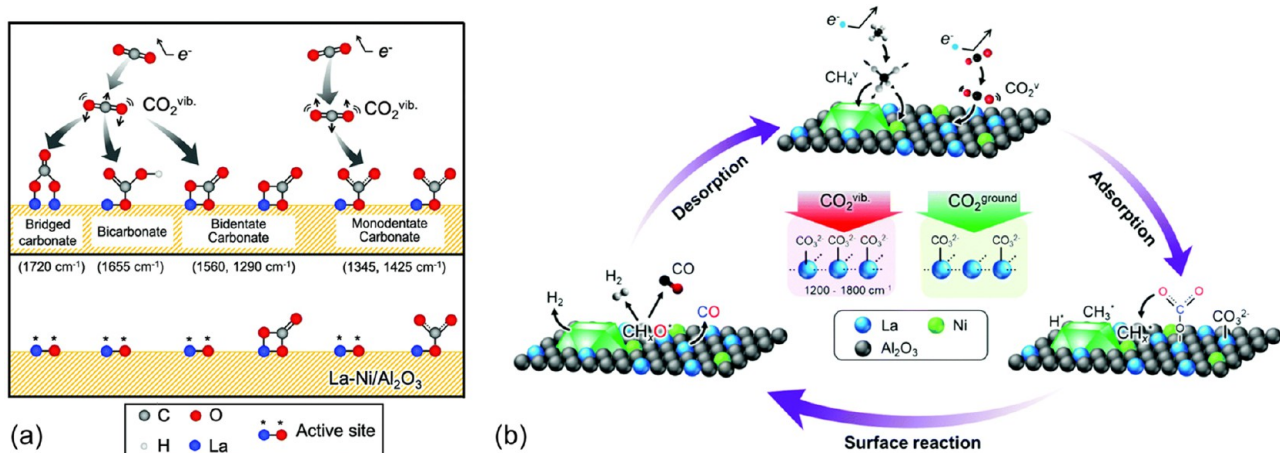


Figure 20. (a) CO₂ activation mechanism on La–Ni/Al₂O₃ at 200 °C via a thermal process and plasma-assisted process. (b) Plasma-assisted reaction pathways in DRM over La–Ni/Al₂O₃. Adapted with permission from ref 229. Copyright 2020 Royal Society of Chemistry.

in the plasma phase, which plays a key role in promoting H₂ production at low temperatures (Figure 20b).²²⁹

3.2.6. Summary. In plasma-assisted oxidative methane reforming processes, achieving an energy efficiency exceeding 60% is essential to be competitive with conventional and emerging technologies (Figure 13). Various types of plasma reactors have emerged for hydrogen production, each with its unique set of advantages and disadvantages. Gliding arc

discharges offer a modest energy efficiency (18–35%) and cost-effectiveness, along with the ability to treat a wide range of feedstocks. However, they tend to consume higher overall power and can experience unstable plasma discharge characteristics. In contrast, microwave plasmas provide the highest hydrogen yield (to date) and exceptional efficiency (~60%) via plasma-assisted SMR, especially when catalysts are introduced to enhance hydrogen selectivity. Nevertheless, issues like hot

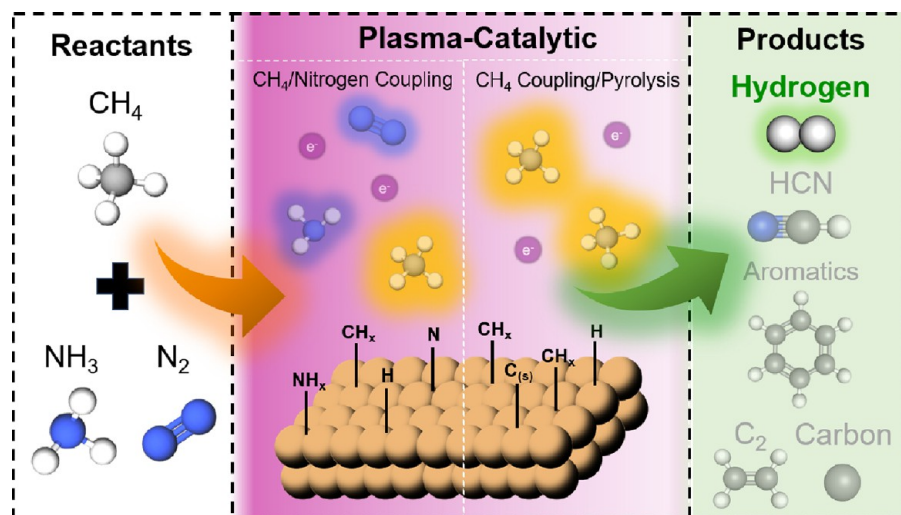


Figure 21. Schematic representation for plasma-catalytic nonoxidative methane conversion to chemicals and H_2 .

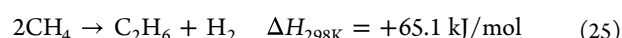
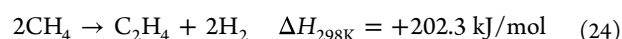
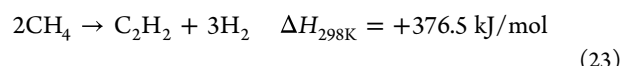
spot formation, variable penetration depth due to microwave instability, and high power consumption for microwave generation limit their application for continuous hydrogen production. Dielectric barrier discharges provide many advantages for H_2 production. However, economic feasibility remains a challenge due to its low energy efficiency (2–20%). Catalyst deactivation due to byproduct contamination is another concern, emphasizing the significant role of catalyst identification and performance in achieving effective plasma-catalyst synergy. It is worth noting that DBD-assisted POX and DRM are gaining popularity for the one-step synthesis of oxygenates.

3.3. Plasma-Assisted Nonoxidative Methane Reforming. Nonoxidative conversion of CH_4 is considered a promising route for the generation of H_2 ; however, most efforts in this area have focused on the production of higher hydrocarbons as valuable fuels and chemicals, with H_2 as a byproduct. Although the selective production of H_2 is not often targeted in nonoxidative CH_4 reforming processes, H_2 remains a valuable product and processes could be re-evaluated with the focus of improving H_2 yields. Within this section, the studies highlighted span various nonoxidative chemistries that lead to the formation of higher hydrocarbons, while forming H_2 as a byproduct.

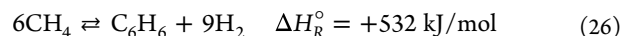
3.3.1. Background/Motivation. Direct conversion of CH_4 is an attractive alternative for the production of fuels and chemicals. Many efforts have been made to advance this chemistry, including approaches such as thermal, homogeneous/heterogeneous catalysis, photocatalysis, electrocatalysis, and plasma catalysis.²³¹ However, due to the high C–H bond strength in CH_4 (434 kJ mol⁻¹),²³² practical implementation of processes targeting the direct conversion of CH_4 are challenging. In contrast to the oxidative conversion of CH_4 , nonoxidative routes for CH_4 activation present high selectivity to target products such as olefins and aromatics. Thus, the chemistries defined within this section primarily focus on the formation of these species, rather than the formation of H_2 , although H_2 is a byproduct for the following reactions.

The direct coupling of CH_4 to C_2 hydrocarbons and H_2 under nonoxidative conditions (eqs 23–25) has received significant attention. This pathway is highly endothermic and involves elevated temperatures (>1273 K) to achieve a higher

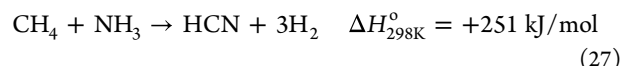
degree of C–C bonding and H_2 yields, where CH_4 can be coupled to products such as acetylene, ethylene, and ethane.²³³



Alternatively, the direct transformation of CH_4 to a mixture of transportable aromatics (e.g., benzene, toluene, and xylenes) and H_2 (eq 26) has also garnered attention. This process is also highly endothermic, requiring reaction temperatures as high as 973 K, where the reaction is restricted by an equilibrium conversion of ~14%. The commercialization of this process remains unfeasible because (1) the high operating reaction temperatures to achieve significant CH_4 conversions and (2) catalyst deactivation caused by the formation of polyaromatic hydrocarbon deposits over the catalysts.

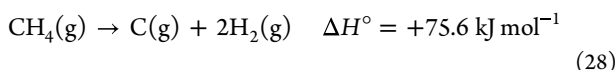


A third possible route to activate CH_4 for H_2 production involves NH_3 reforming. Here, hydrogen cyanide (HCN) is one of the main products obtained from the reaction, and H_2 is formed as a byproduct. The industrial process for HCN production was established by the BASF corporation in 1956,²³⁴ and the main routes for HCN generation are achieved by the Andrussov and Blausaure Methane Anlage (BMA) processes. The Andrussov process is not pertinent for this section, since H_2 is not generated from the reaction; therefore, it will not be further discussed. However, the BMA process directly converts CH_4 and ammonia to H_2 and HCN (eq 27). This process is highly endothermic, requiring temperatures of ~1600 K over a Pt mesh catalyst to achieve high HCN yields.



Thermal decomposition of CH_4 , also known as CH_4 pyrolysis, provides a direct route for the production of carbon and H_2 at high temperatures without the need of an oxygen source as a reactant (eq 28), thereby eliminating the requirement for secondary reactors (e.g., water-gas shift). CH_4 pyrolysis holds significant promise for decarbonization,

primarily due to its capacity to produce solid carbon that can be readily sequestered. Moreover, the production of carbon products through noncatalytic CH₄ pyrolysis has reached a high level of commercial maturity and currently fulfills approximately 95% of the global carbon black market demand.⁶ Nonetheless, in terms of H₂ production, this technology has only seen a limited number of pilot and early-stage commercial sites in operation.



Nonthermal plasmas are suitable for nonoxidative CH₄ conversion to higher hydrocarbons and H₂ due to the ability to operate at low bulk gas temperatures and drive coupling reactions to generate a diverse product slate (Figure 21). Combination of plasma and catalyst, as previously stated, can enhance both CH₄ conversion and product selectivity. Therefore, this process has the potential for efficient utilization of this resource, mitigating the carbon footprint in this process, and paving the way for a sustainable future for the environment and society. The following section highlights significant findings and timelines for the different nonoxidative CH₄ chemistries discussed.

3.3.2. Advancements and Current State-of-the-Art in Plasma-Assisted Nonoxidative Methane Reforming.

3.3.2.1. Methane Coupling to Higher Hydrocarbons and H₂.

As described for the plasma oxidative reforming of CH₄ (Section 3.2), the application of plasmas to convert carbon dioxide, carbon monoxide, and CH₄ can be traced back to the end of the 19th century.²³⁵ Following this discovery, plasma CH₄ reforming into hydrocarbons emerged, and the development of the Huels process began in the 1940s.²³⁶ In this process, a thermal arc, operating at elevated temperature conditions (15,000–20,000 K), was applied for the conversion of CH₄ to acetylene, leading to the production of H₂.²³⁶

Nonoxidative CH₄ coupling with plasma continued through the 1980s and early 1990s, where attention was given to microwave irradiation in the presence of a catalytic material.^{237–240} However, there was a lack in understanding how microwave pulses and heating influenced CH₄ conversion to higher hydrocarbons. In an attempt to address this, Marín et al.²⁴¹ studied the catalytic oligomerization of methane over Ni powder, Fe powder, and activated carbon via microwave heating. With Ni powder in the presence of He as a diluent, a selectivity to C₃ and C₆ species of 16 and 18%, respectively, was observed under microwave heating. When the reaction was performed over activated carbon, a benzene selectivity of 33% was achieved. Fe powder, however, was only active at higher power inputs (1130 W) and no aromatics were produced from the reaction. Diluents such as He participated by absorbing microwave energy and subsequently colliding with CH₄ molecules to form larger molecular weight hydrocarbons. Microwave irradiation, however, results in gas heating which leads to energy efficiencies lower than those observed in cold plasmas. In order to drive this reaction to lower temperatures, Liu et al. reported the plasma-catalytic conversion of CH₄ in a DC corona discharge.¹⁷⁰ The presence of a NaY zeolite catalyst led to higher methane conversions (12% → 37.4%) while increasing hydrogen selectivity (29.0% → 64.2%), when compared to a reactor with no catalyst present.¹⁷⁰ The formation of microdischarges between catalyst particles was responsible for the enhancement in the CH₄ conversion when compared to a reactor with no packing.¹⁷⁰

Most efforts in the 2000s were aimed at upgrading CH₄ through nonoxidative routes, accompanied by the production of H₂. Although noncatalytic, Yang et al.¹⁷¹ investigated a dielectric barrier discharge and corona discharge for the direct nonoxidative conversion of CH₄ to higher hydrocarbons and H₂. In this study, the effects of plasma input power and gas flow rate were also investigated. The SEI was compared between the DBD and corona systems, and it was found that under the same energy per molecule input, an approximate CH₄ conversion of 20% was obtained over the DBD reactor, while an estimated conversion of 60% was achieved in the corona discharge.²⁴² The increase in CH₄ conversion in the corona discharge is due to differences in the electron energy between these two discharges, where a DBD operates with an average electron energy in the range of 0–10 eV while a corona possesses an average energy in the range of 10–20 eV. H₂ selectivity in the corona discharge was ~80% and varied as a function of the energy per molecule input, while H₂ selectivity for the DBD reactor was not reported.²⁴² Corona discharges, in this context, result in a potential route for nonoxidative conversion of CH₄ to produce acetylene and H₂ under low-temperature conditions, outperforming a DBD discharge under identical specific energy input.

To improve CH₄ activation and H₂ selectivity, Indarto¹⁷² investigated a DBD reactor with either Zn or Cr oxide catalysts. Remarkably, the CH₄ conversion of the plasma-catalytic process was ~50% when compared to the noncatalytic process, and the addition of the catalyst increased H₂ selectivity to 40%.¹⁷² Although no quantification of the carbon deposition was reported in this study, carbon was collected on the reactor wall and over the surface of inner electrodes, leading to catalyst and reactor deactivation in the process.

Following this study, Rueangjitt et al.¹⁷³ proposed the plasma-catalytic reforming of CH₄ to H₂ and acetylene in an AC-microsized gliding arc discharge. In this study, the effects of input power (4–12 W) and reactor thickness (0.65, 1.25, 2.25, 3.25, and 4.25 mm) and the role of the catalyst were evaluated. High selectivities for H₂ (~75%) were achieved for a plasma power of 6 W and were independent of the reactor thickness.¹⁷³ The authors suggested that although the reactor thickness was varied, short residence times were still obtained, resulting in unchanged selectivity for H₂.¹⁷³ Despite the presence of a Ni-loaded porous alumina-silica catalyst, the H₂ selectivity remained unchanged.¹⁷³

Using a process variable screening approach, Shuanghui et al.¹⁷⁴ studied the effect of the CH₄/Ar ratio, CH₄ flow rate, input voltage, and electrode gap for the conversion of CH₄ to C₂ hydrocarbons and H₂ in a gliding arc plasma under atmospheric pressure and ambient temperatures. The macroscopic parameters were tuned in order to optimize CH₄ conversion, C₂ hydrocarbon production, and CH₄ yields. Optimum conditions suggested for this process consisted of a CH₄/Ar mole ratio of 0.27, CH₄ flow rate of 14 mL min⁻¹, input voltage of 22 V, and an electrode gap of 4 mm.¹⁷⁴ Under these conditions, a 43.4% CH₄ conversion was achieved, while C₂ and H₂ yields were 37.8% and 35.3%, respectively.¹⁷⁴ The product distribution for C₂ hydrocarbons was not deconvoluted; however, the authors comment that these consisted mainly of unsaturated hydrocarbons.¹⁷⁴ Similar parametric studies were performed by Ghanbari et al.¹⁷⁵ on the effect of Ni–K₂O/Al₂O₃ packing on CH₄ conversion and H₂ selectivity. It was observed that increasing the catalyst packing improved the CH₄ conversion up to a maximum of 88.4% at 6 g catalyst

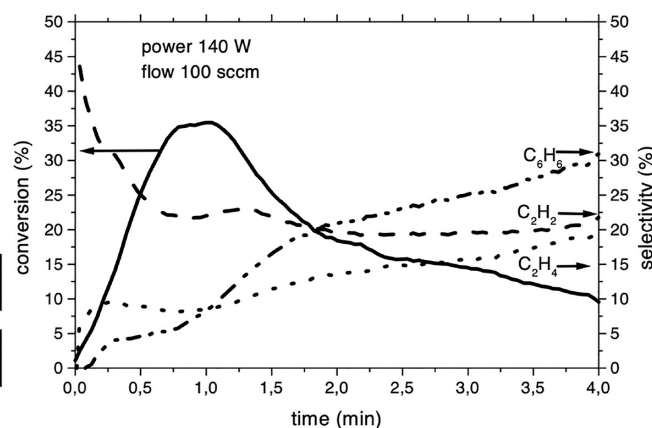
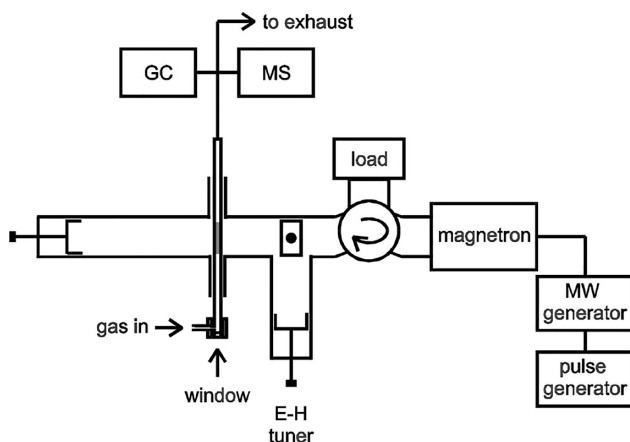


Figure 22. (a) Experimental setup for microwave-pulsed plasmas for methane conversion to aromatics and (b) methane conversion and product selectivity. Adapted with permission from ref 244. Copyright 2002 Elsevier.

packing ($\text{WHSV} = 0.07 \text{ g g}_{\text{cat}}^{-1} \text{ h}^{-1}$).¹⁷⁵ However, complete packing of the plasma zone with the catalyst (10 g) led to decreased CH_4 conversion due to suppression of filamentary behavior and weaker plasma-catalytic interaction.¹⁷⁵

Kasinathan et al.¹⁷⁶ investigated the influence of particle size of $\text{MgO}/\text{Al}_2\text{O}_3$ catalysts over CH_4 activation in a dielectric barrier discharge reactor. An increase in the conversion of CH_4 (9.5–23.0%) was observed with decreasing particle size (1.75–0.25 mm). A similar trend was observed for H_2 production, where H_2 yields increased with decreasing particle size.¹⁷⁶ The authors attributed this enhancement in the activity over smaller catalyst particles to the improved interaction between the surface of the catalyst and reaction species, highlighting the role of catalyst particle size in the conversion of CH_4 to H_2 .¹⁷⁶

As noted here, multiple literature studies are available for the plasma-assisted nonoxidative conversion of CH_4 for both catalytic and noncatalytic systems. These studies show the influence of macroscopic parameters (i.e., plasma power input, feed composition, gas flow rate, SEI, etc.) over CH_4 conversions and H_2 production while showcasing the benefits of coupling a catalyst with a plasma (i.e., one-stage vs two-stage configurations). However, H_2 production is limited in these systems and is accompanied by the formation of higher hydrocarbons (i.e., C_2 species, aromatics).

3.3.2.2. Methane Aromatization. Building on the pioneering work from Wang et al.²⁴³ on thermal methane dehydroaromatization under nonoxidative conditions over a Mo-modified H-ZSM-5 catalyst, many have become interested in the use of nonthermal plasmas for this chemistry since elevated bulk gas temperatures are required for methane activation, and nonthermal plasmas can mitigate this temperature requirement.

Heintze et al.²⁴⁴ first reported the use of a microwave-pulsed plasma for the conversion of CH_4 to aromatics and H_2 using Ni wires, leading to benzene selectivities of up to 30% for an SEI of 84 kJ/L (Figure 22).²⁴⁴ While this study does not explicitly quantify H_2 yields, based on the reaction stoichiometry (e.g., $\text{CH}_4:1.5\text{H}_2$), it can be hypothesized as a byproduct.

A two-stage plasma-catalytic reactor using a Ni-modified H-ZSM-5 catalyst was reported by Li et al. to improve aromatic yields; however, catalysts located downstream from the pulsed spark discharge plasma zone negatively affected the aromatic and H_2 yields.¹⁷⁷ In the absence of catalysts (623 K), a H_2

yield of 62.6% was achieved. Conversely, with Ni/H-ZSM-5, the yield decreased by ~15–20%. The reduction in H_2 selectivity with Ni catalysts was due to the hydrogenolysis capability of the Ni metal.¹⁷⁷ Furthermore, an increase in the H_2 yield was observed with higher reaction temperatures (>673 K) using the Ni-based catalysts, but coke yields increased significantly as well.¹⁷⁷

In a one-stage DBD reactor, Park et al.²⁴⁵ reported a temperature of 500 °C under plasma exposure of Mo/H-ZSM-5 improves methane conversion and benzene production compared to thermal reaction over Mo/H-ZSM-5 at 700 °C.²⁴⁵ Moreover, Van et al.²⁴⁶ considered a different approach for CH_4 conversion to aromatics and H_2 using DBD plasmas, specifically in a dual-stage configuration (i.e., two-stage), where plasma and catalyst are spatially separated. The study found that overlapping a Ga/H-ZSM-5 catalyst with a DBD plasma resulted in poor stability, with a drastic decrease in CH_4 conversion and aromatic production within 1 h of time on stream.²⁴⁶ Therefore, the study explored a dual-stage configuration, where the plasma operated under milder conditions, while a thermal-catalytic reactor containing Ga/H-ZSM-5 operated at 550 °C with a 70% BTX selectivity.²⁴⁶

3.3.2.3. Methane Nitrogen Coupling Chemistry. Production of HCN , NH_3 , and H_2 through carbon–nitrogen coupling, utilizing CH_4 and N_2 as primary sources, has received significant attention from the plasma community. This interest stems from naturally occurring reactions between CH_4 and N_2 observed in the atmosphere of Titan, a moon of Saturn.²⁴⁷ An example of such chemistry was reported by Bai et al.,²⁴⁸ who documented the synthesis of NH_3 through the use of CH_4/N_2 plasmas in a microgap discharge without a catalyst, where H_2 was observed as a byproduct of the reaction. The authors showed that for a residence time of 1.6 s, the yield of NH_3 was 8000 ppm (0.42 mmol g^{-1}).²⁴⁸ In comparison, a previous study reported by the same authors showed the synthesis of NH_3 by strong electric fields over MgO powders, where an NH_3 yield was found to be 5000 ppm, showcasing an improvement with a microgap discharge.²⁴⁹ In terms of H_2 production, the yield and production rate were 9.1% (v/v) and 1879.8 $\mu\text{mol min}^{-1}$.²⁴⁹

A similar approach was adopted by Poirier et al.²⁵⁰ for plasma-assisted hydrocarbon upgrading, utilizing N_2 as a source to produce nitrogen-containing products in a one-pot process. The composition of N_2 was an important factor

affecting the product distribution from a simulated shale gas feed. In N₂-lean environments, the primary products were saturated and unsaturated hydrocarbons.²⁵⁰ Conversely, N₂-rich environments led to the incorporation of N₂ into the products, resulting in the production of chemicals such as NH₃ and nitrogen-containing liquids (including heterocycles, amines, nitriles, and more).²⁵⁰ This study highlights the role of nonthermal plasma in facilitating the breakdown of stable molecules into value-added chemicals using electrical input under mild conditions, and it underscores the impact of nitrogen composition on product selectivity.²⁵⁰

To evaluate catalyst contributions, Yi et al.¹⁷⁸ investigated the NH₃ reforming of CH₄ over Cu-based catalysts using a dielectric barrier discharge plasma reactor. Plasma-catalytic NH₃ reforming of CH₄ was studied at a reaction temperature of 673 K over a Cu/S-1 catalyst, where a CH₄ conversion of 30% occurred with a HCN selectivity of 79% and stoichiometric H₂.¹⁷⁸ It was proposed that HCN production in plasma catalysis undergoes Eley–Rideal (ER) reactions between the radicals generated in the plasma and adsorbed species over the Cu catalyst.¹⁷⁸

More recently, nitrogen incorporation in diamond-like carbon (DLC) microstructures facilitated with the use of nonthermal plasmas was reported by Clarke et al.²⁵¹ The authors showed that light alkane activation leads to carbon deposition and growth over both catalyst and electrode that is spatially controlled by altering the voltage.²⁵¹ DLC materialized in a dielectric barrier discharge reactor with ethane as the hydrocarbon source, and the presence of nitrogen resulted in N-incorporation into the DLC with N/C > 0.25, adding value to this obtained material.²⁵¹ This approach provides an innovative method for the coproduction of clean H₂ (since this reaction is performed in the absence of oxidants) and value-added nitrogen-containing carbon.

A growing area of research involves the plasma-catalytic reforming of CH₄ to H₂ and nitrogen-containing products of added value (i.e., HCN, amines, NH₃, nitriles, etc.). Studies for this chemistry are still ongoing, but the approach has the potential to become a favorable alternative for the production of H₂ and N-containing products.

3.3.2.4. Methane Pyrolysis. Three approaches commonly studied for CH₄ pyrolysis include (1) catalytic pyrolysis, (2) thermal pyrolysis, and (3) plasma pyrolysis.²⁵² For thermal plasma pyrolysis, commercial-scale processes are being developed in the US,²⁵² and operation of this process lies within a temperature range of 1000–3000 °C.²⁵³ Nonthermal plasma CH₄ pyrolysis, however, provides the benefit of operating under lower temperature conditions, and the combination of plasma and catalyst can lead to synergistic effects for the generation of carbon and H₂. This process has the potential of removing carbon from the carbon cycle, while the plasma source is powered by the use of renewable energy. Therefore, the discussion in this section will be centered around recent studies involving nonthermal plasmas in the presence of a catalytic material for the production of carbon and H₂.

Khalifeh et al.¹⁷⁹ evaluated the decomposition of CH₄ to H₂ in a nanosecond pulsed DBD plasma reactor using three different scenarios: plasma-only, plasma with packing material (glass beads), and plasma with catalyst (Pt–Re/Al₂O₃). The results show that for CH₄ flow rates of 20 mL min⁻¹ (or residence times of 9.46 s) and lower, CH₄ conversion increases in the order of plasma + packing > plasma + catalyst > plasma

alone.¹⁷⁹ At a higher flow rate of 30 mL min⁻¹ (or residence time of 8.28 s), the plasma-catalytic reaction dominates with a higher CH₄ conversion in the order of plasma + catalyst > plasma + packing > plasma alone.¹⁷⁹ Further increasing the flow rate to 40 mL min⁻¹ (7.36 s) disrupts the operation of the plasma discharge and no CH₄ conversion is observed. In terms of H₂ production, for a CH₄ flow rate of 20 mL min⁻¹ (9.46 s), the highest production rates are achieved in the packed plasma system (0.891 mmol/min). However, for a CH₄ flow rate of 30 mL min⁻¹, the catalytic plasma system exhibits higher H₂ production rates (1.213 mmol/min).

In a different study, CH₄ conversions and H₂ yields of 87.4% and 67%, respectively, were obtained with a nonthermal plasma in the absence of a catalyst and were heavily dependent on the operating conditions of this process (i.e., discharge power and CH₄ flow rate).¹⁸⁰ The researchers noted that catalytic reactions over Ni/Al₂O₃ were more efficient compared to the low-temperature plasma process, resulting in high CH₄ conversions, although H₂ yields were comparatively lower.¹⁸⁰ The authors identified (1) H₂ production remained unaffected by the CH₄ gas flow rate and discharge power within a temperature range of 400–700 °C and (2) H₂ yields could be enhanced at low discharge powers and high flow rates of CH₄.¹⁸⁰

Using a catalytic DBD, Khoja et al.¹⁸¹ investigated CH₄ cracking for H₂ production with a Ni/MgAl₂O₄ catalyst. Plasma–catalyst synergy led to an improved CH₄ conversion of 80% over Ni/MgAl₂O₄ when compared to MgAl₂O₄ (65%) and plasma-only (73%) experiments. Similarly, an improvement in the H₂ selectivity was also observed, with selectivities of 62%, 68%, and 75% for plasma alone, MgAl₂O₄, and Ni/MgAl₂O₄, respectively.¹⁸¹ A time on stream analysis over Ni/MgAl₂O₄ is depicted in Figure 23, where a 5% decrease in CH₄ conversion and 4% decrease in H₂ selectivity is observed over a period of 16 h, illustrating reasonable stability for the process.¹⁸¹ TGA experiments showed the presence of volatile matter and amorphous carbon, which likely affected the catalyst performance. Further SEM images showed the presence of carbon nanotubes (CNTs). Although the

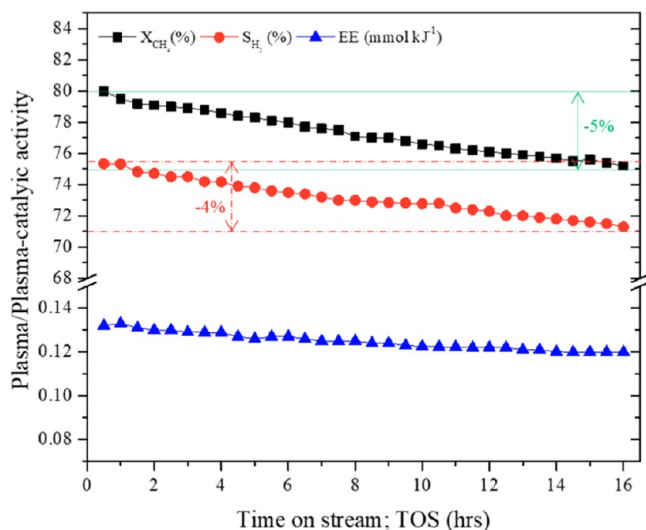


Figure 23. CH₄ conversion and H₂ selectivity as a function of time on stream. Experimental conditions consisted of a GHSV of 364 h⁻¹, a catalyst loading of 0.5 g, and a reaction temperature of 350 °C. Reprinted with permission from ref 181. Copyright 2020 MDPI.

regeneration of the catalyst was not reported in this study, the energy efficiency for the process is shown in Figure 23 as well, and it is relatively constant as a function of time on stream. This study demonstrates the potential of plasma-catalytic systems for H₂ and carbon nanotube (CNT) formation using CH₄ as a hydrocarbon source.

3.3.3. Process Parameters. The influence of macroscopic parameters on the activation of CH₄ and subsequent conversion to H₂ has been a topic of interest in the plasma-catalysis community. Although preliminary discussion of these parameters was provided in earlier sections, this section will focus on how these parameters influence CH₄ conversions, H₂ yields, product selectivity, and energy efficiency.

3.3.3.1. Plasma Power. With an increase in plasma power input, high-energy electrons become more available to promote neutral-electron collisions, resulting in higher reactant conversions. For instance, Rueangjitt et al.¹⁷³ investigated nonoxidative methane reforming in a gliding arc microreactor in the absence of a catalyst, where the input power was varied in the range of 4–12 W. Within this range, a CH₄ conversion increase of ~25–32% was observed.¹⁷³ However, the plasma input power had no effect over the H₂ selectivity, where an ~75% selectivity toward H₂ was maintained across the input power range studied.¹⁷³

In contrast, Shuanghui et al.¹⁷⁴ varied the input voltage between 20 and 23 V with a CH₄ feed, and a decrease in the CH₄ conversion was observed at 23 V.¹⁷⁴ However, an optimum was obtained for H₂ yield at 22 V. Coke was deposited over the electrode surface as a result of CH₄ decomposition, leading to a decrease in both CH₄ conversions and H₂ yields. Further, the authors hypothesized that the increase in voltage inhibited the formation of methyl radicals, although no quantification or evidence of these species was presented.¹⁷⁴

Ghanbari et al.¹⁷⁵ investigated the effect of applied voltage for the conversion of CH₄ over Ni-K₂O/Al₂O₃ in a nanosecond pulsed DBD plasma reactor. The presence of the Ni-K₂O/Al₂O₃ catalyst with an applied voltage of 8 kV increased the CH₄ conversion from 76.4% to 79.3% and the H₂ production from 64.1% to 73.9%, when compared to the plasma-only system (i.e., no catalyst present).¹⁷⁵ In addition, for an applied voltage of 8 kV, the presence of Ni-K₂O/Al₂O₃ reduced the required discharge power from 162 to 141.4 W, corresponding to a 10% reduction while also increasing the energy efficiency of the process.¹⁷⁵

These studies showcase the influence of plasma power input over CH₄ conversion and H₂ generation for CH₄ activation in a nonoxidative environment. Although CH₄ conversion has a positive dependence on plasma input power, achieving higher voltages can lead to extensive carbon deposition over the surface of the reactor and inner electrode, which negatively influences CH₄ conversions. Therefore, the plasma input power should be carefully considered in order to achieve desired CH₄ conversion and H₂ generation while maintaining operational stability.

3.3.3.2. Reaction Temperature. The plasma catalysis community has studied the influence of bulk gas temperature with reaction performance for plasma-assisted CH₄ reforming chemistries.^{107,123,163,254} Despite the current findings in this field, there is a limited understanding of the effect of bulk gas temperature on plasma properties and chemistry, especially in the context of nonoxidative methane conversion to higher hydrocarbons and H₂.

Recent studies have shown that bulk gas temperature inhibits CH₄ conversion under nonoxidative conditions.²⁵⁴ Akintola et al.²⁵⁴ investigated this phenomenon and concluded that an increase in the bulk gas temperature leads to a decrease in the gas density, resulting in a reduction of the gas gap resistance prior to plasma ignition. This effect on gas density influences plasma characteristics and enables a transition in the mode of the plasma, shifting it from a filamentary mode to a more diffusive mode.²⁵⁴ Plasma properties such as the filament lifetime, total and average charge, and filament intensity influenced CH₄ activation, where an increase in the bulk gas temperature led to a decrease in the filament lifetime from 7.46 ± 0.12 to 5.95 ± 0.12 ns within a temperature range of 400–700 °C.²⁵⁴ The same behavior was observed for the total and average charge, where a decrease of 41.4 ± 4.14 to 1.27 ± 0.11 nC and 235 ± 13.8 to 16.1 ± 1.26 pC, respectively, was observed with an increase in temperature.²⁵⁴

In order to elucidate temperature effects for CH₄ conversion to aromatics under plasma stimulation, Rivera-Castro et al.²⁵⁵ investigated the influence of the bulk gas temperature over Mo/H-ZSM-5. Although not quantified, stoichiometric amounts of H₂ were purportedly produced for the plasma-assisted CH₄ conversion in the temperature range of 573–773 K, where CH₄ conversions up to 15% were obtained, and a 2-fold increase in the benzene production was achieved over Mo/H-ZSM-5 at 773 K.²⁵⁵ At a bulk gas temperature of 873 K, a decrease in CH₄ conversion for the plasma-catalytic system was obtained. The remaining activity was largely due to thermal catalytic pathways taking place at the higher temperature conditions.

Overall, these findings show that the operating temperature for the nonoxidative conversion of CH₄ can drastically affect CH₄ conversion and ultimately H₂ yield. Not only can bulk gas temperature influence plasma characteristics, but in the presence of a catalytic material, variation in reaction temperature can alter the product distribution (i.e., aromatization), increase the contribution from thermal-catalytic pathways, and minimize the contribution from plasma phase reactions.

3.3.3.3. Gas Feed Composition and Flow Rate. Gas feed composition and flow rate are two common parameters often varied in plasma catalysis studies. Shuanghui et al.¹⁷⁴ studied the influence of the CH₄ flow rate in a gliding arc plasma reaction for C₂ and H₂ production. It was found that as the CH₄ gas flow rate increased, the CH₄ conversion as well as the H₂ yield decreased, where a decrease from 81.28% to 59.66% was observed within the range of 14–66 mL min⁻¹. The authors suggested that a decrease in the residence time reduces the time for methyl radicals and H radicals to generate C₂ hydrocarbons and H₂.¹⁷⁴

In a separate study, Ghanbari et al.¹⁷⁵ investigated the effect of carrier gas flow on CH₄ conversion and H₂ production for the catalytic conversion of CH₄ to H₂ in a nanosecond pulsed DBD plasma reactor. The volumetric gas flow rate was varied between 50 and 80 mL min⁻¹, and these specific studies were conducted in the absence of a catalyst. The maximum H₂ production was observed for a volumetric flow rate of 70 mL min⁻¹, while a further increase in the carrier gas flow rate resulted in a reduction over the H₂ production.¹⁷⁵ The authors suggested that this effect on H₂ production occurred because (1) an increase in the argon flow rate allows for a higher number of argon molecules to participate in electron collisions which produce more argon active species and (2) a reduction in the residence time of argon in the plasma discharge reduces

interactions between CH_4 and active Ar species, which negatively affects CH_4 conversion.¹⁷⁵

Rather than using a carrier gas to cofeed with CH_4 , Rahimpour et al.¹⁸² investigated the cocracking of CH_4 and *n*-hexadecane over a Mo–Ni/ Al_2O_3 catalyst in a packed-bed DBD plasma reactor. The authors found that this process predominantly leads to the formation of H_2 , accompanied by light hydrocarbons in the range of C_1 through C_4 .¹⁸² The results of this investigation provides evidence that the in-phase plasma-catalysis system shows significant improvement in H_2 production and energy efficiency over the postplasma process (i.e., where the catalyst is placed downstream).

3.3.4. Plasma Reactor Types. Plasma reactor types, designs, and configurations are of crucial importance for the plasma-assisted conversion of CH_4 to higher hydrocarbons and H_2 , and the selection of the appropriate plasma reactor type may determine the outcome of the plasma CH_4 chemistry. Herein, studies are highlighted for different plasma reactor types and innovative designs to improve performance for these configurations. These include corona and spark discharge, microwave plasma, gliding arc, and DBD plasma.

3.3.4.1. Corona and Spark Discharge. It is widely recognized that an increase in the applied voltage in a corona discharge system can lead to a transition toward a spark discharge.²⁵⁶ Using a spark discharge, Wang et al.¹⁸³ investigated the nonoxidative conversion of CH_4 in a plasma-followed-by-catalyst system to generate ethylene and H_2 . In the absence of a catalytic material, the spark discharge resulted in CH_4 conversions of 80%, with yields of 64.1% for acetylene, 2.5% for ethylene, and 59% for H_2 .¹⁸³ The introduction of a Pd–Ag/SiO₂ catalyst downstream of the spark discharge notably increased the ethylene yield to 17.1% and the H_2 yield to 62.6%, while eliminating acetylene production in this configuration.¹⁸³ Energy efficiency and H_2 yield of this system, as depicted in Figure 13, were approximately ~5% and 36%, respectively. These values are comparable to those of other plasma reactor types discussed for nonoxidative CH_4 chemistries.

3.3.4.2. Dielectric Barrier Discharge (DBD). DBD plasmas are commonly used for the conversion of CH_4 to value-added fuels and chemicals at ambient pressure due to their scalability and ease of plasma operation.²⁵⁷ An example was reported by García-Moncada,¹⁸⁴ where a DBD reactor contained catalytic layers with varying thicknesses loaded on the reactor walls. Pd/ Al_2O_3 was chosen as a dehydrogenation catalyst to decrease the formation of carbonaceous deposits for CH_4 conversion in the nonoxidative environment.¹⁸⁴ The catalytic coating of the reactor walls was intended to reduce the impact of the catalyst on plasma discharge characteristics, phenomena typically observed in packed-bed plasma systems.¹⁸⁴ It was found that the CH_4 conversion decreased in the presence of the catalytic layer (Figure 24) due to hydrogenation of methyl radicals with chemisorbed H_2 .¹⁸⁴ Interestingly, variation of the thickness of the Pd catalyst had no influence on the CH_4 conversion. However, the thickness of the Pd catalyst layer affected the product distribution, where carbon deposits decreased as the layer thickness was increased.¹⁸⁴ In terms of H_2 selectivity, addition of the thinnest catalyst layer led to a sharp increase (Figure 24).¹⁸⁴ A comparison between the Pd catalytic wall reactor and a packed-bed reactor containing the same amount of catalyst demonstrated improved performance in the wall-coated reactor, characterized by reduced carbon deposits.¹⁸⁴

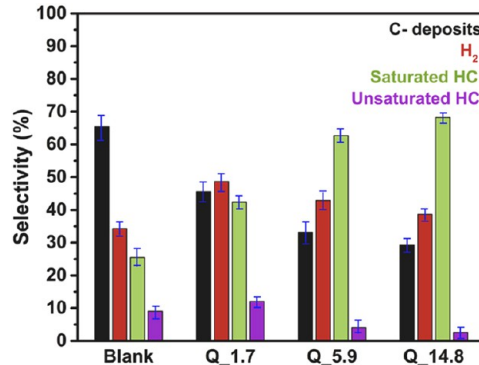


Figure 24. Product distribution obtained from plasma methane dissociation in a structured DBD plasma. Reprinted in part with permission from ref 184. Copyright 2021 Elsevier.

When compared to the corona discharge discussed earlier, DBD systems exhibit lower efficiency (3.27%) and H_2 yield (31.28%). Nevertheless, these values still fall within the range of energy efficiencies and H_2 yields reported for all plasma reactor types used for nonoxidative CH_4 activation, as shown in Figure 13.

3.3.4.3. Microwave (MW) Plasma. The primary benefits of microwave discharges include their ease of igniting plasma, flexibility in operating pressure, capacity to process large volume of gases, and the avoidance of gas phase contamination from electrode erosion debris.²⁵⁸ Nagazoe et al.²⁵⁹ conducted a study on CH_4 dissociation using microwave irradiation with a Pt/ Al_2O_3 catalyst positioned downstream of the microwave plasma zone. The microwave irradiation of CH_4 predominantly produced acetylene and H_2 as products; however, the presence of the Pt/ Al_2O_3 catalyst promoted hydrogenation pathways, leading to the formation of ethylene.²⁵⁹ The research revealed that as the distance between the microwave plasma zone and the catalyst bed increased, the ethylene yield decreased. Conversely, when the catalyst and microwave plasma zone came into close proximity, higher yields of ethylene were achieved. Therefore, this study underscores the significance of the plasma-catalyst configuration and its impact on product distribution in microwave-assisted CH_4 conversion.²⁵⁹

A more recent study involving microwave irradiation was conducted by Julian et al.²⁶⁰ focusing on the nonoxidative conversion of CH_4 using a Mo/H-ZSM-5 catalyst. Specifically, a Mo/H-ZSM-5 catalyst was coated onto a silicon carbide (SiC) monolith, demonstrating stable operation for 19 h at a reaction temperature of 700 °C. The Mo/H-ZSM-5 catalyst on SiC was assessed under both conventional heating and microwave conditions at 700 °C, revealing a noteworthy reduction of coke deposits under microwave irradiation, approximately halving the amount of coke formed.²⁶⁰ Furthermore, the product distribution was influenced by the microwave environment, yielding benzene, ethylene, and negligible amounts of naphthalene.²⁶⁰ In contrast, conventional heating under the same conditions led to the formation of heavy aromatic hydrocarbons and coke precursors, which were notably absent under microwave irradiation. It was found that microwave heating alters the nature of the active Mo_2C sites, thereby influencing the resulting product distribution.²⁶⁰

3.3.4.4. Gliding Arc. In contrast to other nonthermal plasma reforming systems, gliding arcs are able to operate with low specific power consumption and thus achieve relatively high energy efficiency.²⁶¹ Rueangjitt et al.¹⁷³ conducted a perform-

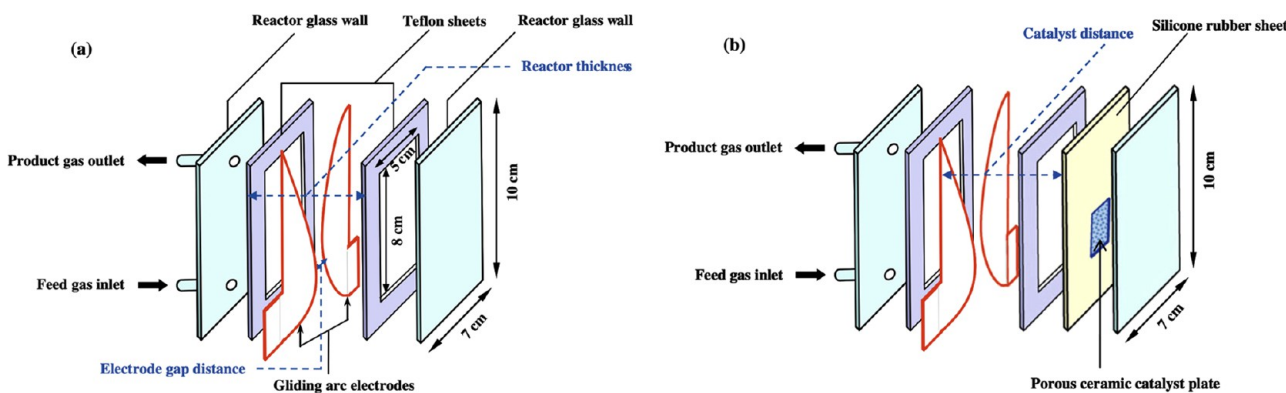


Figure 25. Mini-gliding arc discharge reactor configurations (a) in the absence of a catalyst and (b) in the presence of a catalyst. Adapted with permission from ref 173. Copyright 2009 Elsevier.

ance comparison of a mini-gliding arc under three different configurations: (1) in the absence of a catalytic material, (2) with an unloaded catalyst, and (3) over a Ni-catalyst-loaded plate for CH_4 reforming, as shown in Figure 25. The presence of both unloaded and Ni-loaded catalysts in the plasma system exhibited a synergistic effect, enhancing CH_4 conversion.¹⁷³ The gas flow feed rate and catalyst distance were varied in these studies, and it was found that over the Ni-loaded catalyst plate, CH_4 conversions greater than 50% were obtained for a feed flow rate of 75 mL min^{-1} and a catalyst distance of 0.2 mm. The reported enhancement was attributed to the adsorption and desorption capabilities of plasma-excited species over the catalyst and support surfaces.¹⁷³ H_2 yields were also shown to have an enhancement, with an $\sim 10\%$ increase observed for the plasma Ni-loaded system compared to the plasma-alone configuration.¹⁷³

Lee and Sekiguchi²⁶² explored an alternative approach to plasma-assisted CH_4 reforming by employing a spouted catalytic bed within a gliding arc reactor (see Figure 26). In this setup, Pt, Pd, Rh, and Ru catalysts supported on Al_2O_3 were assessed for their performance. The product distribution was influenced by the presence of the catalyst. Acetylene was

the primary product formed in the absence of a catalytic material, while Pt and Pd catalysts promoted formation of ethylene and ethane.²⁶² Interestingly, the presence of a catalyst in this system inhibited CH_4 conversions, which was attributed to the distortion of the discharge from the catalyst.²⁶²

As shown in Figure 13, gliding arc systems used for nonoxidative CH_4 upgrading result in a higher energy efficiency and H_2 yield when compared to DBD and corona discharge systems. This difference could be due to the ability of gliding arcs to operate under lower power inputs, as previously discussed. However, it is evident that significant room is available for improvement in both energy efficiency and H_2 yield for all of these plasma processes (Figure 13).

3.3.5. Mechanistic Evaluation. The most significant challenge in plasma catalysis is understanding the underlying mechanisms and contributions from the plasma, catalysts, or combination. Plasma–catalytic interactions give rise to a range of effects, such as electrical field enhancements, alteration of the plasma discharge mode, and the formation of micro-discharges within porous materials, among others. Hence, the cumulative impact of these effects adds greater complexity to the system, making the design process notably challenging. Thus, the combination of experimental and computational studies is important in obtaining insights into the nonoxidative conversion of CH_4 to higher hydrocarbons and H_2 over catalytic materials under plasma stimulation.

Given the many reaction pathways, we initially highlight plasma-phase CH_4 reactions in the absence of a catalyst. For instance, De Bie et al.²⁶³ developed a one-dimensional fluid model for a CH_4 DBD plasma, describing the conversion process and pathways to higher hydrocarbons and H_2 . The spatial averaged densities of plasma species present in a CH_4 plasma as a function of time are highlighted in Figure 27.²⁶³ Here, the molecular density of CH_4 is observed to decrease, mainly due to dissociation and ionization reactions taking place. Consequently, the evolution of H_2 accompanied by higher hydrocarbon species is observed in the discharge at significant densities. Interestingly, the molecular density of H_2 increases as a function of time, and at 20 s, both CH_4 and H_2 densities are comparable.²⁶³

Predominant pathways for H_2 production consist of the dissociation reaction of (1) ethane (eq 29), with a contribution of 56%, (2) dissociation of propane (eq 30), with a contribution of 23%, and dissociation of methane (eq 31), accounting for 7%.²⁶³

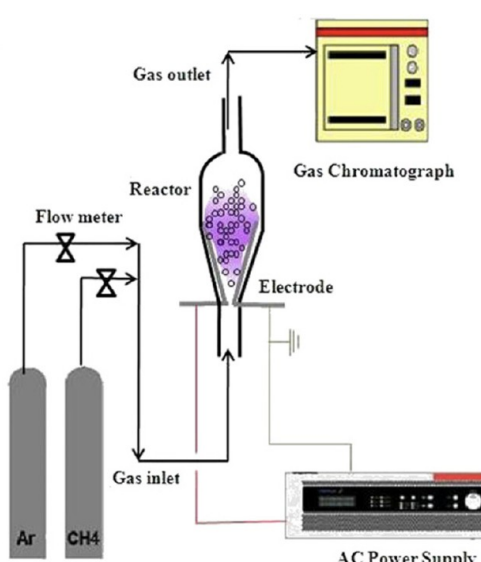


Figure 26. Spouted catalyst bed experimental apparatus for plasma-catalytic methane reforming. Reprinted in part with permission from ref 262. Copyright 2011 IOP Publishing Ltd.

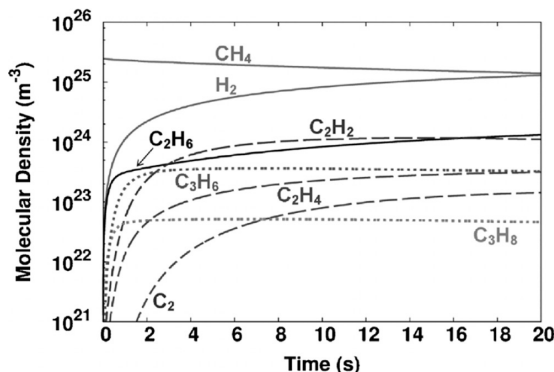
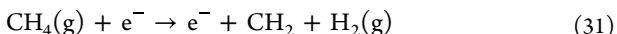
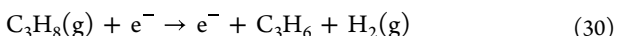
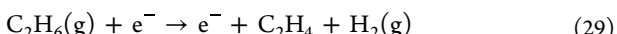


Figure 27. Molecular densities as a function of the residence time in a pure CH_4 plasma. Reprinted with permission from ref 263. Copyright 2011 John Wiley and Sons.



Somers et al.²⁶⁴ studied interaction mechanisms of CH_x radicals in plasmas over various Ni catalyst surfaces using molecular dynamics (MD) simulations utilizing the ReaxFF potential at 400 K to simulate plasma-catalytic conditions. It was found that the decomposition of CH_x radicals over various Ni surfaces at 400 K leads to the formation of H_2 , CH_4 , C_2H_4 , and C_2H_6 molecules, followed by the desorption of these species to the gas phase. This is likely attributed to the diffusion of H_2 atoms over Ni surfaces, stemming from the dissociation of C–H bonds in adsorbed CH_x species. Later studies by Somers et al. showed temperature effects for CH_x radicals over Ni (111) surfaces for H_2 formation.²⁶⁵ Significant H_2 generation was observed at temperatures >1400 K, corresponding to temperatures for warm plasmas.²⁶⁶ These studies showcase the application of molecular dynamics to explore interactions between plasma-excited species and metal surfaces, such as Ni in this case, to provide a better understanding of the plasma-catalytic systems.

In terms of experimental insights, Spiess et al.²⁶⁶ studied the effect of metal electrodes on the decomposition of CH_4 for the generation of H_2 in a silent glow discharge plasma and suggested possible plasma-catalytic reaction pathways based on mass spectrometry and GC/MS measurements. The proposed mechanism is initiated by the plasma activation of CH_4 through electron-impact reactions, leading to the formation of coke, alkanes, alkenes, cycloalkanes, and H_2 .²⁶⁶ The authors suggested that the metal surface plays a role in the initiation of the radical reaction and is important for recombination and termination reactions.²⁶⁶

Yi et al.¹⁷⁸ reported mechanistic insights on the NH_3 reforming of CH_4 for HCN and H_2 production over Cu-based catalysts. It was demonstrated that NH_3 reforming of CH_4 can occur at 673 K (in contrast to the thermal process, which operates at around 1600 K) in the presence of a nonthermal plasma.¹⁷⁸ Through the combination of experimental and DFT calculations, plasma-catalytic production of HCN was proposed to follow an Eley–Rideal (E-R) mechanism between radicals generated in the plasma and adsorbed species over a Cu surface, as depicted in Figure 28.¹⁷⁸

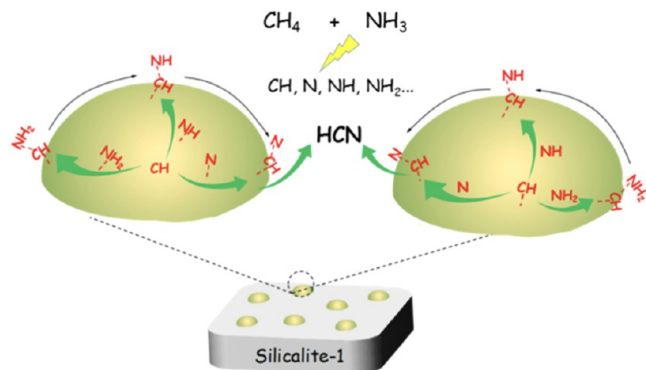


Figure 28. Schematic diagram for the production of HCN from the ammonia reforming of methane via E-R mechanism. Reprinted with permission from ref 178. Copyright 2021 American Chemical Society.

More recently, Engelmann et al.²⁶⁷ investigated interactions between vibrationally excited species and plasma-generated radicals with transition metal catalysts and the influence of the catalytic material on conversion rates and product selectivity. These interactions were studied by developing a microkinetic model, which shows that both vibrational excitations and plasma-generated radicals can impact conversion rates and selectivity over different transition metals.²⁶⁷ The formation of ethylene was favored over noble metals (i.e., Pt, Rh, and Pd) from vibrationally excited CH_4 species, whereas a mixed product selectivity was obtained over non-noble catalysts, indicating the products are dependent on the catalyst type, plasma type, and plasma characteristics.²⁶⁷

3.6. Summary. Nonoxidative CH_4 conversion presents a promising pathway for the production of valuable fuels and chemicals and the generation of H_2 . One distinctive advantage of utilizing nonthermal plasmas is the reduced demand for high bulk gas temperatures and energy input, a clear departure from conventional thermal processes employed for CH_4 activation. Nonetheless, the challenge of achieving high energy efficiencies remains a significant hurdle on the path to commercializing nonthermal plasma applications in hydrocarbon reforming.

Thus far, we have discussed significant findings in the field, dissecting various CH_4 reforming chemistries for the production of higher hydrocarbons and H_2 as a byproduct. Although the discussion within this section primarily focused on the upgrading of CH_4 to higher hydrocarbons, we have attempted to showcase alternative routes to generate H_2 . Focus was placed on plasma-catalyst systems that lead to synergistic effects that can improve conversions, selectivity, H_2 yields, and energy efficiency. Figure 13 compares the H_2 yield and energy efficiency of all plasma reactor types discussed in the studies, showing similar behavior but also highlighting their limitations. Nonoxidative conversion of CH_4 , however, encounters many issues, such as catalyst deactivation due to extensive coke formation, which can also lead to suppression of the plasma discharge. Plasma pyrolysis, however, stands out as one of the most promising technologies for emission-free H_2 production.²⁵² Combined with renewable energy sources, this motivates the utilization of methane as a viable source for this process.

3.4. Plasma-Assisted Ammonia Decomposition.

3.4.1. Background/Motivation. Ammonia (NH_3) is one of the most extensively manufactured chemicals globally.²⁶⁸ Due to the potential of NH_3 to be produced cleanly and efficiently transported, NH_3 decomposition has emerged as a viable

option for CO_x -free H_2 production. NH_3 has an energy density of 3000 Wh kg^{-1} and a chemical hydrogen storage capacity of 17.8% (120 g L^{-1}), which is more than that of methanol, synthesis gas, and other hydrogen-containing chemicals, making it an ideal candidate for H_2 storage/production technologies.^{269,270}

Typically, NH_3 is produced from the Haber–Bosch process, which uses H_2 derived from natural gas sources and N_2 from air. This process is highly energy-intensive, accounting for 2% of global energy consumption and ~2% of global CO_2 emissions.²⁷¹ Decarbonizing NH_3 decomposition effectively requires green ammonia (produced from electrolytic hydrogen),^{272–274} ammonia synthesis from plasma catalysis, or blue ammonia (where the associated CO_2 is captured and stored).²⁷⁹ The NH_3 decomposition reaction is endothermic (eq 32), with thermal equilibrium conversion of >99% at 673 K (Figure 29).²⁸⁰ Therefore, lowering the temperature of NH_3

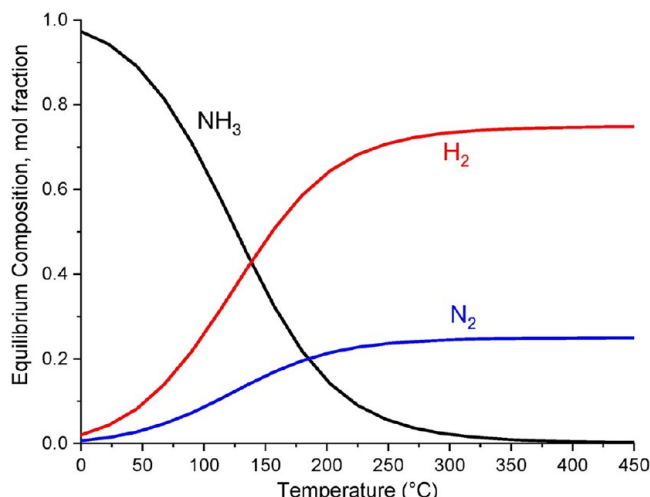
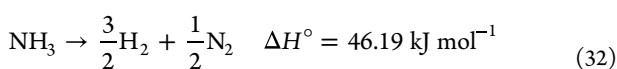


Figure 29. Thermal NH_3 decomposition equilibrium concentration of NH_3 , H_2 , and N_2 with respect to reaction temperature at 1 atm. Reprinted with permission from ref 280. Copyright 2022 Elsevier.

decomposition through nonthermal routes may reduce energy consumption associated with the process and ultimately reduce the associated CO_2 footprint. Additionally, the utilization of renewable energy sources (such as wind and solar) further improves the decarbonization potential of the process.



Plasma-catalytic NH_3 decomposition is recognized for its low-temperature approach to hydrogen production (Figure 30). Notably, external heating of the reactor is often unnecessary, as the plasma can generate energetic electrons that effectively aid in the breakdown of NH_3 to H_2 .^{281,282} The design space for plasma-catalysis is immense, and many parameters can be varied to determine optimal conditions. Therefore, this section provides an overview of the current state-of-the-art in plasma-catalytic ammonia decomposition, followed by a detailed description of the different parameters, process conditions, and plasma properties that influence the reaction.

3.4.2. Advancements and Current State-of-the-Art in Plasma-Assisted NH_3 Decomposition. Plasma NH_3 decomposition experiments can be traced back to the 1950s when

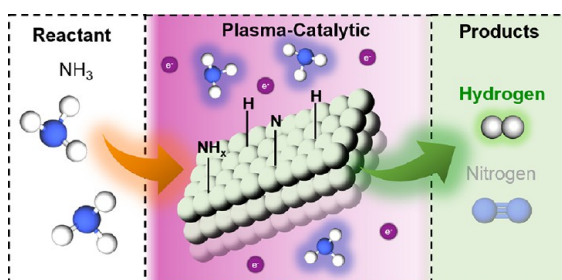


Figure 30. Reaction scheme for the plasma-catalytic NH_3 decomposition.

Devins and Burton investigated the formation of hydrazine (N_2H_4) from NH_3 using an electric discharge tube.²⁸³ In an attempt to study the influence of chemical reagents on surfaces exposed to a plasma jet, Freeman and Skrivan of the American Cyanamid Company studied plasma-activated NH_3 decomposition to H_2 .²⁸⁴ The authors exposed an NH_3 feed to an Ar plasma jet and observed that the reaction was limited by the diffusion of the NH_3 in the effluent plasma stream. It took up to 20 years before d'Agostino et al. (1980) provided spectroscopic and kinetic measurements into the role of excited species on an RF plasma NH_3 decomposition reaction.²⁸⁵ The NH_3 decomposition process was postulated to follow zero-order kinetics, with the initial step being the cleavage of the N–H bond from vibrationally and electronically excited species, leading to NH_2 radical formation.²⁸⁵ Soucy et al.²⁸⁶ provided another report of plasma-assisted NH_3 decomposition using a mixed feed (consisting of NH_3 , Ar, and H_2) in the 1990s using RF induction plasma. The authors evaluated the effect of plasma power, NH_3 , and total gas flow rate (SEI) on NH_3 conversion.²⁸⁶ It was found that an increase in the discharge power increased the NH_3 conversion with a conversion of 88% at a 25 kW power input. However, a decrease in the SEI through an increase in the gas flow rate at constant power decreased the NH_3 conversion.²⁸⁶ Analysis of the product concentration profiles showed that the reaction was transport-controlled rather than kinetically controlled.²⁸⁶ It was not until the early 2000s when Arkhipenko et al. provided another report of NH_3 decomposition in mixed He/ NH_3 and Ar/ NH_3 feed streams using an atmospheric pressure glow discharge (APGD) plasma.²⁸⁷ The authors observed NH_3 conversion of ~60% at a flow rate of 0.5 L/min. Interestingly, the authors observed that the nature of the diluent gas played a significant role in the H_2 yield, where the H_2 yield was 2–3 times higher in the NH_3/He mixed feed when compared to the NH_3/Ar mixed feed for the same flow rate and power input.²⁸⁷ Only at NH_3 concentrations <20% was the H_2 yield similar for both diluents. The Ar was observed to affect the discharge stability negatively compared to when He was used as the diluent.²⁸⁷ However, as the NH_3 concentration increases, the influence of the diluent on the NH_3 activation and conversion decreases. It should also be noted that the plasma discharge power was not reported in this work, making the reproduction or comparison across different studies rather difficult.²⁸⁷

It was not until 2013 that plasma-catalytic approaches were investigated for the NH_3 decomposition reaction.¹⁸⁷ Perhaps the most widely varied parameter in plasma-catalysis studies is the catalyst type, which has been motivated by the discovery that the ideal catalyst in thermal processes is not necessarily the ideal catalyst in plasma-assisted processes.^{275,276,288} The catalyst type can influence N adsorption and desorption after

decomposition, as well as the plasma properties of the reactor.¹⁹⁰ Much recent effort has been targeted on the material design and appropriate catalyst selection for this chemistry. Wang et al.¹⁹⁰ studied different supported transition metal catalysts (Cu, Fe, Ni, and Co) with different N-bond affinities. The authors described a criterion referred to as the synergistic capability (Q_c , %), described as

$$Q_c (\%) = X_{\text{NH}_3(\text{P+C})} - X_{\text{NH}_3(\text{p})} - X_{\text{NH}_3(\text{c})} \quad (33)$$

where $X_{\text{NH}_3(\text{P+C})}$ is the % conversion of the combined plasma-catalyst system, $X_{\text{NH}_3(\text{p})}$ is the % conversion of the plasma-only system and $X_{\text{NH}_3(\text{c})}$ is the % conversion of the thermal-catalyst-only system.¹⁹⁰ For example, Figure 31 shows the NH_3

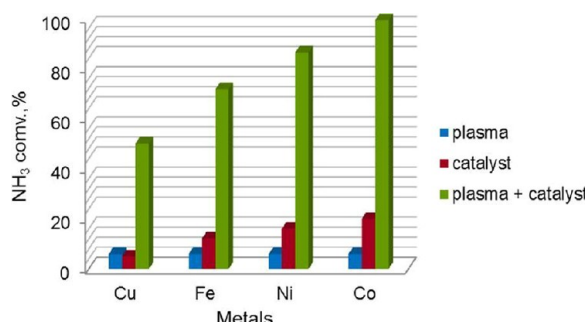


Figure 31. NH_3 conversion over Cu, Fe, Ni, and Co in different operation modes (plasma only, catalyst only, plasma + catalyst) at 450 °C. Reprinted with permission from ref 190. Copyright 2015 American Chemical Society.

conversion from the different catalysts under different operational modes (plasma only, catalyst only, and plasma + catalyst). Significant enhancement in NH_3 conversion was observed when the plasma was coupled with a catalyst. Q_c was determined for various catalysts following the order of Co (73%) > Ni (64%) > Fe (54%) > Cu (39%), and the authors concluded that Co, which has an intermediate N-bond strength, was optimum for the reaction.¹⁹⁰ One thing to point out here is that the plasma-only performance was evaluated in an empty reactor. It is preferable to perform such studies with the packing (support) material to delineate the packing effect from the metallic enhancement effectively. Further analysis on support effects with Co catalysts showed that the Co/fumed silica behaved similarly to the Co/r'- Al_2O_3 and both catalysts outperformed the other supports tested (TiO_2 , HZSM-5, NaZSM-5, TS-1).¹⁹⁰

In a separate paper by the same authors, the metal dispersion was evaluated as an approach to improve NH_3 decomposition.¹⁸⁹ Using a vacuum-freeze-drying and plasma calcination technique, Wang et al.¹⁸⁹ prepared well-dispersed Co nanoparticles on fumed silica and compared them with the incipient wetness-impregnation Co/fumed silica. The vacuum-freeze prepared Co/fumed silica displayed a 47% increase in NH_3 conversion compared to the conventional impregnated catalysts, and the enhancement was attributed to the improved dispersion and narrow particle size range (2–3 nm) of the Co nanoparticles. Similarly, particle size dependence on ammonia conversion and energy efficiency over unmodified alumina support material has also been reported by El-Shafie et al.¹⁸⁵ Although more description about the nature of alumina used

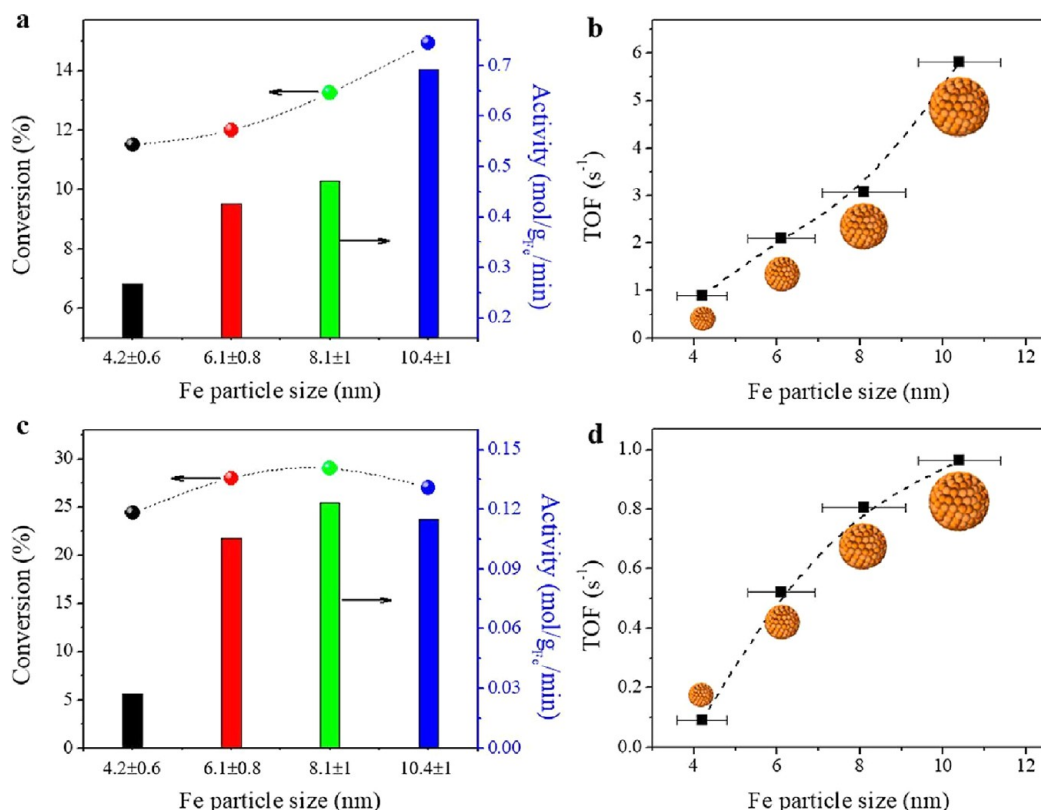


Figure 32. Effect of Fe particle size on catalytic NH_3 decomposition at 600 °C: (a, b) conversion, specific activity, and TOF during the thermocatalytic reaction at 600 °C; (c, d) conversion, specific activity, and TOF during plasma catalytic reaction without external heating. Reprinted with permission from ref 186. Copyright 2022 American Chemical Society.

was not reported in this study, the authors observed that increasing the alumina particle size from 1 to 2 mm led to a decrease in NH_3 conversion from 83.19% to 80.35%, with a corresponding decrease in energy efficiency.¹⁸⁵

Chen et al.¹⁸⁶ studied the particle size dependence of Fe on the NH_3 conversion with a particle size range of 4.2–10.4 nm. Different Fe_2O_3 nanoparticles were prepared using the polyol method and dispersed on the Al_2O_3 using impregnation techniques. However, the researchers observed that as the particle size increased from 4.2 to 8.1 nm, the TOF values increased to a maximum of 0.96 s^{-1} (Figure 32d), highlighting a structure sensitivity dependence on the NH_3 decomposition reaction. Similarly, the thermocatalytic NH_3 conversion and TOF at 600°C also increased with particle size (Figure 32a,b).¹⁸⁶ However, it should be noted that the plasma-catalytic studies were performed with no external heating and with a measured bulk gas temperature of $\sim 200^\circ\text{C}$ at a discharge power of 11 W. The plasma NH_3 conversion over the Al_2O_3 support alone was 22%. This shows that packed-bed effects account for $\sim 76\text{--}90\%$ of the catalytic enhancement over the Fe_2O_3 catalyst, depending on the Fe particle size.¹⁸⁶ This result is somewhat contradictory to the previous report, where improved Co dispersion led to improved NH_3 conversion. It is evident that studies on the effect of particle size using different metals stimulated by nonthermal plasma are still needed.

To improve the Fe NH_3 decomposition activity, Yi et al.¹⁹¹ prepared a series of bimetallic catalysts (Fe–Co, Fe–Mn, Fe–Ni) of different ratios. They observed that the Fe–Ni bimetallic catalysts (with a Fe/Ni molar ratio of 6/4) displayed the most improved activity, with $>99.99\%$ NH_3 conversion at 500°C .¹⁹¹ The hydrogen production rate and energy consumption were maximized at $0.96 \text{ mol}/(\text{g h})$ and $0.050 \text{ kWh}/(\text{mol g})$, respectively. Interestingly, the thermocatalytic NH_3 conversion for the Fe/Ni alloy was less than that of the Ni-only thermal reaction. However, under plasma exposure, the bimetallic Fe/Ni catalyst displayed better NH_3 conversion than Ni, indicating a synergistic benefit under plasma stimulation. Further, the optimal conversion was observed for the Fe/Ni 6/4 ratio.¹⁹¹ More increase in Fe content beyond this ratio led to a decrease in NH_3 conversion. This increased activity was attributed to the formation of Fe_3NiN alloy, which created more sites for NH_3 adsorption and facile adoption of NH_x intermediates.¹⁹¹ Additionally, the preferential adsorption of N and H over Fe and Ni sites respectively enabled the recombination desorption of N_2 and H_2 from the different sites. In addition, this Fe–Ni catalyst displayed good stability for over 200 h of continuous operation.¹⁹¹ Gao et al.¹⁹² recently investigated the plasma-catalytic NH_3 decomposition over transition metal (Fe, Co, and Ni) doped ceria catalysts. The bimetallic codoped metals improved the desorption of NH_3 , evidenced by the NH_3 TPD peak shift to lower temperatures compared to single metal doped ceria catalysts.¹⁹² Further, all bimetallic doped ceria catalysts displayed improved performance over the single metal doped catalyst, with the bimetallic doped FeCo/CeO_2 displaying the best performance with a TOF of 0.275 s^{-1} and hydrogen production rate of $29.3 \text{ mmol}/(\text{g}_{\text{cat}} \text{ min})$ at 450°C .¹⁹² The stability test conducted showed excellent stability of the catalysts for over 48 h time-on-stream operation at 600°C . This enhancement in performance with the FeCo/CeO_2 catalyst was attributed to strong metal–support interactions

(SMSI), the presence of oxygen vacancies, and the moderate nitrogen binding energies between Fe and Co.¹⁹²

Yu et al.¹⁹³ investigated the plasma-catalytic NH_3 decomposition using a Mo_2N catalyst, and they observed a 95% NH_3 conversion at a plasma power input of 40 W, which is more than double the plasma-only or thermal-only catalyst efficiency. The nitridation temperature for catalyst preparation was also observed to affect the conversion of NH_3 , with the catalyst prepared at 850°C displaying an optimum NH_3 conversion of 95% (Figure 33).¹⁹³ However, the MoO_2 precursor used

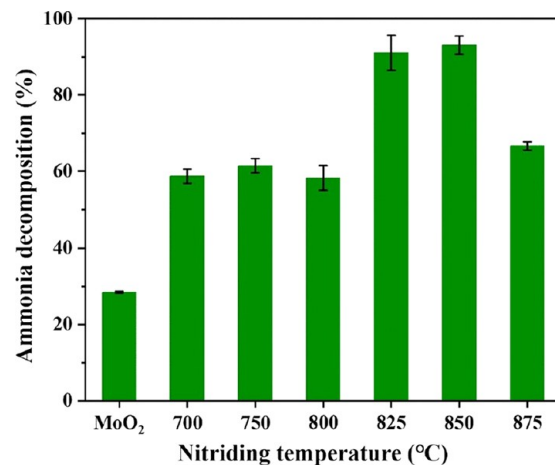


Figure 33. Plasma NH_3 conversion over MoO_2 and Mo_2N catalysts prepared at different nitriding temperatures. Reprinted with permission from ref 193. Copyright 2022 Springer Nature.

showed very low NH_3 conversion (28%) at the same plasma conditions (Figure 33). This improvement in performance with nitridation temperature was attributed to the increase in Mo_2N content and the emergence of the Mo^0 phase.¹⁹³ This study demonstrates the importance of nitride formation and catalyst surface composition in NH_3 decomposition activity over metal catalysts.¹⁹³

Andersen et al.²⁸⁰ investigated the influence of different dielectric materials on plasma-catalytic NH_3 decomposition. Materials with a dielectric constant between 4 and 30 significantly improved the NH_3 decomposition.²⁸⁰ Compared to the plasma-only NH_3 conversion of 5%, MgAl_2O_4 yielded a conversion of $\sim 15\%$, which decreased slightly with an increase in particle size.²⁸⁰ Higher dielectric materials such as TiO_2 and BaTiO_3 delivered lower performance than plasma-only reactions, likely due to reduced gas phase electron density.^{289,290} Interestingly, when metals (Ni, Fe, Co) and bimetallic (Fe–Ni) were impregnated upon the MgAl_2O_4 , the NH_3 conversion decreased significantly.²⁸⁰ While Fe/ MgAl_2O_4 , Co/ MgAl_2O_4 , and Fe–Ni/ MgAl_2O_4 yielded $\sim 1\%$ conversion of NH_3 , Ni/ MgAl_2O_4 yielded the highest NH_3 conversion (7%).²⁸⁰ This value was less than half ($\sim 46\%$) of the MgAl_2O_4 NH_3 conversion.²⁸⁰ The metal reduction of NH_3 conversion was attributed to the metal's ability to quickly remove gas phase electrons due to their high conductivity and significantly decreasing the formation of microdischarges.²⁸⁰

Zhao et al.¹⁹⁴ investigated the catalytic effect of the metal electrodes in enhancing plasma-catalytic ammonia decomposition. They studied the effect of Cu, stainless steel (SS), and Ni and observed the electrode performance to increase in the order of Cu < SS < Ni.¹⁹⁴ While the Cu electrode was relatively inert, they observed the Ni and SS electrodes were

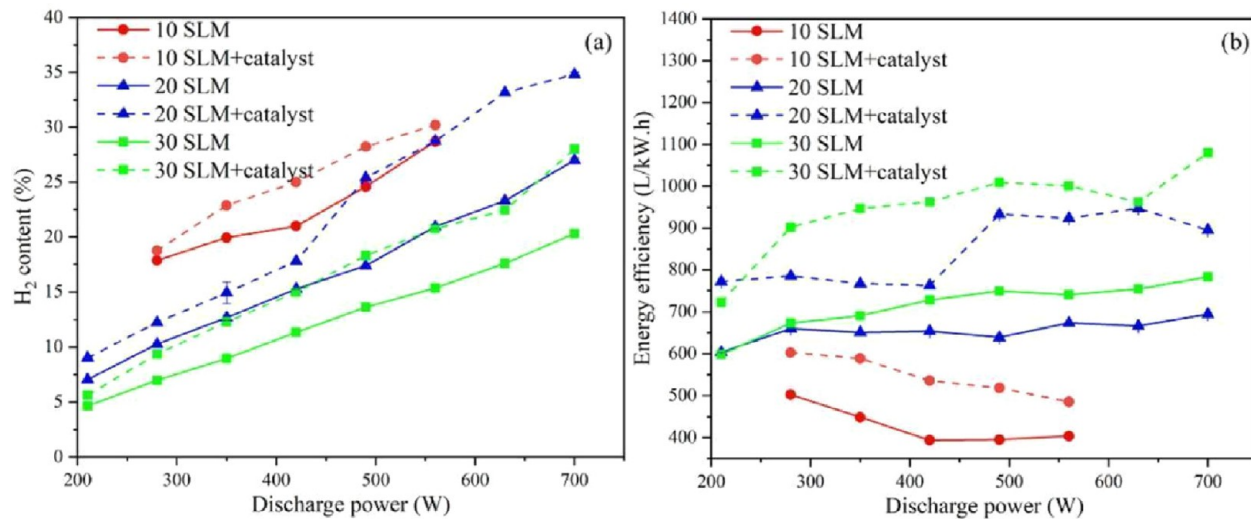


Figure 34. (a) Effect of plasma power on H₂ content. (b) Effect of plasma power on the energy efficiency of the system. Reprinted with permission from ref 198. Copyright 2021 Elsevier.

active catalysts for ammonia decomposition, with the Ni and Fe and their corresponding nitrides identified as the active phases for the reaction.¹⁹⁴ Interestingly, these electrodes contributed up to 50% of the NH₃ decomposition. To improve the energy efficiency of the process, the authors worked on increasing the effective discharge and plasma bulk temperature by decreasing the reactor diameter.²⁹¹ Therefore, the plasma gap is reduced, and the ammonia is forced through the plasma volume with reactor insulation so the electrodes reach high temperatures. Further, they decreased the discharge frequency, which increased the discharge time, plasma volume, and electrode temperature.¹⁹⁴ This could enhance the plasma phase decomposition and the catalytic decomposition over the inner electrode.

The majority of the studies in the emerging area of plasma-catalytic NH₃ decomposition have been directed toward novel material designs to enhance NH₃ conversion rates and H₂ yield in contrast to the conventional thermocatalytic process. To this point, bimetallic catalysts have shown improved performance and stability compared to the monometallic analogues, which is due to the moderate nitrogen adsorption strengths of these bimetallics and, in some instances, improved metal–support interactions. Recent works using nitride-based catalysts also point to the importance of catalyst surface properties in improving NH₃ conversion. Such an understanding is fundamental in designing newer materials for enhanced NH₃ conversion and H₂ yield, specifically at lower temperatures.

3.4.3. Process Parameters. Operating conditions and process parameters exert a significant influence on ammonia decomposition activity. As discussed earlier, the temperature can alter the rate-limiting step of the reaction, with nitrogen desorption limiting at lower temperatures and N–H cleavage limiting at higher temperatures.^{190,270} In addition, other parameters such as feed composition, flow rate, and plasma input parameters such as the plasma power influence the NH₃ conversion. This section discusses the influences of such process parameters on the plasma-catalytic NH₃ decomposition.

3.4.3.1. Plasma Power. Typically, the increase in energy density with power increases the number of electrons that participate in the formation of radicals and energy exchange

reactions, leading to more breakdown of NH₃ and the formation of H₂.^{198,292} Additionally, for the NH₃ decomposition reaction, increasing power has also been reported to facilitate the desorption of adsorbed N on the catalyst surface.^{188,189} For example, Yu et al.¹⁹³ showed that increasing the plasma power from 25 to 40 W (corresponding to an SEI increase from 37.5 to 60 kJ/L) in a DBD reactor increased the NH₃ conversion over a Mo₂N catalyst from 71% to 92%. In these experiments, an optimum power was achieved (40 W), above which an additional increase in discharge power was unable to increase the reactant conversion.¹⁹³ Akiyama et al.¹⁹⁵ also showed a similar plasma power dependence on the NH₃ decomposition rate. The authors observed that increasing the plasma power to 50 W led to a 100% hydrogen yield.¹⁹⁵

Similar parametric studies performed by Lin et al.¹⁹⁸ in a nonthermal arc plasma (NTAP) showed that increasing the power to 700 W significantly increased the H₂ content of the product stream up to ~35%. In this report, the H₂ yield increased continually with increasing power, and no optimum was observed.¹⁹⁸ The energy efficiency of the system was influenced by increasing plasma power (Figure 34). Further OES measurements show the abundance of NH^{*}, N₂^{*}, H₂^{*}, and NH₂^{*} emission bands and the atomic spectra of H_α and H_β.¹⁹⁸ This indicated that the NTAP was effective in dissociating the NH₃. A calculated energy efficiency up to 22.7% was obtained at an NH₃ gas flow rate of 20 SLM. Surprisingly the energy efficiency was observed to increase from ~5.7% to 22.7% as power was increased from 200 to 700 W at a gas flow rate of 20 SLM when a catalyst was incorporated.¹⁹⁸ This increase in efficiency with discharge power is somewhat contrary to observations in a DBD plasma. However, the temperature of the NTAP increased significantly by ~200 K across the power range tested, which could have also influenced the reaction performance.¹⁹⁸

Moszczyńska et al.²⁹³ also reported a plasma power dependence for NH₃ decomposition over carbonaceous catalyst material. The authors show increased NH₃ conversion from 40% to ~100% when the normalized power was increased from 150 to 900 W/m.²⁹³ Gorky et al.²⁹⁴ investigated the effect of NH₃ decomposition on MgTiO₃ metal-based perovskites under cold plasma conditions. Similar to other reports, the

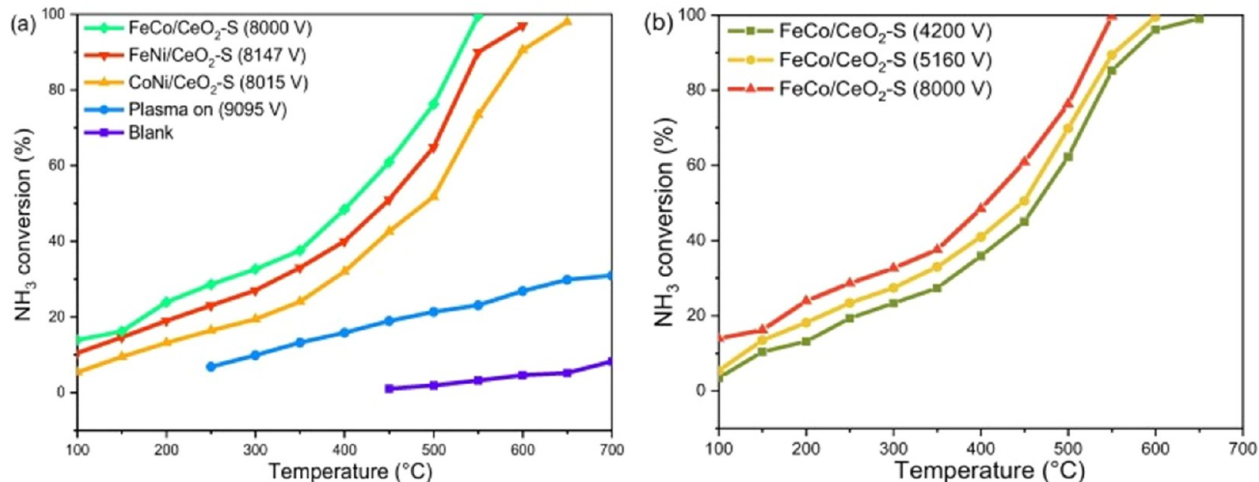


Figure 35. (a) Temperature dependence for plasma-catalytic NH₃ conversion over transition metal (Fe, Ni, Co) doped CeO₂ catalysts at ~8000 V (blank at 9095 V). (b) Temperature dependence for plasma-catalytic NH₃ conversion over FeCo/CeO₂ catalyst at different applied voltages. Reprinted in part with permission from ref 192. Copyright 2023 Elsevier.

NH₃ conversion increased with increasing plasma power, resulting in an NH₃ conversion of ~44% at a discharge power of 20 W with a corresponding energy requirement of 5.06 g_{NH₃}/kWh.²⁹⁴ The plasma power has also been postulated to increase the concentration of NH₃* and NH· intermediates in the gas phase, which helps to consume N from the catalyst surface and prevent the catalyst surface from poisoning due to the reaction.²⁹⁴ Such N consumption pathways have been shown to reduce the temperature of N desorption by over 100 °C.¹⁸⁷ Moreover, studies by Wang et al.¹⁸⁸ show direct evidence using OES that as plasma power increases, the intensity of NH₃* increases, which leads to a corresponding increase in NH₃ conversion.

3.4.3.2. Reaction Temperature. The temperature is a critical parameter that influences the plasma-catalytic NH₃ decomposition reaction, as it affects both the NH₃ activation and N₂ desorption over the catalyst surface. Wang et al.¹⁸⁷ reported a temperature dependence for NH₃ decomposition studies using a DBD plasma over Fe catalysts. In this work, increasing the temperature from 573 to 683 K increased the NH₃ conversion from 1.5% to 99.9%. Although the temperature effect was achieved by changing the plasma power, further studies were performed by the same research group using the same Fe catalyst to delineate the temperature effect further.¹⁸⁸ Here, the authors used a water-cooled reactor at the same exposure power. The results show much lower NH₃ conversion (<20%) using the water-cooled reactor (for the same power input), thus highlighting that the increase in temperature leads to improved NH₃ conversion.¹⁸⁸ Additionally, the enhancement in NH₃ conversion with temperature was also attributed to the favorable N₂ desorption from the Fe surface at higher temperatures.¹⁸⁸

Gao et al.¹⁹² also studied the temperature influence for the NH₃ decomposition reaction over transition metal doped CeO₂. The NH₃ conversion increased with temperature over the single and bimetallic doped CeO₂. Figure 35a shows that with increasing temperature from 300 to 700 °C, a plasma-catalytic enhancement is observed.¹⁹² Though the same increasing trend with temperature was observed for all catalysts tested, the bimetallic doped FeCo/CeO₂ displayed the highest NH₃ conversion with temperature reaching 100% conversion

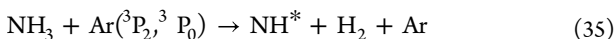
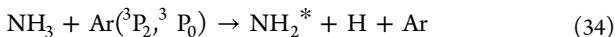
at 550 °C.¹⁹² The temperature of maximum conversion increased with reducing plasma voltage (Figure 35b), whereas the NH₃ conversion reached 100% at 550 °C for 8000 V and a temperature of ~650 °C was required to reach the same conversion at 4200 V.¹⁹² A similar increase in NH₃ conversion with temperature has also been reported for a Fe–Ni bimetallic catalyst, with the NH₃ conversion increasing from ~18% at 370 °C to ~60% at 460 °C.¹⁹¹

A challenge with some of the reported temperature studies is that they are conducted in conditions where an increase in discharge power is used as a knob for temperature control. It would be ideal to conduct such temperature studies at conditions where the temperatures are controlled by an external furnace and increased independent of the discharge power. This would enable proper isolation of temperature effects, which would be highly beneficial for material design. There are still opportunities to improve plasma-catalytic performance at lower temperatures. Future work could leverage the design and selection of materials and the modification of plasma properties to enhance low-temperature activity.

3.4.3.3. Gas Feed Composition and Flow Rate. While some studies have utilized pure NH₃ streams for the decomposition studies,^{190,191} dilution of the NH₃ feed in an inert gas (such as argon or He) has been employed to achieve higher conversions. The presence of inert diluent benefits the NH₃ decomposition reaction because these inert gases, such as He and Ar, have lower breakdown voltages compared to the reactant gases. Ar has also been reported to possess a lower breakdown voltage compared to He, with reported breakdown voltages of 309 and 363 V for Ar and He, respectively.²⁹⁵ Additionally, reports have shown that adding an inert gas such as Ar increases the electron energy and enhances the electric field.²⁹⁶ This increases electron impact reaction with gas phase molecules and promotes plasma-phase chemistry.^{296–298} There is also the potential to create metastable species, which undergo Penning ionization through impact collision and energy exchange with neutral species such as NH₃.^{196,299}

Fateev et al.²⁹⁹ demonstrated the influence of diluent when they investigated the plasma decomposition of an NH₃/Ar stream. The authors studied different NH₃ composition ranges (0.1–10%) and observed that in the lower concentration

regions (0.1–3% NH₃), the predominant reaction pathway is the penning ionization of NH₃ from metastable Ar (Ar(³P₂, ³P₀)) leading to the formation of electronically excited NH₂^{*} and NH^{*} (eqs 34 and 35).²⁹⁹ However, as the concentration of NH₃ increases (3–10%), the electron impact collisions of NH₃ dominate, leading to NH₂^{*} and NH^{*} formation.²⁹⁹



Further, Mlotek et al.²⁶⁹ also investigated the influence of NH₃ concentration using different diluents such as Ar and N₂ in a gliding arc reactor. The NH₃ conversion was observed to increase with decreasing NH₃ concentration. While a similar trend is observed when NH₃ is diluted with N₂, the increase in NH₃ conversion is much higher with N₂ as diluent compared to Ar at the same discharge power. This is due to higher stability for the metastable N₂ (N₂(A³S_u) compared to the metastable Ar (Ar(³P₂, ³P₀)) species.²⁶⁹ However, when NH₃ concentration reaches 33%, the choice of gas diluent does not affect the NH₃ conversion.²⁶⁹ This is consistent with previously reported studies that as the NH₃ concentration increases, the direct electron impact ionization dominates the metastable species-driven-Penning ionization pathway.²⁹⁹ Further analysis shows that at much higher NH₃ concentrations, the reaction rate increases while the energy consumption decreases.²⁶⁹ When pure NH₃ feed is used, the energy consumption is 443 kJ/mol_{NH₃} (which is equivalent to 3.6 kWh/m_{H₂}³ and more than 10 times the minimum thermodynamic requirement).²⁶⁹ Overall, these observations highlight that the nature of the gas used as the diluent is also an important factor in the plasma phase chemistry for NH₃ decomposition. However, the dilution of NH₃ using inert gases presents a challenge in practical implementation owing to the cost and availability of the appropriate diluent gas.

Inoue et al.³⁰⁰ also investigated the effect of NH₃ concentration on reaction conversion and H₂ production. The lower NH₃ concentration (0.5% in Ar) led to a high conversion of 100%, while the higher NH₃ composition (100% pure feed) led to a lower conversion of ~15%.³⁰⁰ Similarly, the energy efficiency was observed to be 800-fold higher for the pure feed compared to the diluted feed.³⁰⁰

The NH₃ reactant flow rate also affects the reaction conversion and H₂ production rate. As described earlier, increasing the gas flow rate at the same power input reduces the SEI, which affects the energy available for a molecule to be excited, ionized, or dissociated. Mlotek et al.²⁶⁹ investigated the influence of flow rate and specific energy input on plasma-assisted NH₃ decomposition. Increasing the gas flow rate at the same specific energy input increases the reaction rate. This increase in reaction rate is consistent for both high and low NH₃ feed concentration regimes and with different diluents, Ar and N₂.²⁶⁹

Akiyama et al.¹⁹⁵ also studied the influence of gas flow rate (residence time) on the NH₃ decomposition rate. The rate of NH₃ decomposition was dependent on the gas residence time in the discharge zone. Increasing the gas residence time to 1.2 s led to a 100% hydrogen yield at a 50 W power input. Similarly, Hayakawa et al.⁶⁸ investigated the influence of NH₃ flow rate in a combined catalytic reactor and plasma membrane reactor. However, in this system, the authors observed that by

increasing the NH₃ flow rate, the H₂ production flow rate increased as well. Increasing the NH₃ flow rate from up to 150 L/h led to a maximum H₂ production rate of 120 L/h at a 110 V input.⁶⁸

Overall, the NH₃ flow rate and composition strongly influence the NH₃ conversion, reaction rate, and energy consumption. While the presence of diluents such as inert gases (Ar, He) or N₂ produces metastable species that could help activate NH₃, the increase in flow rate affects the specific energy input and reaction rate. Thus, to prevent drawing inaccurate conclusions, catalyst material should be tested at the same feed concentrations to compare reaction performance adequately. Moreover, operating with pure NH₃ feed streams rather than diluted feed is beneficial from an economic standpoint.

3.4.4. Plasma Reactor Types. To date, the majority of NH₃ decomposition studies have been conducted in a DBD plasma, and we discuss the different DBD reactor designs and configurations that have been employed in these studies. For instance, Guo and co-workers¹⁹⁰ provided early studies on plasma-catalytic NH₃ decomposition over different supported catalysts in a coaxial DBD reactor. A shell quartz tube of 10 mm o.d. × 8 mm i.d. was used as the dielectric material, with an aluminum foil of 0.1 mm thickness wrapped around the dielectric as the ground electrode.¹⁹⁰ The HV electrode consisted of a 2 mm o.d. stainless steel rod inserted in the reactor. An AC voltage source was used to power the plasma reactor, and the total power was measured by means of a power meter. While the AC power was evaluated from the product of apparent voltage and AC current, the input power was measured using an oscilloscope.¹⁹⁰ This reactor configuration was used to evaluate the effect of transition metals (Fe, Co, Ni, and Cu) for the NH₃ decomposition reaction.¹⁹⁰ Additionally, it allowed for the elucidation of support effects¹⁹⁰ and also for the effect of N poisoning on Fe catalysts¹⁸⁷ for the plasma NH₃ decomposition. The highest energy yield for H₂ production from the system was 5.98 mol/(g kWh).¹⁹⁰

In a follow-up study using the same DBD reactor, the same research group studied the effect of DBD plasma volume on the plasma-catalytic NH₃ decomposition over a finely dispersed Co catalyst.¹⁸⁹ Here, the authors adjusted the volume of the plasma zone (with a constant catalyst packing) by adjusting the length of the inner HV electrode to obtain volumes ranging from 0.4 mL up to 3.3 mL.¹⁸⁹ The catalyst packing volume was held constant at 3.1 mL, resulting in a partially immersed catalyst with lower plasma discharge volumes (Figure 36). Interestingly, the authors observed that decreasing plasma discharge volume increased NH₃ conversion (Figure 37a) and energy yield (Figure 37b).¹⁸⁹ The increase in NH₃ conversion and energy yield was attributed to the increase in SEI at the lower plasma discharge volumes. The SEI here was defined as the ratio of the plasma input power to the

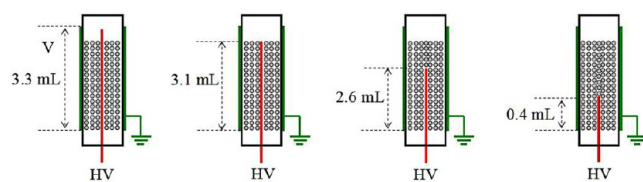


Figure 36. Different DBD plasma volumes for NH₃ decomposition over Co/SiO₂ catalyst. Reprinted with permission from ref 189. Copyright 2019 MDPI.

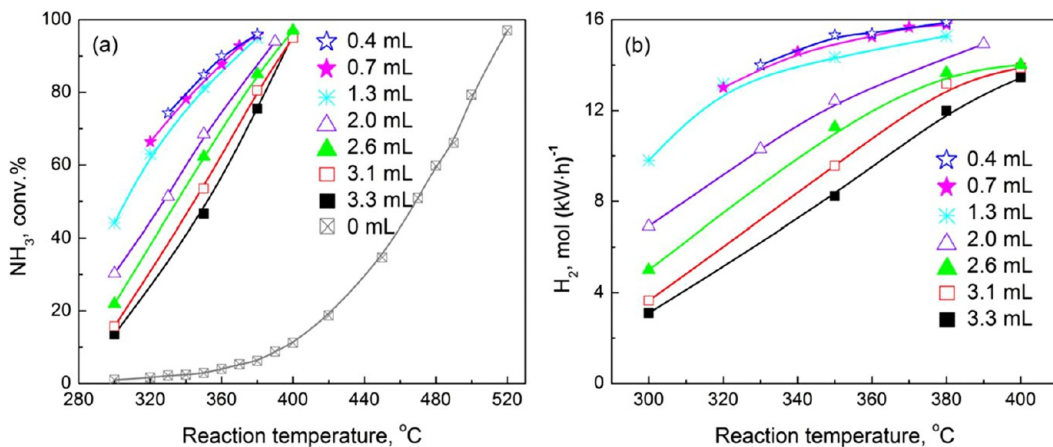


Figure 37. (a) NH₃ conversion as a function of DBD plasma volumes. (b) H₂ energy yield as a function of DBD plasma volumes. Reprinted in part with permission from ref 189. Copyright 2019 MDPI.

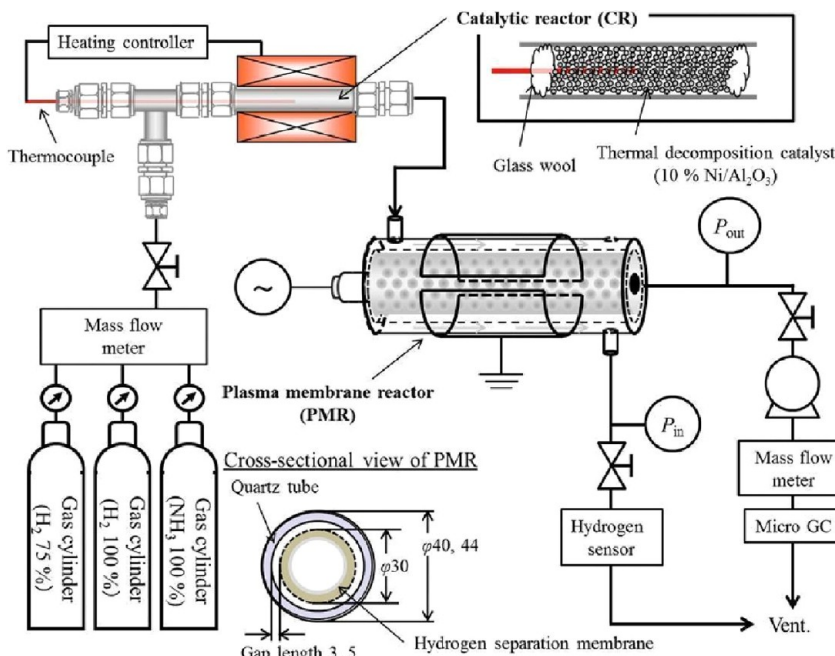


Figure 38. Plasma membrane reactor (PMR) setup. Reprinted with permission from ref 68. Copyright 2019 Elsevier.

plasma discharge volume (W/mL).¹⁸⁹ Additionally, a higher energy yield of 15.9 mol/(g kWh) was obtained with a plasma discharge volume of 0.4 mL.¹⁸⁹

Other groups have employed DBD plasma with different electrode materials and dimensions. Chen et al.¹⁸⁶ used a coaxial quartz tube DBD plasma with an inner diameter of 4 mm. The outer electrode was a 6 cm long stainless steel mesh (20 mesh) material, while the inner electrode was 1/16 in. tungsten rod.¹⁸⁶ Gao et al.¹⁹² also made use of a quartz DBD reactor with a wall thickness of 2 mm, a 19 mm o.d., and a copper ring material as an outer electrode. A copper rod (5 mm diameter) served as an inner electrode with a nanosecond pulsed power source.¹⁹² Interestingly, the inner electrode was wrapped with a 1 mm thick quartz tube to reduce any catalytic influence on the inner electrode.¹⁹² This innovative design is necessary to delineate electrode contribution from catalyst performance. Andersen et al.²⁸⁰ employed the use of a stainless steel mesh (5 cm length) wrapped around the quartz reactor as the outer electrode and a stainless steel rod (10 mm o.d.) as

the inner electrode. With a wall thickness and inner diameter of 1.5 and 19 mm, respectively, a discharge gap of 4.5 mm and plasma discharge volume of 10.2 mL were obtained.²⁸⁰ The plasma discharge volume was higher than those reported by Guo and co-workers¹⁸⁹ and Chen et al.¹⁸⁶ As indicated in these studies, various electrodes, plasma volumes, and power sources have been examined for DBD reactors for NH₃ decomposition, showcasing versatility and adaptability in reactor design. On the other hand, careful normalization of reaction results could help place newer findings that advance the field in proper perspective.

Alternatively, Hayakawa et al.⁶⁸ utilized a novel plasma membrane reactor system where a plasma membrane reactor (PMR) was connected downstream of a catalytic reactor (10% Ni/Al₂O₃) to separate H₂ and produce a high-purity product stream. Figure 38 shows that the plasma membrane reactor comprises a coaxial quartz tube and a hydrogen separation module.⁶⁸ The plasma was generated in the gap by means of a DBD. The hydrogen separation module, which also acts as the

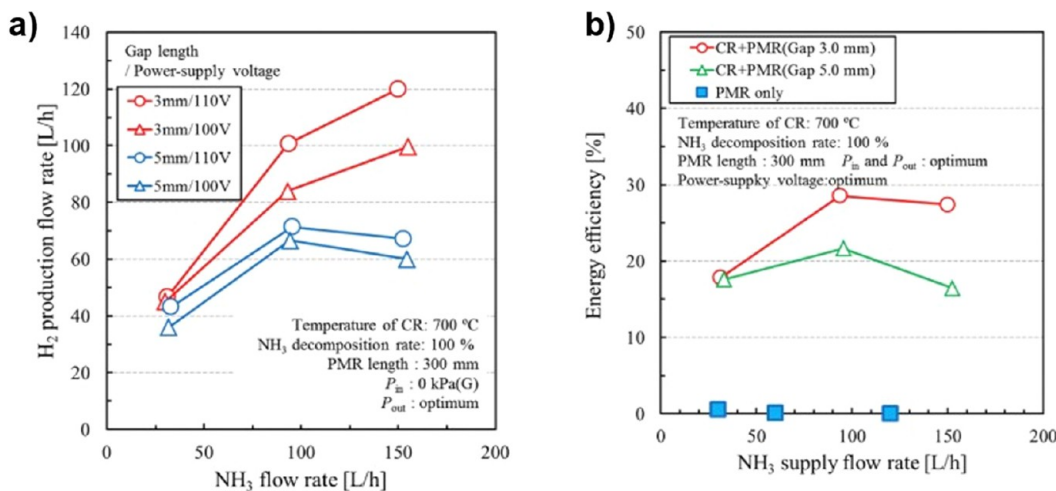


Figure 39. (a) H₂ production rate as a function of NH₃ flow rate at different reaction gap lengths. (b) Energy efficiency as a function of NH₃ flow rate at different reaction gap lengths. Reprinted in part with permission from ref 68. Copyright 2019 Elsevier.

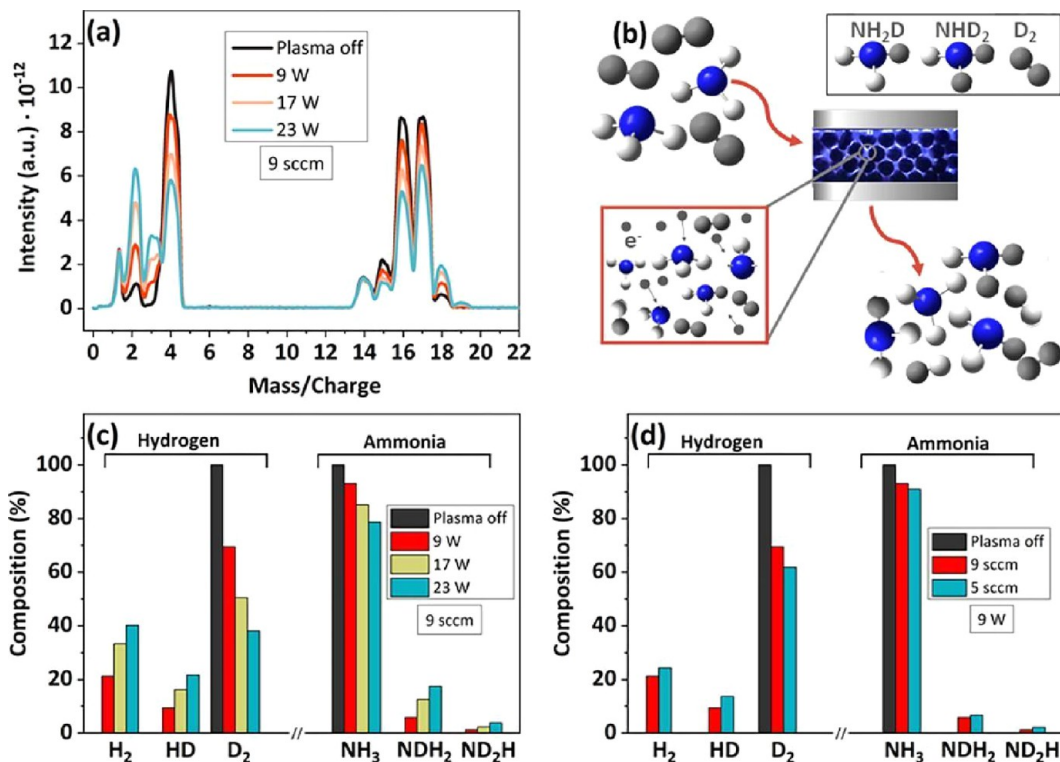


Figure 40. (a) Recorded mass spectra from plasma NH₃ + D₂ exposure. (b) Schematic representation of reaction and exchange leading to NH₃ and H₂ formation. (c) Percentage composition of the different product molecules as a function of plasma power (total flow 9 sccm). (d) Percentage composition of the different product molecules as a function of gas flow rate (plasma power 9 W). Reprinted with permission from ref 197. Copyright 2020 American Chemical Society.

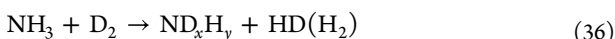
high-voltage electrode, consisted of a 40% Pd–Cu alloy separation membrane. Ammonia is initially decomposed to H₂ and N₂ in the catalytic reactor, after which the product stream comprising unreacted NH₃, H₂, and N₂ is fed to the PMR, where 99.99% purity H₂ is separated.⁶⁸ Additionally, the gap length between the quartz tube and the hydrogen separation module varied between 3 and 5 mm. The hydrogen production rate (Figure 39a) and energy efficiency (Figure 39b) decreased when the reaction gap was increased from 3 to 5 mm, due to the increase in electron density with the shortening of the plasma gap, facilitating the production of radicals.⁶⁸ This

plasma membrane reactor module provides a novel approach to producing high-purity H₂ streams from NH₃, although the efficiency remains an area to improve.⁶⁸

Due to the robust nature and flexible operation of a DBD plasma and the relative ease of coupling with a catalyst, it has become ubiquitous in plasma-catalytic NH₃ decomposition. NH₃ decomposition studies have highlighted that the DBD reactor provides a good setup for rapid material screening and detailed interrogation of the catalytic enhancement for plasma-catalytic ammonia synthesis. Challenges with the DBD reactor lie with its low energy efficiency; as shown in Figure 13, the

reported energy efficiency for this process using the DBD plasma is around 22%. This would need to be enhanced significantly to allow for large-scale implementation of this technology. Further, the materials of construction (electrodes), discharge parameters (gaps), and methods for calculating plasma discharge powers often vary from research groups and between different studies, making it difficult to consolidate findings to adequately advance the field.

3.4.5. Mechanistic Evaluation. Multiple reports have investigated the reaction mechanism for plasma-catalytic NH₃ decomposition.^{191,197} The desorption of adsorbed N₂ (N₂^{*}) is typically agreed upon as the rate-limiting step for the thermal NH₃ decomposition reaction.^{188–190,197,301} Plasma is proposed to generate active species and radicals that can react over the catalyst surface. Navascués et al.¹⁹⁷ used isotope labeling experiments where deuterium (D₂) was cored with NH₃ to interrogate the plasma NH₃ decomposition pathway. Figure 40 shows the different mass intensities (Figure 40a), the proposed reaction scheme (Figure 40b) according to eq 36, and the percentage composition of the different gas products as a function of power (Figure 40c) and total gas flow rate (Figure 40d).¹⁹⁷ From the results, the NH₃ and D₂ amounts decreased with increasing plasma powers while the products (H₂, HD, NDH₂, ND₂H) increased with plasma power, indicating the exchange of the consequent H/D atoms. Also, a decrease in the gas flow rate (Figure 40d) increased the SEI and led to higher NH₃ conversion.¹⁹⁷



Using mass spectrometry measurements, the authors show that high-energy electrons lead to the formation of NH[•] and NH₂[•] radical species, as shown in eqs 37 and 38.¹⁹⁷



However, a series of ineffective reactions where hydrogen radicals or excited hydrogen species may exchange or combine with other NH_x species could take place, leading to low energy efficiencies.¹⁹⁷ Equations 39 and 40 show the interaction of D₂ with NH[•] and NH₂[•], respectively. Equation 40 was reported to happen very quickly since NH₂[•] was not detected from OES spectrum analysis.¹⁹⁷



Although the plasma activation and NH₃ dissociation in the plasma phase have been described, the complete plasma-catalytic reaction, including surface-mediated pathways, has not been fully elucidated. Further, it would be important to study the different elementary steps from a plasma-activated NH₃ up to the H₂ associative desorption step and understand how the activation barriers vary from metal to metal. Another possible approach would be to conduct sequentially designed experiments, as reported recently for NH₃ synthesis.²⁷⁶ In this case, plasma NH₃ activation can be followed by thermal treatments to readily observe associative desorption of H₂ and N₂ over the catalyst surface. Also, other spectroscopic tools, such as inelastic neutron scattering (INS) explored by Barbour et al.³⁰² for NH₃ synthesis and molecular beam mass spectrometry (MBMS),³⁰³ could be utilized to further elucidate the reaction mechanism.

3.4.6. Summary. The plasma-catalytic NH₃ decomposition reaction provides a promising process for H₂ storage and production. Different plasma reactor types have been employed for this process, with DBD being the most prevalent. Most of the research works have focused on designing new materials: bimetallic, bimetallic-doped oxides, nitrides, and highly dispersed metals to enhance the NH₃ decomposition and hydrogen yield. Moreover, some researchers have investigated the influence of particle sizes and dielectric materials on NH₃ decomposition. In some instances, the NH₃ feed is diluted with an inert gas, which helps activate NH₃ molecules by generating metastable species. However, this poses a challenge from a cost standpoint and makes it difficult to compare materials across different studies. The temperature is another critical parameter owing to the endothermic nature of the reaction, and plasma provides an opportunity to operate at lower temperature conditions. On the mechanistic side, more studies are still required to fully unravel and elucidate the reaction pathways for the plasma NH₃ decomposition chemistry. Such a fundamental understanding would be pivotal to inform better material selection and design to improve the NH₃ conversion at lower temperatures.

3.5. Alternative Processes for Hydrogen Generation using Plasmas. Other nonconventional processes have also been explored for plasma-catalytic hydrogen production, including the gasification of biomass and the conversion of oxygenates (e.g., alcohols). Here, we briefly highlight these promising directions for hydrogen production.

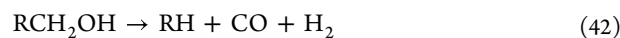
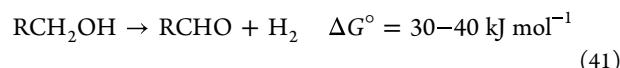
3.5.1. Alcohol Conversion to Hydrogen. **3.5.1.1. Background.** The conversion of alcohols is another interesting opportunity for hydrogen generation, owing to the fact that alcohols could also be derived from biomass (bioalcohols).^{304,305} Equation 41 shows that the process is thermodynamically uphill with a standard Gibbs free energy between 30– and 40 kJ/mol. Additionally, there is the added potential of a decarbonization process where CO is also produced, as shown in eq 42. Table 2 shows that this second

Table 2. Standard Gibbs Free Energy (ΔG°) for Reaction 42 over Selected Alcohols^{a,308}

alcohol	reaction	ΔG° (kJ mol ⁻¹)
methanol	CH ₃ OH → CO + 2H ₂	28.9
ethanol	C ₂ H ₅ OH → CH ₄ + CO + H ₂	-13.9
1-propanol	C ₃ H ₇ OH → C ₂ H ₆ + CO + H ₂	0.4
1-butanol	C ₄ H ₉ OH → C ₃ H ₈ + CO + H ₂	0.8
1-pentanol	C ₅ H ₁₁ OH → C ₄ H ₁₀ + CO + H ₂	7.0

^aStandard Gibbs free energies obtained from Lange's Handbook of Chemistry.

pathway (eq 42) has favorable energetics over different alcohols and is even exergonic when ethanol is used. Since this earlier report, many reports have investigated the application of molecular catalysts for hydrogen production from alcohols.^{306,307} However, these systems rely heavily on rare-earth metals, which are also expensive and can sometimes be toxic.



More recently, conventional supported metal catalysts have been explored to reform alcohols to produce hydrogen. He et al. investigated the use of Pt supported on different transition metal oxides (ZrO_2 , TiO_2 , and CeO_2) for bioethanol reforming to produce H_2 , concluding that the support oxygen vacancy and acidity play vital roles in improving catalyst performance and suppressing coke formation.³⁰⁴ Transition metal catalysts such as Ni, Co, and Cu have also been examined for the alcohol reforming to hydrogen.^{309,310} Improvements in material design for higher hydrogen selectivity, better stability, and improved resistance to coke deactivation are still challenges plaguing the use of these materials. The reforming of alcohol is typically performed with steam and sometimes with oxygen (oxidative reforming). The steam reforming reaction is highly endothermic (eqs 47 and 48). However, introducing oxygen leads to a more favorable autothermal energetic pathway, as seen in eq 49. The ratio of steam to alcohol and oxygen to alcohol is an important factor that affects the alcohol reforming temperature and product selectivity, as seen in eqs 43–49. Figure 41 shows the

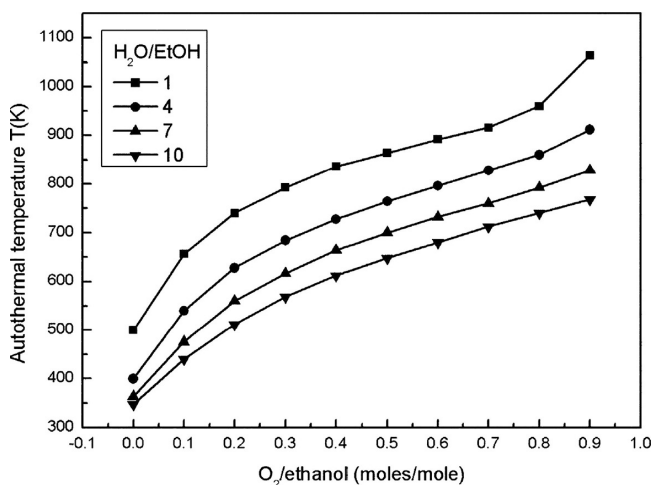
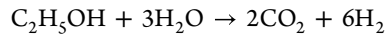
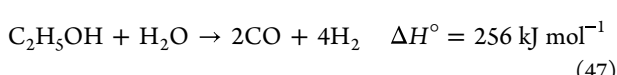
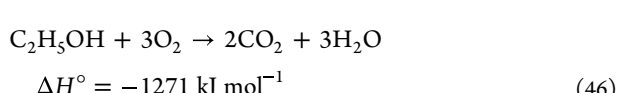
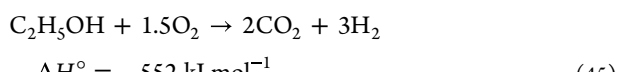
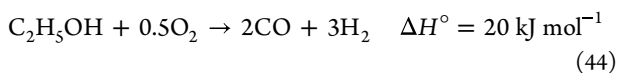
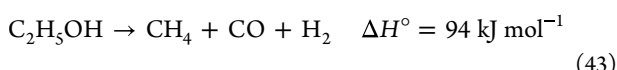
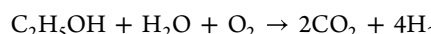


Figure 41. Autothermal temperature as a function of $\text{O}_2/\text{ethanol}$ and $\text{H}_2\text{O}/\text{ethanol}$ ratios at 1 bar pressure. Reprinted with permission from ref 311. Copyright 2008 American Chemical Society.

relationship between the equilibrium (autothermal) temperature and the $\text{H}_2\text{O}/\text{ethanol}$ and $\text{O}_2/\text{ethanol}$ feed ratios.³¹¹ For a particular $\text{O}_2/\text{ethanol}$ ratio, increasing the $\text{H}_2\text{O}/\text{ethanol}$ ratio leads to a decrease in the equilibrium temperature.



$$\Delta H^\circ = 174 \text{ kJ mol}^{-1} \quad (48)$$



$$\Delta H^\circ = -68 \text{ kJ mol}^{-1} \quad (49)$$

3.5.1.2. Plasma-Assisted Alcohol Conversion to Hydrogen.

Earlier works were conducted by Zhu et al.³¹² for bioethanol reforming using a corona plasma and WGS shift catalysts (Pt/TiO_2 and $\text{Pt}-\text{Re}/\text{TiO}_2$ stacked bed) downstream. The combined plasma–WGS system led to a significant improvement in H_2 gas phase selectivity (73.3%) and production rate (3.56 mmol/min). Further, Du et al.³¹³ studied the steam-oxidative reforming of ethanol to produce hydrogen using a nonthermal arc plasma-catalytic system. In this study, an ethanol/water/air mixture was first mixed in a spray nozzle and fed to the plasma discharge zone, with a $\text{Ni}/\gamma\text{-Al}_2\text{O}_3$ catalyst placed downstream of the plasma discharge zone.³¹³ Parametric studies were conducted using variations in the reactant feed ratios, such as oxygen/ethanol (O/C), steam/ethanol (S/C), and discharge power. The results show that H_2 productions increased with increasing O/C ratio (Figure 42a) and S/C ratio (Figure 42b) up to maxima of 1.358 and 1.440 mmol $_{\text{H}_2}$ /s, respectively.³¹³ Increasing the ethanol flow rate also increases the H_2 production rate (Figure 42c) and energy efficiency with an optimum at an ethanol flow rate of 0.1 g/s (Figure 42d). The specific energy requirement (SER) for H_2 decreased with ethanol flow rate to a minimum H_2 SER of 39.8 kJ/mol at an ethanol flow rate of 0.14 g/s.³¹³

Du et al.³¹⁴ further investigated the ethanol conversion to H_2 over three different supported catalysts ($\text{Ni}/\gamma\text{-Al}_2\text{O}_3$, $\text{Co}/\gamma\text{-Al}_2\text{O}_3$, and $\text{Cu}/\gamma\text{-Al}_2\text{O}_3$). The best performance was observed over $\text{Ni}/\gamma\text{-Al}_2\text{O}_3$, with a SER for H_2 of 6.7 kJ/mol at an ethanol conversion of 88.2% and H_2 selectivity of 46.3%.³¹⁴ The reaction condition for maximum H_2 also varied among the catalysts, with an optimum O/C ratio of 0.3 over Ni and Cu, while the optimum O/C yield was 0.5 over Co when the S/C ratio was 1.0 and the ethanol flow rate was 0.10 g/s.³¹⁴ The mechanism of catalytic enhancement for the plasma-catalytic system for ethanol conversion to H_2 is shown in Figure 43. The plasma generates electrons which activate the reactant molecules, creating highly energetic species (ions, radicals) which are then converted over the catalyst surface, yielding products (H_2 , CO, CO_2).³¹⁴

Recent investigations have shown that plasma could also be employed for the conversion of alcohol/water mixtures to produce H_2 .³¹⁵ Olejczyk et al.³¹⁶ utilized a hybrid plasma-catalytic reactor for the conversion of ethanol to hydrogen. The authors used a spark discharge plasma reactor in which an ethanol/water mixed stream was fed into the reactor. An unsupported cobalt catalyst was used with operating temperatures of 250–600 °C, discharge powers of 15–35 W, and ethanol/water ratios of 1:3.³¹⁶ Ethanol conversions and hydrogen yields increased with temperature and also with power due to increase in electron density and more effective collisions for ethanol breakdown.³¹⁶ Further studies conducted on ethanol conversion to hydrogen using a multisegment plasma-catalytic reactor and a Co/ZrO_2 catalyst showed a high hydrogen yield of up to ~0.45 mol $_{\text{H}_2}$ /h (Figure 44a).³¹⁷ Figure 44b shows that the ethanol conversion increased from 34 to 55% after the discharge power was increased from 20 to 60 W.

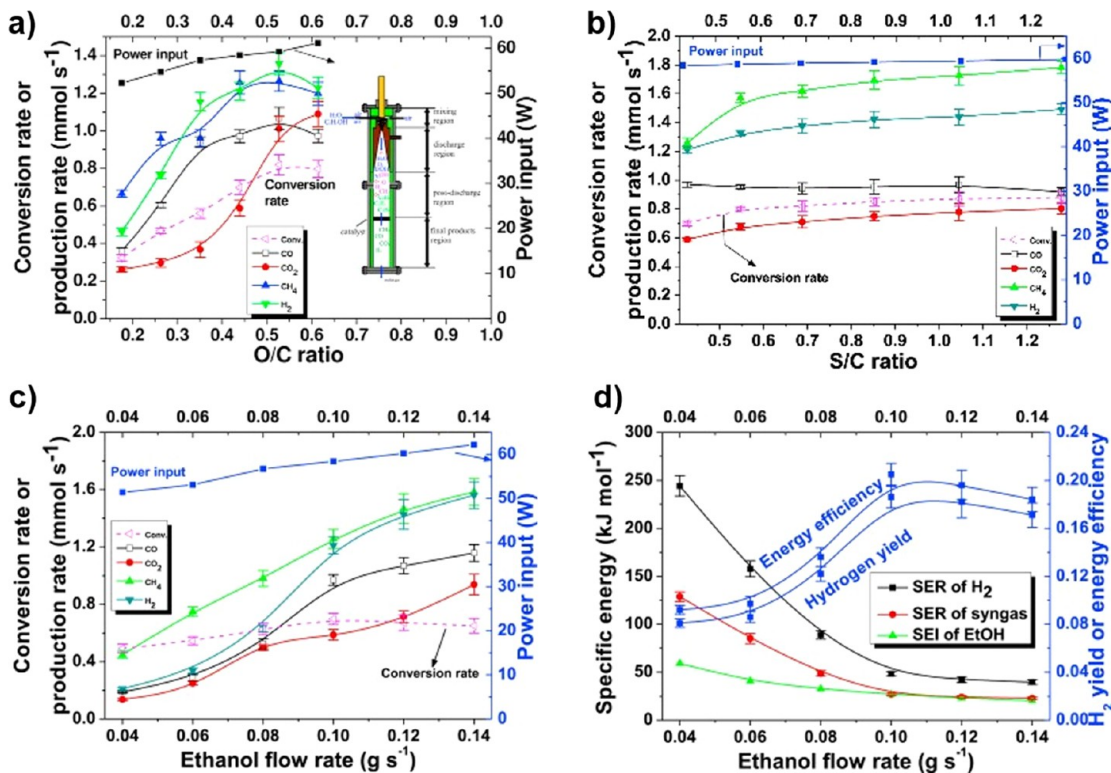


Figure 42. (a) Influence of O/C on the conversion, production rate, and plasma power (process conditions: S/C 0.43, ethanol flow rate 0.10 g/s). (b) Influence of S/C on the conversion, production rate, and plasma power (process conditions: O/C 0.44, ethanol flow rate 0.10 g/s). (c) Influence of ethanol flow rate on the conversion, production rate, and plasma power (process conditions: O/C 0.44, S/C 0.43). (d) Influence of ethanol flow rate on ethanol reforming performance (process conditions: O/C 0.44, S/C 0.43). Adapted with permission from ref 313. Copyright 2014 Elsevier.

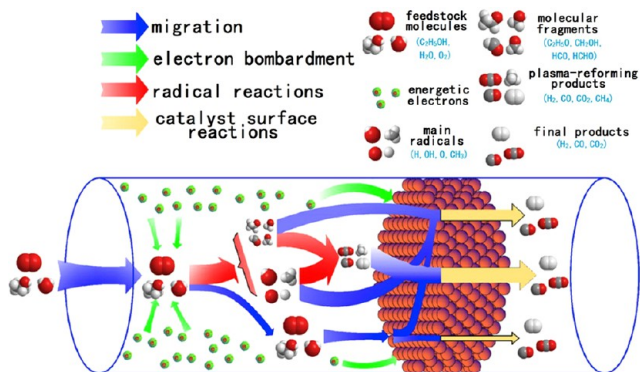


Figure 43. Plasma activation, species migration, and reaction scheme over catalyst surface. Reprinted with permission from ref 314. Copyright 2015 Elsevier.

Moreover, a high H₂ yield of 7.7 mol_{H₂}/kWh was obtained at 60 W from the plasma-catalytic reactor, which was ~2.4 times greater than that from the plasma-only reactor.³¹⁷ Similar studies were performed by the same research group with methanol/water feed using a Ni/Al₂O₃ catalyst, which showed that with increasing discharge power, methanol conversion increased up to a maximum conversion of 64% and a corresponding H₂ production rate of 1.38 mol/h.³¹⁸

Using a gliding arc plasma, Lian et al.³¹⁹ converted methanol to hydrogen for fuel cell applications. Two feed streams comprising a methanol/air/steam mixture and a methanol/steam mixture were fed into the plasma-catalytic system to prevent soot formation and catalyst sintering. Also, the process

comprised a two-stage catalyst process, where a plasma pyrolysis process is followed by a high-temperature pyrolysis reaction and steam reforming in the first catalyst stage (NiCu/γ-Al₂O₃) and a steam reforming and water-gas shift in the second catalyst reactor (FeCu/γ-Al₂O₃).³¹⁹ This combined process resulted in a H₂ selectivity of 99% at a methanol conversion of 92%. Additionally, the process exhibited an energy efficiency of 91% at a low energy cost of 0.22 kWh/Nm³. Cost analysis showed that the process can be competitive with existing technologies, such as steam methane reforming, and allows for a transient response, which provides a good scale-up operation.³¹⁹

3.5.1.3. Summary. Alcohol conversion has been explored as an alternative pathway for hydrogen production. Predominantly aliphatic alcohols such as ethanol and methanol have been investigated. In all cases, the plasma-catalytic process shows significant enhancement compared to the analogous plasma-only or thermocatalytic processes. In many instances, steam (and sometimes air) is fed along with the alcohol to facilitate the reforming reaction to produce syngas rich in hydrogen. In terms of catalyst performance, supported Ni, Co, and Cu catalysts have been predominantly explored, with Ni mostly displaying the best performance across different studies. Experimental results also showed increased alcohol conversion and hydrogen production rate with plasma power, alcohol flow rate, and the steam/alcohol and oxygen/alcohol ratio, sometimes observing an optimum at intermediate feed ratios and feed flow rate. However, this particular route for hydrogen production is still in the infancy stage, and more work is still needed on the material selection and catalyst design, as well as

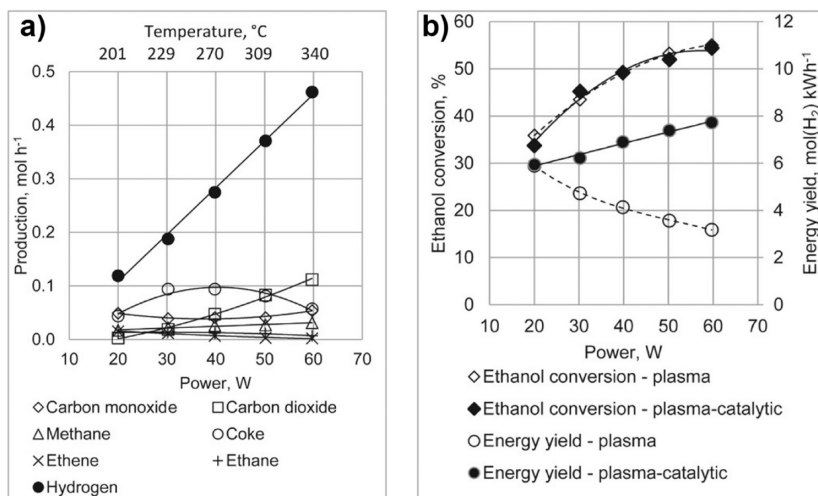
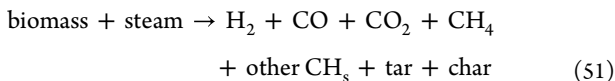
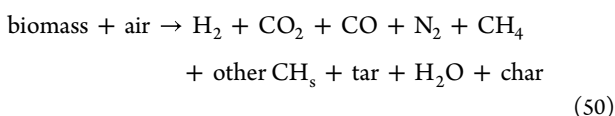


Figure 44. (a) Production of H₂, CO, CO₂, CH₄, C₂H₄, C₂H₆, and coke from the plasma-catalytic reaction at different discharge powers. (b) Ethanol conversion and energy yield of H₂ at different discharge powers in the plasma-only and plasma-catalytic reactor. Adapted with permission from ref 317. Copyright 2021 Elsevier.

fundamental studies that provide mechanistic insights on the alcohol conversion under plasma stimulation.

3.5.2. Biomass Conversion to Hydrogen. **3.5.2.1. Biomass Gasification and Pyrolysis.** Biomass is a renewable source of energy derived from various plant and animal materials, encompassing crops, wood, and forest residues, grass, industrial byproducts, consumer waste, and an array of other materials.⁶⁶ Biomass gasification is a critical element that presents a more substantial H₂ yield in contrast to biological methods.³²⁰ During gasification, biomass is introduced with a gasification medium (e.g., air, oxygen, and/or steam) to generate syngas (eqs 50 and 51), typically at temperatures ranging from 500 to 1400 °C and pressures within the range of 1–33 bar.³²⁰ Then, produced CH₄ and other hydrocarbon gases are passed to the steam reformer and WGS units to boost H₂ yield. Despite the release of significant quantities of CO₂ (~4.5 kg_{CO₂}/kg_{H₂}),¹⁴ the produced hydrogen is classified as “green” when coupled with carbon capture technologies (~14.5 kg_{CO₂}/kg_{H₂}) and provides a promising route for clean hydrogen production.¹¹



Generally, the primary parameters influencing hydrogen yield are the type of biomass, particle size, temperature, steam-to-biomass ratio, and the specific catalyst employed. This method demonstrates a good energy efficiency ranging from 55% to 65% and boasts a relatively economical hydrogen production cost of around \$2/kg H₂.^{14,66} Nonetheless, the hydrogen content fluctuates due to seasonal availability and the presence of impurities in the feedstock. The removal of byproducts, specifically tar, also presents an ongoing challenge in biomass gasification.

Biomass pyrolysis, on the other hand, refers to the thermal decomposition of biomass at elevated temperatures in the absence of air and typically results in the production of

gaseous, liquid (bio-oil and tar), and solid (char) products.^{321,322} The gaseous product consists primarily of light hydrocarbons, CO, and H₂. To this end, biomass pyrolysis and gasification have been touted as an avenue for hydrogen production.³²³ Recently, plasma technologies have been investigated for biomass gasification and conversion approaches.^{324–330} While some plasma studies have investigated the direct conversion of biomass sources such as wood and cellulose, others have looked at the conversion of tar and biogas to produce H₂ and/or syngas.

3.5.2.2. Plasma-Assisted Biomass/Polymer Gasification and Pyrolysis. Typically, these systems comprise a two-stage process that incorporates a plasma-catalyst reactor downstream of a pyrolysis chamber where initial products are reformed to yield more gaseous (H₂) products. Blanquet et al.³³¹ studied the conversion of waste biomass to hydrogen using a two-stage pyrolysis-plasma catalysis process. Figure 45 shows the process schematic where the waste wood biomass source was pyrolyzed upstream, and the product was fed into a plasma-catalyst system consisting of a Ni/Al₂O₃ catalyst.³³¹ While the pyrolysis reactor was maintained at 600 °C, the plasma reactor was maintained at 250 °C for the steam reforming reaction. A 4-fold increase in hydrogen yield (1 to 4 mmol_{H₂}/g_{biomass}) was observed in the pyrolysis-plasma/catalytic system compared to the thermal-only pyrolysis system, with a 3-fold decrease in tar production compared to the thermal-only process.³³¹ Further, the two-stage approach allowed for the catalyst to be regenerated and recycled effectively.³³¹ The same group investigated the influence of biomass components as well as promoters and support effects on the Ni-based catalyst.³³² It was observed that lignin-based biomass led to a higher H₂ production compared to cellulose (4.29 to 4.07 mmol_{H₂}/g_{cellulose}). Additionally, they showed that using different metallic promoters, the yield of hydrogen could be enhanced in the order of Ce–Ni > Co–Ni > Mg–Ni > Fe–Ni > Ni–Ni > Cu–Ni, while the support effect was in the order of Ni/Al₂O₃ > Ni/TiO₂ > Ni/Y-Zeolite.³³² Likewise, Zeng et al.³³³ studied the effect of K loading on promoted Ni catalyst (Ni–K/Al₂O₃) for biogas conversion and summarized that the 2 wt % K-promoted catalyst displayed the best activity. The same research group went further to evaluate the effect of

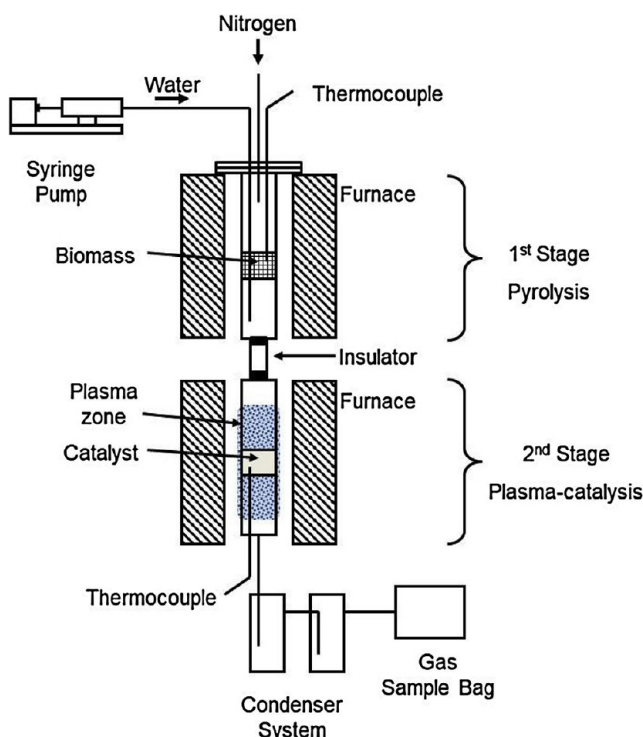


Figure 45. Process schematic for the two-stage pyrolysis-plasma/catalyst system for biomass conversion. Reprinted with permission from ref 331. Copyright 2019 Elsevier.

temperature on this Ni–K/Al₂O₃ catalyst and observed the highest conversion at 160 °C.³³⁴ Similarly, Wang et al.³³⁵ used a tandem pyrolysis-plasma/catalyst system to convert cellulose over a Ni–Co/γ-Al₂O₃ bimetallic catalyst. The authors observed an ~8-fold increase in H₂ yield (from 0.2 to 1.7 mmol_{H₂}/g) when compared to thermal-only conditions.³³⁵ Parametric studies showed that plasma power improved H₂ yields with the highest H₂ yield of 5 mmol_{H₂}/g obtained at a 15 W plasma power.³³⁵ However, the reforming temperature had an adverse effect on H₂ production, with the highest H₂ yield and selectivity (35%) obtained at the lowest temperature (250 °C). Further increase in temperature led to an increase in yields of other products such as CO, CO₂, CH₄, and C₂–C₃ gases.³³⁵

Enhanced conversion of biomass volatiles has also been reported to increase hydrogen production (47.65 mmol_{H₂}/g) from pine sawdust using a plasma-catalyst system with a bimetallic Ni–Fe/Al₂O₃ catalyst at a reforming temperature of 500 °C.³³⁶ The synergistic enhancement of the plasma/catalyst system was also shown to increase with reforming temperature up to 500 °C as depicted in Figure 46.³³⁶ The catalyst displaced good stability with plasma after 10 cyclic measurements, with the energetic electrons generated by plasma poised to alleviate tar formation and carbon deposition. Figure 47 shows the plasma/catalyst process mechanism, whereby the plasma generates reactive intermediates, which are then converted over the catalyst surface to produce H₂ with the Boudart reaction pathway responsible for coke inhibition.³³⁶ Another group of materials that is gaining some traction is the perovskite-based catalyst La₈Ce₂–M₅Ti₅O_{3–δ} (M = Fe, Co, Ni, and Cu), where the oxygen mobility and plasma-activated surface oxygen species were determined to play a vital role in

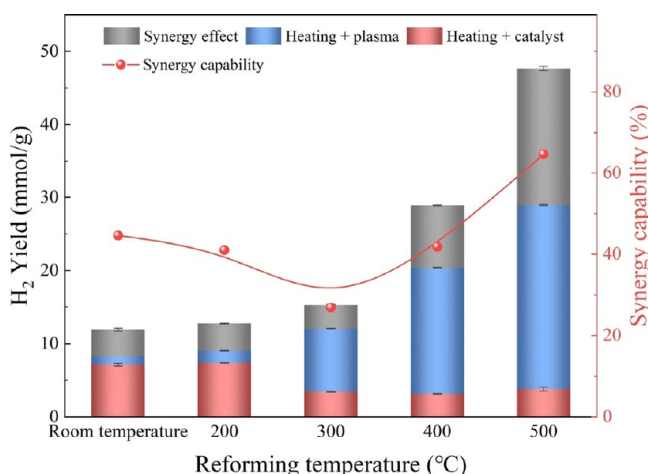


Figure 46. Synergistic effect and hydrogen production at different reforming temperatures over a Ni–Fe/Al₂O₃ catalyst. Reprinted with permission from ref 336. Copyright 2023 Elsevier.

reforming biomass tar, enhancing the conversions of compounds such as toluene to gaseous product (H₂, CO, CO₂, and CH₄).³³⁷

While the previous works highlighted made use of a DBD plasma reactor, Mei et al.³³⁸ used a gliding arc plasma (GAD) to convert mixed biomass tar (consisting of naphthalene and toluene) to H₂. They observed an improvement in product yield when plasma was coupled with a catalyst. Moreover, a bimetallic Ni/Co (7.5% Ni/7.5% Co) alloy catalyst displayed a better H₂ yield (42.3%) and energy yield of 40.3 g/kWh compared to the monometallic (Ni/Al₂O₃ and Co/Al₂O₃) materials.³³⁸ This improved performance was attributed to the improved reducibility of the Ni/Co alloy, which led to better reactant conversion and minimized the formation of by-products.³³⁸ More recently, the same research group explored the use of a honeycomb material comprising a blank substrate and a coated catalyst material (γ-Al₂O₃ and Ni/γ-Al₂O₃) for converting the mixed biomass tar (naphthalene and toluene) in a GAD plasma reactor.³³⁹ A higher energy yield of 50.9 g/kWh and better catalyst stability against coke deposition was obtained.³³⁹ Zhang et al.³⁴⁰ looked at the effect of Ni and bimetallic alloys on a rotating gliding arc (RGA) plasma, with the bimetallic NiCu and NiCo catalysts displaying better stability and biomass conversion compared to the pristine Ni catalyst. Further, Xu et al.³⁴¹ investigated the influence of catalyst poison and Ni loading in biomass tar (toluene) conversion using a rotating gliding arc plasma. They observed an increase of 91.9% to 94.7% when Ni loading was increased from 4% to 16%.³⁴¹ However, the highest H₂ yield (29.3%) was obtained at a Ni loading of 8%. Moreover, the catalyst poison was shown to influence the discharge mode in one stage (in-plasma catalysis (IPC)) and two stages (postplasma catalysis (PPC)), which affected the plasma discharge properties and nature of reactive species formed.³⁴¹ Another recent report using a gliding arc plasma investigated the influence of different oxidants (CO₂, O₂, and steam (H₂O)) in reforming toluene and observed that steam had the largest effect on product yield and energy yield.³⁴²

Similar to biomass conversion, plasma-assisted polymer deconstruction is gaining research traction as a route for hydrogen generation from waste plastics. Particularly, plasma gasification of polymers (plastics) has been touted to be more

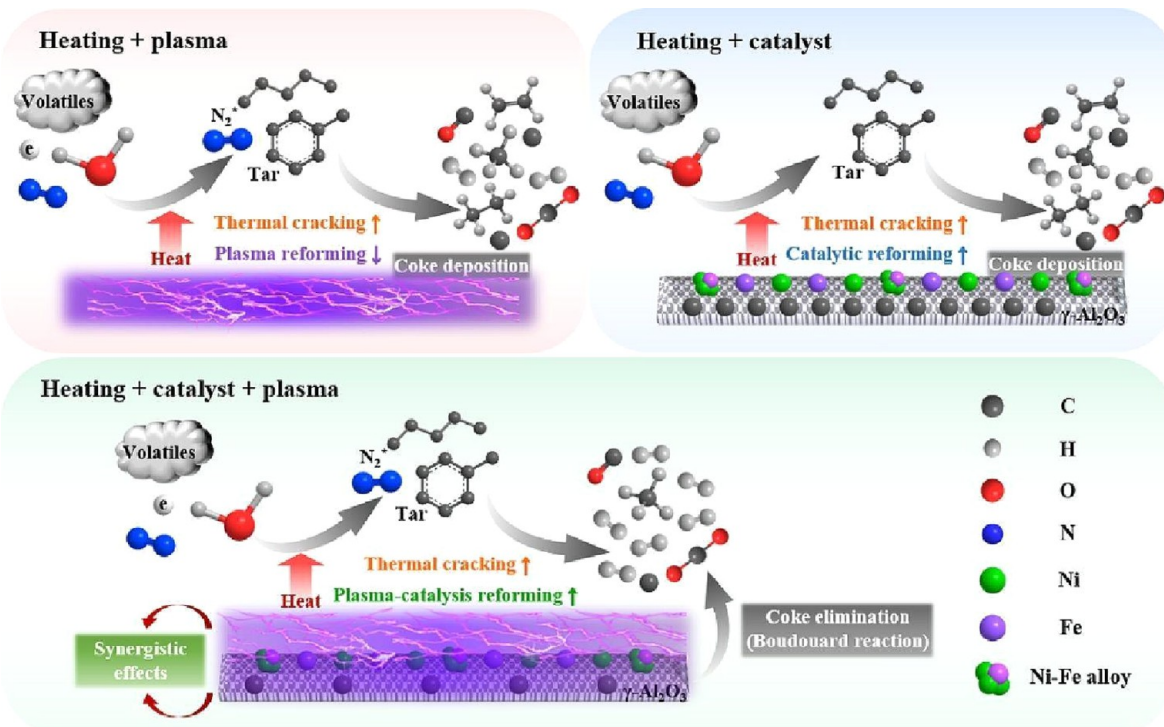


Figure 47. Postulated reaction mechanism for the plasma-catalytic system for biomass volatiles. Reprinted with permission from ref 336. Copyright 2023 Elsevier.

efficient.³⁴³ The influence of catalyst materials for such reactions was investigated by Williams and co-workers,³⁴⁴ who studied the generation of H₂ from waste propylene using different alumina-supported metal catalysts (Ni/Al₂O₃, Fe/Al₂O₃, Co/Al₂O₃, Cu/Al₂O₃). Their results show that a Ni/Al₂O₃ catalyst displayed the highest yield of 1.5 mmol_{H₂}/g_{plastic}. Moreover, the addition of steam enhanced H₂ yield further, resulting in 4.56 mmol_{H₂}/g_{plastic} at a steam weight hourly space velocity (WHSV) of 4 g/(h g_{catalyst}).³⁴⁴ Further, the same authors studied support effects using various support materials (MCM-41, Y-Zeolite, ZSM-5, Al₂O₃, TiO₂, dolomite, BaTiO₃, CaTiO₃, and Mo₂C) and observed that MCM-41 gave the highest H₂ yield of 11 mmol_{H₂}/g_{plastic}.³⁴⁵ Impregnating Ni on the MCM-41 support further improved the H₂ yield to 18 mmol_{H₂}/g_{plastic}, providing evidence of a metallic contribution to the reaction.³⁴⁵ Xiao et al.³⁴⁶ investigated the pyrolysis of polypropylene for H₂ generation using a coaxial DBD plasma reactor. Conversely to previously discussed works that used supported metal catalysts, this work focused on using a Brønsted acid catalyst (HZSM-5).³⁴⁶ The plasma-HZSM-5 system led to an improvement in gas product yield with a H₂ yield of 4.19 mmol/g. Further, an improved selectivity to BTX was observed with complete suppression of wax formation. Interestingly, the researchers demonstrated remarkable stability of the plasma-catalyst systems, with the catalyst activity remaining unaffected after 10 cyclic operations.³⁴⁶ The plasma-catalytic stability was attributed to the generation of radicals, which enhanced the cracking of the volatile components, limiting coke deposition on the catalyst surface.³⁴⁶ Similarly, HZSM-5 has also been applied in the plasma-assisted deconstruction of high-density polyethylene (HDPE) to produce H₂.³⁴⁷ The HZSM-5 catalyst was postulated to act as microreactors, enabling the conversion

of plasma-activated intermediate species to produce H₂.³⁴⁷ In another similar study on polypropylene pyrolysis over Fe/Al₂O₃, a high yield of H₂ was obtained (30 mmolH₂/g_{plastic}).³⁴⁸ The conversion of volatiles by the plasma helps improve the yield of light gases such as H₂ with the added production of carbon nanotubes (CNT).³⁴⁸

3.5.2.3. Summary. Overall, biomass pyrolysis and gasification provide an excellent opportunity for waste valorization and production of hydrogen. Notably, the plasma catalytic processes allow for improved conversion and higher H₂ production yields when compared to the thermal-only or thermocatalytic methods. Most plasma processes have relied on a 2-stage approach, with a thermal pyrolysis reactor upstream of a plasma reforming reactor. While most studies conducted primarily used a DBD plasma reactor, a few recent studies have looked at gliding arc plasma reactors for such biomass transformations. Further, on the biomass conversion front, efforts have focused on the direct conversion of biomass sources (wood, cellulose), conversion of biotar (toluene and naphthalene), and biogas (such as CO₂ and CH₄). Conversion of these different forms of biomass or biomass-derived intermediates will be pivotal in the hydrogen production economy. From a catalyst viewpoint, Ni is the most studied, with the effect of promoters, bimetallic alloys, and support also being evaluated. The plasma has also been shown to improve the stability of these catalysts by eliminating or limiting coke formation. Further efforts should also be geared toward improved material selection and application of novel materials in converting these biomass compounds and derivatives into hydrogen. Additionally, polymer conversion is another promising route for H₂ generation, as this aids in the valorization of waste plastic as a fuel source.

4. CHALLENGES AND CONCLUDING THOUGHTS

4.1. Energy Efficiency and Scale-up Challenges

Associated with Plasma-Assisted Technologies. Plasma catalysis is an alternative that holds the potential to address on-demand hydrogen production while either mitigating or significantly reducing greenhouse gas (GHG) emissions, particularly when integrated with other renewable energy sources such as photovoltaics and wind power. As a result, its applicability extends to various mobile and stationary applications, including eco-friendly electricity generation with fuel cells, as well as diverse chemical uses such as food hydrogenation, metallurgical processes, and supplying the semiconductor industry with hydrogen. Plasma catalysis presents a competitive or relatively lower capital cost than conventional reforming methods, owing to its ability to address energy-intensive storage/transportation-related issues, small-scale and distributed installations, and its further advantage of being compatible with various feedstocks for establishing efficient on-board hydrogen production systems.⁶⁵

However, certain challenges still affect the plasma-catalysis processes for hydrogen generation. One notable concern is the energy efficiency of the system (Figure 13). Broadly speaking, energy efficiency is the ratio of the energy accumulated in the product gas to the energy cost of producing the gas.³⁴ The reported energy efficiency for plasma-assisted hydrocarbon reforming is still well below the required threshold for commercial application. For instance, the highest reported energy efficiency for plasma-assisted steam reforming is 60% at a methane conversion of 74%.¹⁰⁷ The conversions of hydrocarbons, such as methane, with a DBD plasma in other reforming processes have been reported at even lower energy efficiencies. However, coupling the DBD plasma with a catalyst significantly increases the energy efficiency.³⁴⁹ Much earlier studies conducted in a ferroelectric pellet packed-bed reactor showed that the energy efficiency of hydrogen production from water was 10-fold higher compared to photocatalysis, although it fell short in comparison with the electrolysis process.³⁵⁰ The plasma source employed can also influence the energy efficiency of the system. For example, microwave plasma has been demonstrated to have the highest energy efficiency for CO₂ conversion at moderate pressures.³⁵¹ Additionally, due to the much higher reduced electric fields, DBD plasma has been reported to facilitate electronic excitation and bond dissociation, which are less energetically favorable pathways.³⁵² Appropriate catalyst identification for plasma-driven processes can improve energy efficiency by (1) improvement of the process selectivity and moles of desired product at a specific energy input or (2) packed-bed polarization, which enhances the electric fields around the catalyst.³⁵² Therefore, it remains a critical goal to design the plasma-catalytic reactor to efficiently utilize the electric power input and channel it for direct transformation of the reactants.³⁵³

Scale-up from laboratory experimentation to commercial operation is another challenge.^{353,354} Direct modification of industrial systems with plasma technology is also challenging and dependent on the plasma type, particular reaction chemistry, and operating conditions. For instance, the high-pressure demands in reforming reactions pose a challenge to the plasma operation as well as the dependence on electrical energy input.³⁵⁵ Although high-pressure and -temperature operation is achievable, it significantly impairs electrode lifetimes due to increased erosion of the electrodes and

requires a higher input power due to the increase in breakdown voltage for the gas following Paschen's law.³⁵⁵ These challenges have limited the scale-up of high-pressure and thermal plasma processes to date.^{353,354} On the other hand, the subatmospheric pressure conditions commonly used in many plasma systems, such as RF and microwave plasma, also pose a scale-up and process design challenge. A nonthermal plasma, such as a DBD plasma, offers distinct advantages in this context, primarily owing to its ability to operate at atmospheric pressure and relatively straightforward setup. Scaling up can be achieved by configuring numerous DBD systems in parallel, similar to plasma-ozone production.³⁵² However, perturbations in operating temperatures and reduced electric fields lead to instabilities in nonthermal plasma generation at higher production levels.³⁵⁴

Martini et al. analyzed the cost of a nonthermal plasma for VOC abatement technologies and estimated the cost of scale-up.³⁵⁶ The lab-scale plasma reactor cost was estimated at € 5000 (\$5346 US). While the fixed cost (for plasma reactions, connection, and maintenance) was quite high, the variable cost from the power supply was estimated at € 0.1789 (\$0.19 US) per kWh. The large-scale plasma reactor was analyzed in 3 configurations: (1) multiple reactors in parallel operating at the same efficiency, (2) multiple reactors in parallel but with different efficiencies, and (3) a group of parallel reactors in series with one another. It was concluded that multiple reactors in series was the optimum of all three configurations. While the above processes were applied to VOC abatement technologies, the mode of operation and scale-up for hydrogen production would be critical in the cost of the processes. As already mentioned, plasma-catalytic hydrogen generation would be competitive when the cost of hydrogen production gets to < \$2/kg. Additionally, as the price of renewable electricity from wind and solar systems continues to decrease, the cost of the plasma system will be considerably lowered.

4.2. Integration with Renewable Energy Systems.

One significant advantage of plasma-catalytic systems is the capability to integrate plasma generation with renewable energy systems, offering a sustainable approach to both plasma generation and utilization. In this scenario, the electricity necessary to fuel the plasma could be derived from various renewable sources such as wind and solar, as well as emerging systems like hydro, wave, and tidal power.³⁵² For example, Ueckerdt et al.³⁵⁷ conducted some comparative studies and concluded that solar PV would be easier to implement in the US, whereas the integration of wind energy was found to have similar limitations in the US compared to Germany. It is important to note that in the electrification approaches for H₂ production, the operation cost (OPEX) have been reported to be highly dependent on electricity cost.⁶⁷ However, the cost of renewable electricity from wind and solar has been projected to decrease for large-scale plasma operations.³⁵⁸ Additionally, the US Department of Energy (DOE) has targets for the cost of solar energy and to reduce the cost of electricity generation from 4.6 cents per kWh to 2 cents per kWh by 2030.³⁵⁹ With ongoing efforts to enhance the generation, distribution, and cost efficiency of these renewable energy systems, the utilization of such systems for the production of decarbonized H₂ would likely be accelerated. Additionally, the integration of plasma systems with other technologies, such as electrolysis, is of significant interest. Bespal'ko et al.³⁶⁰ recently provided an overview of plasma-driven solution electrolysis (PDSE) approaches for H₂ generation. In this process, a plasma

discharge is subjected to a gas-vapor system in proximity to an electrode immersed in an electrolyte solution.^{360,361} This PDSE process leads to significant improvement in H₂ production yields and higher Faradaic efficiencies when compared to alkaline electrolysis (AEL) or polymer electrolyte membrane electrolysis (PEMEL) and does not require the use of precious metals. Certain drawbacks that need to be addressed with the PDSE are electrode breakdown, low energy efficiency, and challenges with gas separation.

4.3. Concluding Thoughts and Opportunities. Within the plasma catalysis community, more emphasis should be placed on normalizing results in a way that allows for comparison across different plasma studies. Key metrics such as H₂ yields and energy efficiencies are usually calculated differently, which makes it difficult to establish clear advances in the field. Furthermore, parametric evaluations are sometimes convoluted with the variation of multiple parameters (such as powers and temperatures) simultaneously. This makes it difficult to isolate individual contributions of the process parameters to optimize the H₂ productivity effectively. Researchers working on plasma-assisted technologies for H₂ production should focus on performing careful experiments with appropriate plasma control experiments that allow for better comparison and reproducibility by others.

Plasma technologies undeniably open up many opportunities for decarbonized H₂ production. To date, plasma-catalytic processes involving natural-gas-sourced methane (oxidative and nonoxidative) have been studied extensively. Under oxidative environments, the major challenge is in improving reaction selectivity to H₂. To this end, variation in key process parameters such as feed composition, SEI, and discharge power have been made to improve the H₂ selectivities. Similarly, nonoxidative plasma routes also experience challenges with H₂ selectivities, along with the persistent issue of catalyst deactivation, representing a significant obstacle in the commercialization of large-scale plasma processes for hydrocarbon reforming. Nonetheless, plasma pyrolysis of hydrocarbons, biomass, and/or waste plastics has been identified as a promising route to the generation of H₂ with reduced CO₂ emissions. Moreover, hydrocarbon pyrolysis has the potential to provide high-value materials such as carbon nanotubes or carbon fibers with abundant industrial applications. Nonthermal plasmas provide an alternative in lowering the temperature requirement for this process. Furthermore, catalyst and plasma combinations in these nonthermal plasma systems lead to synergistic effects, enhancing methane conversion and H₂ yields. In contrast, due to the elevated operating temperatures in thermal plasmas, the incorporation of catalysts is not as feasible.

The NH₃ decomposition process provides a unique opportunity for producing CO_x-free H₂. As emphasized previously, the source of NH₃ is very important in closing the carbon loop and fully decarbonizing the process. This pathway represents an opportunity where plasma, combined with other processes like electrolysis, could play an essential role. However, compared to other processes, NH₃ decomposition does not suffer from a selectivity issue, as the sole products from the reaction are H₂ and N₂. Most efforts have been targeted toward material screening for improved H₂ yields and energy efficiencies. Nevertheless, there are few mechanistic studies related to plasma-catalytic NH₃ decomposition reactions. Future studies could focus on elucidating this reaction mechanism, emphasizing the influence of catalytic

properties, including N adsorption strength and activation barriers for elementary steps involving the recombinative desorption of H₂ and N₂. Such fundamental studies would provide a better understanding of the reaction and improve catalyst design and material selection. Further, most studies for NH₃ decomposition have been primarily limited to DBD plasma reactors, and other plasma types may be optimal for improving H₂ yields and energy efficiencies.

■ ASSOCIATED CONTENT

SI Supporting Information

The Supporting Information is available free of charge at <https://pubs.acs.org/doi/10.1021/acscatal.3c05434>.

Table of energy efficiency and H₂ yields for each technology and plasma type ([PDF](#))

■ AUTHOR INFORMATION

Corresponding Author

Jason C. Hicks – Department of Chemical and Biomolecular Engineering, University of Notre Dame, Notre Dame, Indiana 46556, United States;  orcid.org/0000-0002-5054-2874; Email: jhicks3@nd.edu

Authors

Ni Wang – Department of Chemical and Biomolecular Engineering, University of Notre Dame, Notre Dame, Indiana 46556, United States

Hope O. Otor – Department of Chemical and Biomolecular Engineering, University of Notre Dame, Notre Dame, Indiana 46556, United States

Gerardo Rivera-Castro – Department of Chemical and Biomolecular Engineering, University of Notre Dame, Notre Dame, Indiana 46556, United States

Complete contact information is available at: <https://pubs.acs.org/10.1021/acscatal.3c05434>

Author Contributions

[†]N.W., H.O.O., and G.R.-C. contributed equally.

Author Contributions

The manuscript was written through contributions of all authors. All authors have given approval to the final version of the manuscript.

Funding

This project was supported by the U.S. Department of Energy, Office of Science, Office of Basic Energy Sciences, under Award DE-SC0021107. This project was also funded in part by the U.S. Department of Energy (DOE), National Energy Technology Laboratory (NETL), under award number DE-FE0031862 and by the Engineering Research Centers Program of the National Science Foundation under NSF Cooperative Agreement no. EEC1647722.

Notes

The authors declare no competing financial interest.

■ REFERENCES

- (1) McManus, M. C. Environmental Consequences of the Use of Batteries in Low Carbon Systems: The Impact of Battery Production. *Appl. Energy* **2012**, *93*, 288–295.
- (2) Li, P.; Xia, X.; Guo, J. A Review of the Life Cycle Carbon Footprint of Electric Vehicle Batteries. *Sep. Purif. Technol.* **2022**, *296* (May), No. 121389.

- (3) Aunedi, M.; Olympios, A. V.; Pantaleo, A. M.; Markides, C. N.; Strbac, G. System-Driven Design and Integration of Low-Carbon Domestic Heating Technologies. *Renew. Sustain. Energy Rev.* **2023**, 187, No. 113695.
- (4) Gaur, A. S.; Fitiwi, D. Z.; Curtis, J. Heat Pumps and Our Low-Carbon Future: A Comprehensive Review. *Energy Res. Soc. Sci.* **2021**, 71, No. 101764.
- (5) Tan, X.; Nielsen, J. The Integration of Bio-Catalysis and Electrocatalysis to Produce Fuels and Chemicals from Carbon Dioxide. *Chem. Soc. Rev.* **2022**, 51 (11), 4763–4785.
- (6) Ruiz-López, E.; Gandara-Loe, J.; Baena-Moreno, F.; Reina, T. R.; Odriozola, J. A. Electrocatalytic CO₂ Conversion to C₂ Products: Catalysts Design, Market Perspectives and Techno-Economic Aspects. *Renew. Sustain. Energy Rev.* **2022**, 161, No. 112329.
- (7) Hwang, J.; Maharjan, K.; Cho, H. J. A Review of Hydrogen Utilization in Power Generation and Transportation Sectors: Achievements and Future Challenges. *Int. J. Hydrogen Energy* **2023**, 48 (74), 28629–28648.
- (8) Ravi, S. S.; Aziz, M. Clean Hydrogen for Mobility – Quo Vadis? *Int. J. Hydrogen Energy* **2022**, 47 (47), 20632–20661.
- (9) Guilbert, D.; Vitale, G. Hydrogen as a Clean and Sustainable Energy Vector for Global Transition from Fossil-Based to Zero-Carbon. *Clean Technol.* **2021**, 3 (4), 881–909.
- (10) IEA. *Global Hydrogen Review 2023*. International Energy Agency: 2023; <https://www.iea.org/reports/global-hydrogen-review-2023> (accessed 2023-09-01).
- (11) Parkinson, B.; Balcombe, P.; Speirs, J. F.; Hawkes, A. D.; Hellgardt, K. Levelized Cost of CO₂Mitigation from Hydrogen Production Routes. *Energy Environ. Sci.* **2019**, 12 (1), 19–40.
- (12) Nazir, H.; Louis, C.; Jose, S.; Prakash, J.; Muthuswamy, N.; Buan, M. E. M.; Flox, C.; Chavan, S.; Shi, X.; Kauranen, P.; Kallio, T.; Maia, G.; Tammeveski, K.; Lymperopoulos, N.; Carcdea, E.; Veziroglu, E.; Iranzo, A.; Kannan, A. M. Is the H₂ Economy Realizable in the Foreseeable Future? Part I: H₂ Production Methods. *Int. J. Hydrogen Energy* **2020**, 45 (27), 13777–13788.
- (13) Hallenbeck, P. C.; Benemann, J. R. Biological Hydrogen Production: Fundamentals and Limiting Processes. *Int. J. Hydrogen Energy* **2002**, 27 (11–12), 1185–1193.
- (14) Dincer, I.; Acar, C. Review and Evaluation of Hydrogen Production Methods for Better Sustainability. *Int. J. Hydrogen Energy* **2015**, 40 (34), 11094–11111.
- (15) Nazir, H.; Muthuswamy, N.; Louis, C.; Jose, S.; Prakash, J.; Buan, M. E. M.; Flox, C.; Chavan, S.; Shi, X.; Kauranen, P.; Kallio, T.; Maia, G.; Tammeveski, K.; Lymperopoulos, N.; Carcdea, E.; Veziroglu, E.; Iranzo, A.; M. Kannan, A. Is the H₂ Economy Realizable in the Foreseeable Future? Part III: H₂ Usage Technologies, Applications, and Challenges and Opportunities. *Int. J. Hydrogen Energy* **2020**, 45 (53), 28217–28239.
- (16) DOE. *Department of Energy Hydrogen Program Plan*. U.S. Department of Energy: 2020; <https://www.energy.gov/articles/energy-department-releases-its-hydrogen-program-plan> (accessed 2020-11-12).
- (17) Chung, W. C.; Chang, M. B. Review of Catalysis and Plasma Performance on Dry Reforming of CH₄ and Possible Synergistic Effects. *Renew. Sustain. Energy Rev.* **2016**, 62, 13–31.
- (18) Xu, Y.; Zhang, B. Recent Advances in Electrochemical Hydrogen Production from Water Assisted by Alternative Oxidation Reactions. *ChemElectroChem.* **2019**, 6 (13), 3214–3226.
- (19) Lagadec, M. F.; Grimaud, A. Water Electrolyzers with Closed and Open Electrochemical Systems. *Nat. Mater.* **2020**, 19 (11), 1140–1150.
- (20) Zhu, J.; Hu, L.; Zhao, P.; Lee, L. Y. S.; Wong, K. Y. Recent Advances in Electrocatalytic Hydrogen Evolution Using Nanoparticles. *Chem. Rev.* **2020**, 120 (2), 851–918.
- (21) Akhade, S. A.; Singh, N.; Gutierrez, O. Y.; Lopez-Ruiz, J.; Wang, H.; Holladay, J. D.; Liu, Y.; Karkamkar, A.; Weber, R. S.; Padmaperuma, A. B.; Lee, M. S.; Whyatt, G. A.; Elliott, M.; Holladay, J. E.; Male, J. L.; Lercher, J. A.; Rousseau, R.; Glezakou, V. A. Electrocatalytic Hydrogenation of Biomass-Derived Organics: A Review. *Chem. Rev.* **2020**, 120 (20), 11370–11419.
- (22) Cao, L.; Yu, I. K. M.; Xiong, X.; Tsang, D. C. W.; Zhang, S.; Clark, J. H.; Hu, C.; Ng, Y. H.; Shang, J.; Ok, Y. S. Biorenewable Hydrogen Production through Biomass Gasification: A Review and Future Prospects. *Environ. Res.* **2020**, 186 (April), No. 109547.
- (23) Snoeckx, R.; Bogaerts, A. Plasma Technology—a Novel Solution for CO₂ Conversion? *Chem. Soc. Rev.* **2017**, 46 (19), 5805–5863.
- (24) Conrads, H.; Schmidt, M. Plasma Generation and Plasma Sources. *Plasma Sources Sci. Technol.* **2000**, 9 (4), 441–454.
- (25) Neyts, E. C.; Ostrikov, K.; Sunkara, M. K.; Bogaerts, A. Plasma Catalysis: Synergistic Effects at the Nanoscale. *Chem. Rev.* **2015**, 115 (24), 13408–13446.
- (26) Fridman, A.; Kennedy, L. A. *Plasma Physics and Engineering*; CRC Press: 2021.
- (27) Tendero, C.; Tixier, C.; Tristant, P.; Desmaison, J.; Leprince, P. Atmospheric Pressure Plasmas: A Review. *Spectrochim. Acta - Part B At. Spectrosc.* **2006**, 61 (1), 2–30.
- (28) Tao, X.; Bai, M.; Wu, Q.; Huang, Z.; Yin, Y.; Dai, X. CO₂ Reforming of CH₄ by Binode Thermal Plasma. *Int. J. Hydrogen Energy* **2009**, 34 (23), 9373–9378.
- (29) Shapoval, V.; Marotta, E. Investigation on Plasma-Driven Methane Dry Reforming in a Self-Triggered Spark Reactor. *Plasma Process. Polym.* **2015**, 12 (8), 808–816.
- (30) Chung, W. C.; Chang, M. B. Dry Reforming of Methane by Combined Spark Discharge with a Ferroelectric. *Energy Convers. Manag.* **2016**, 124 (15), 305–314.
- (31) Chung, W. C.; Chang, M. B. Review of Catalysis and Plasma Performance on Dry Reforming of CH₄ and Possible Synergistic Effects. *Renew. Sustain. Energy Rev.* **2016**, 62, 13–31.
- (32) Fridman, A. *Plasma Chemistry*; Cambridge University Press: 2008.
- (33) Dębek, R.; Azzolina-Jury, F.; Travert, A.; Maugé, F. A Review on Plasma-Catalytic Methanation of Carbon Dioxide – Looking for an Efficient Catalyst. *Renew. Sustain. Energy Rev.* **2019**, 116, No. 109427.
- (34) Tatarova, E.; Bundaleska, N.; Sarrette, J. P.; Ferreira, C. M. Plasmas for Environmental Issues: From Hydrogen Production to 2D Materials Assembly. *Plasma Sources Sci. Technol.* **2014**, 23 (6), No. 063002.
- (35) Zhang, H.; Li, L.; Li, X.; Wang, W.; Yan, J.; Tu, X. Warm Plasma Activation of CO₂ in a Rotating Gliding Arc Discharge Reactor. *J. CO₂ Util.* **2018**, 27, 472–479.
- (36) Chang, J. S.; Lawless, P. A.; Yamamoto, T. Corona Discharge Processes. *IEEE Trans. Plasma Sci.* **1991**, 19 (6), 1152–1166.
- (37) Taghvaei, H.; Rahimpour, M. R. Upgrading of Anisole Using: In Situ Generated Hydrogen in Pin to Plate Pulsed Corona Discharge. *RSC Adv.* **2016**, 6 (100), 98369–98380.
- (38) Subedi, D. P.; Joshi, U. M.; Wong, C. S. Dielectric Barrier Discharge (DBD) Plasmas and Their Applications. In *Plasma Science and Technology for Emerging Economies: An AAAPT Experience*; Springer: 2017; pp 693–737. DOI: 10.1007/978-981-10-4217-1_13.
- (39) Francke, K. P.; Rudolph, R.; Miessner, H. Design and Operating Characteristics of a Simple and Reliable DBD Reactor for Use with Atmospheric Air. *Plasma Chem. Plasma Process.* **2003**, 23 (1), 47–57.
- (40) He, J.; Wen, X.; Wu, L.; Chen, H.; Hu, J.; Hou, X. Dielectric Barrier Discharge Plasma for Nanomaterials: Fabrication, Modification and Analytical Applications. *TrAC - Trends Anal. Chem.* **2022**, 156, No. 116715.
- (41) Brandenburg, R. Corrigendum: Dielectric Barrier Discharges: Progress on Plasma Sources and on the Understanding of Regimes and Single Filaments. *Plasma Sources Sci. Technol.* **2018**, 27, No. 079501.
- (42) Ollegott, K.; Wirth, P.; Oberste-Beulmann, C.; Awakowicz, P.; Muhler, M. Fundamental Properties and Applications of Dielectric Barrier Discharges in Plasma-Catalytic Processes at Atmospheric Pressure. *Chem.-Ing.-Technol.* **2020**, 92 (10), 1542–1558.

- (43) Chirokov, A.; Gutsol, A.; Fridman, A. Atmospheric Pressure Plasma of Dielectric Barrier Discharges. *Pure Appl. Chem.* **2005**, *77* (2), 487–495.
- (44) Jukes, T. N.; Choi, K. S. On the Formation of Streamwise Vortices by Plasma Vortex Generators. *J. Fluid Mech.* **2013**, *733*, 370–393.
- (45) Von Woedtke, T.; Laroussi, M.; Gherardi, M. Foundations of Plasmas for Medical Applications. *Plasma Sources Sci. Technol.* **2022**, *31* (5), No. 054002.
- (46) Lu, W.; Abbas, Y.; Mustafa, M. F.; Pan, C.; Wang, H. A Review on Application of Dielectric Barrier Discharge Plasma Technology on the Abatement of Volatile Organic Compounds. *Front. Environ. Sci. Eng.* **2019**, *13* (2), 1–19.
- (47) Peeters, F.; Butterworth, T. Electrical Diagnostics of Dielectric Barrier Discharges. *Atmospheric Pressure Plasma—from Diagnostics to Applications* **2019**, 23–49.
- (48) Kunhardt, E. E. Generation of Large-Volume, Atmospheric-Pressure, Nonequilibrium Plasmas. *IEEE Trans. Plasma Sci.* **2000**, *28* (1), 189–200.
- (49) Li, J.; Ma, C.; Zhu, S.; Yu, F.; Dai, B.; Yang, D. A Review of Recent Advances of Dielectric Barrier Discharge Plasma in Catalysis. *Nanomaterials* **2019**, *9* (10), 1428.
- (50) Bogaerts, A.; Tu, X.; Whitehead, J. C.; Centi, G.; Lefferts, L.; Guaitella, O.; Azzolina-jury, F.; Kim, H.; Murphy, A. B.; Schneider, W. F.; Nozaki, T.; Jason, C.; Rousseau, A.; Thevenet, F.; Khacef, A.; et al. The 2020 Plasma Catalysis Roadmap. *J. Phys. D. Appl. Phys.* **2020**, *53*, No. 443001.
- (51) Birau, M.; Krasil'nikov, M. A.; Kuzelev, M. V.; Rukhadze, A. A. Nonlinear Theory of a Plasma Microwave Oscillator Using Cable Waves. *J. Exp. Theor. Phys.* **1997**, *84* (4), 694–702.
- (52) Chen, G.; Georgieva, V.; Godfroid, T.; Snyders, R.; Delplancke-Ogletree, M. P. Plasma Assisted Catalytic Decomposition of CO₂. *Appl. Catal. B Environ.* **2016**, *190*, 115–124.
- (53) Kim, Y.; Lee, M.; Kim, Y. J. Selective Growth and Contact Gap-Fill of Low Resistivity Si via Microwave Plasma-Enhanced CVD. *Micromachines* **2019**, *10* (10), 689.
- (54) Ehlbeck, J.; Schnabel, U.; Polak, M.; Winter, J.; Von Woedtke, T.; Brandenburg, R.; Von Dem Hagen, T.; Weltmann, K. D. Low Temperature Atmospheric Pressure Plasma Sources for Microbial Decontamination. *J. Phys. D. Appl. Phys.* **2011**, *44* (1), No. 013002.
- (55) Uhm, H. S.; Hong, Y. C.; Shin, D. H. A Microwave Plasma Torch and Its Applications. *Plasma Sources Sci. Technol.* **2006**, *15* (2), S26.
- (56) Zamri, A. A.; Ong, M. Y.; Nomanbhay, S.; Show, P. L. Microwave Plasma Technology for Sustainable Energy Production and the Electromagnetic Interaction within the Plasma System: A Review. *Environ. Res.* **2021**, *197*, No. 111204.
- (57) Zhang, J. Q.; Zhang, J. S.; Yang, Y. J.; Liu, Q. Oxidative Coupling and Reforming of Methane with Carbon Dioxide Using a Pulsed Microwave Plasma under Atmospheric Pressure. *Energy Fuels* **2003**, *17* (1), 54–59.
- (58) Feng, J.; Sun, X.; Li, Z.; Hao, X.; Fan, M.; Ning, P.; Li, K. Plasma-Assisted Reforming of Methane. *Adv. Sci.* **2022**, *9* (34), 1–36.
- (59) Fridman, A.; Chirokov, A.; Gutsol, A. Non-Thermal Atmospheric Pressure Discharges. *J. Phys. D. Appl. Phys.* **2005**, *38* (2), R1.
- (60) Sun, S. R.; Wang, H. X.; Mei, D. H.; Tu, X.; Bogaerts, A. CO₂ Conversion in a Gliding Arc Plasma: Performance Improvement Based on Chemical Reaction Modeling. *J. CO₂ Util.* **2017**, *17*, 220–234.
- (61) Wang, W.; Mei, D.; Tu, X.; Bogaerts, A. Gliding Arc Plasma for CO₂ Conversion: Better Insights by a Combined Experimental and Modelling Approach. *Chem. Eng. J.* **2017**, *330* (April), 11–25.
- (62) de Medeiros, F. G. M.; Lopes, F. W. B.; Rego de Vasconcelos, B. Prospects and Technical Challenges in Hydrogen Production through Dry Reforming of Methane. *Catalysts* **2022**, *12* (4), 363.
- (63) Bo, Z.; Yan, J.; Li, X.; Chi, Y.; Cen, K. Plasma Assisted Dry Methane Reforming Using Gliding Arc Gas Discharge: Effect of Feed Gases Proportion. *Int. J. Hydrogen Energy* **2008**, *33* (20), 5545–5553.
- (64) IEA. *Hydrogen patents for a clean energy future*; International Energy Agency: 2023; <https://www.iea.org/reports/hydrogen-patents-for-a-clean-energy-future> (accessed 2023-01-01).
- (65) Holladay, J. D.; Hu, J.; King, D. L.; Wang, Y. An Overview of Hydrogen Production Technologies. *Catal. Today* **2009**, *139* (4), 244–260.
- (66) Nikolaidis, P.; Poullikkas, A. A Comparative Overview of Hydrogen Production Processes. *Renew. Sustain. Energy Rev.* **2017**, *67*, 597–611.
- (67) Rojas, J.; Zhai, S.; Sun, E.; Haribal, V.; Marin-Quiros, S.; Sarkar, A.; Gupta, R.; Cargnello, M.; Chueh, W.; Majumdar, A. Technoeconomics and Carbon Footprint of Hydrogen Production. *Int. J. Hydrogen Energy* **2024**, *49*, 59–74.
- (68) Hayakawa, Y.; Miura, T.; Shizuya, K.; Wakazono, S.; Tokunaga, K.; Kambara, S. Hydrogen Production System Combined with a Catalytic Reactor and a Plasma Membrane Reactor from Ammonia. *Int. J. Hydrogen Energy* **2019**, *44* (20), 9987–9993.
- (69) Spallina, V.; Shams, A.; Battistella, A.; Gallucci, F.; Annaland, M. V. S. Chemical Looping Technologies for H₂ Production with CO₂ Capture: Thermodynamic Assessment and Economic Comparison. *Energy Procedia* **2017**, *114*, 419–428.
- (70) Wang, Z.; Li, L.; Zhang, G. Life Cycle Greenhouse Gas Assessment of Hydrogen Production via Chemical Looping Combustion Thermally Coupled Steam Reforming. *J. Clean. Prod.* **2018**, *179*, 335–346.
- (71) Goujard, V.; Tatibouët, J. M.; Batiot-Dupeyrat, C. Use of a Non-Thermal Plasma for the Production of Synthesis Gas from Biogas. *Appl. Catal. A Gen.* **2009**, *353* (2), 228–235.
- (72) Spiliopoulos, N.; Mataras, D.; Rapakoulias, D. E. Power Dissipation and Impedance Measurements in Radio-frequency Discharges. *J. Vac. Sci. Technol. A* **1996**, *14* (5), 2757–2765.
- (73) Eckert, H. U. Dual Magnetic Probe System for Phase Measurements in Thermal Induction Plasmas. *J. Appl. Phys.* **1972**, *43* (6), 2707–2713.
- (74) Bradley, J. W.; Bäcker, H.; Kelly, P. J.; Arnell, R. D. Time-Resolved Langmuir Probe Measurements at the Substrate Position in a Pulsed Mid-Frequency DC Magnetron Plasma. *Surf. Coat. Technol.* **2001**, *135* (2), 221–228.
- (75) Mahoney, J.; Zhu, W.; Johnson, V. S.; Becker, K. H.; Lopez, J. L. Electrical and Optical Emission Measurements of a Capillary Dielectric Barrier Discharge. *Eur. Phys. J. D* **2010**, *60* (3), 441–447.
- (76) Snoeckx, R.; Zeng, Y. X.; Tu, X.; Bogaerts, A. Plasma-Based Dry Reforming: Improving the Conversion and Energy Efficiency in a Dielectric Barrier Discharge. *RSC Adv.* **2015**, *5* (38), 29799–29808.
- (77) Li, M.; Xu, G.; Tian, Y.; Chen, L.; Fu, H. Carbon Dioxide Reforming of Methane Using DC Corona Discharge Plasma Reaction. *J. Phys. Chem. A* **2004**, *108* (10), 1687–1693.
- (78) Ozkan, A.; Dufour, T.; Arnoult, G.; De Keyzer, P.; Bogaerts, A.; Reniers, F. CO₂-CH₄ Conversion and Syngas Formation at Atmospheric Pressure Using a Multi-Electrode Dielectric Barrier Discharge. *J. CO₂ Util.* **2015**, *9*, 74–81.
- (79) Nguyen, D. B.; Lee, W. G. Analysis of Helium Addition for Enhancement of Reactivity between CH₄ and CO₂ in Atmospheric Pressure Plasma. *J. Ind. Eng. Chem.* **2015**, *32*, 187–194.
- (80) Zhang, A. J.; Zhu, A. M.; Guo, J.; Xu, Y.; Shi, C. Conversion of Greenhouse Gases into Syngas via Combined Effects of Discharge Activation and Catalysis. *Chem. Eng. J.* **2010**, *156* (3), 601–606.
- (81) Joussot, R.; Hong, D.; Rabat, H.; Boucinha, V.; Weber-Rozenbaum, R.; Leroy-Chesneau, A. Thermal Characterization of a DBD Plasma Actuator: Dielectric Temperature Measurements Using Infrared Thermography. *40th AIAA Fluid Dyn. Conf.* **2010**, No. July, 1–8.
- (82) Doyle, S. J.; Xu, K. G. Use of Thermocouples and Argon Line Broadening for Gas Temperature Measurement in a Radio Frequency Atmospheric Microplasma Jet. *Rev. Sci. Instrum.* **2017**, *88* (2), No. 023114.
- (83) Wei, G. D.; Ren, C. S.; Qian, M. Y.; Nie, Q. Y. Optical and Electrical Diagnostics of Cold Ar Atmospheric Pressure Plasma Jet

- Generated with a Simple DBD Configuration. *IEEE Trans. Plasma Sci.* **2011**, *39* (9), 1842–1848.
- (84) Kim, J.; Abbott, M. S.; Go, D. B.; Hicks, J. C. Enhancing C-H Bond Activation of Methane via Temperature-Controlled, Catalyst-Plasma Interactions. *ACS Energy Lett.* **2016**, *1* (1), 94–99.
- (85) Liu, J. L.; Snoeckx, R.; Cha, M. S. Steam Reforming of Methane in a Temperature-Controlled Dielectric Barrier Discharge Reactor: The Role of Electron-Induced Chemistry versus Thermochemistry. *J. Phys. D. Appl. Phys.* **2018**, *51* (38), No. 385201.
- (86) Neyts, E. C.; Bogaerts, A. Understanding Plasma Catalysis through Modelling and Simulation - A Review. *J. Phys. D. Appl. Phys.* **2014**, *47* (22), No. 224010.
- (87) Loenders, B.; Michiels, R.; Bogaerts, A. Is a Catalyst Always Beneficial in Plasma Catalysis? Insights from the Many Physical and Chemical Interactions. *J. Energy Chem.* **2023**, *85*, 501–533.
- (88) Hong, J.; Chu, W.; Chernavskii, P. A.; Khodakov, A. Y. Cobalt Species and Cobalt-Support Interaction in Glow Discharge Plasma-Assisted Fischer-Tropsch Catalysts. *J. Catal.* **2010**, *273* (1), 9–17.
- (89) Martínez, R.; Romero, E.; Guimon, C.; Bilbao, R. CO₂ Reforming of Methane over Coprecipitated Ni-Al Catalysts Modified with Lanthanum. *Appl. Catal. A Gen.* **2004**, *274* (1–2), 139–149.
- (90) Ostrivov, K.; Neyts, E. C.; Meyyappan, M. Plasma Nanoscience: From Nano-Solids in Plasmas to Nano-Plasmas in Solids. *Adv. Phys.* **2013**, *62* (2), 113–224.
- (91) Guo, Y. F.; Ye, D. Q.; Chen, K. F.; He, J. C.; Chen, W. L. Toluene Decomposition Using a Wire-Plate Dielectric Barrier Discharge Reactor with Manganese Oxide Catalyst in Situ. *J. Mol. Catal. A Chem.* **2006**, *245* (1–2), 93–100.
- (92) Tu, X.; Gallon, H. J.; Twigg, M. V.; Gorry, P. A.; Whitehead, J. C. Dry Reforming of Methane over a Ni/Al₂O₃ Catalyst in a Coaxial Dielectric Barrier Discharge Reactor. *J. Phys. D. Appl. Phys.* **2011**, *44* (27), No. 274007.
- (93) Van Durme, J.; Dewulf, J.; Leys, C.; Van Langenhove, H. Combining Non-Thermal Plasma with Heterogeneous Catalysis in Waste Gas Treatment: A Review. *Appl. Catal. B Environ.* **2008**, *78* (3–4), 324–333.
- (94) Blankenship, A.; Artsiusheuski, M.; Sushkevich, V.; van Bokhoven, J. A. Recent Trends, Current Challenges and Future Prospects for Syngas-Free Methane Partial Oxidation. *Nat. Catal.* **2023**, *6* (9), 748–762.
- (95) Akande, O.; Lee, B. J. Plasma Steam Methane Reforming (PSMR) Using a Microwave Torch for Commercial-Scale Distributed Hydrogen Production. *Int. J. Hydrogen Energy* **2022**, *47* (5), 2874–2884.
- (96) Balthasar, W. Hydrogen Production and Technology: Today, Tomorrow and Beyond. *Int. J. Hydrogen Energy* **1984**, *9* (8), 649–668.
- (97) Kelly, S.; Mercer, E.; De Meyer, R.; Ciocarlan, R. G.; Bals, S.; Bogaerts, A. Microwave Plasma-Based Dry Reforming of Methane: Reaction Performance and Carbon Formation. *J. CO₂ Util.* **2023**, *75*, No. 102564.
- (98) Mixer, W. G. ART. VIII.—on Electrosynthesis:Carbonic Oxide and Oxygen. Methane and Oxygen. Ethylene and Oxygen. Acetylene and Oxygen. Ethane and Oxygen. *Molecular Changes. Am. J. Sci.* **1897**, *4* (19), 51.
- (99) MOTT-SMITH, H. M. History of “Plasmas. *Nature* **1971**, *233* (5316), 219–219.
- (100) Coward, H. F.; Meiter, E. G. CHEMICAL ACTION IN THE ELECTRIC SPARK DISCHARGE. THE IGNITION OF METHANE. *J. Am. Chem. Soc.* **1927**, *49* (2), 396–409.
- (101) Bone, W. A.; Fraser, R. P.; Witt, F. The Initial Stages of Gaseous Explosions.— Part III. The Behaviour of an Equimolecular Methane-Oxygen Mixture When Fired with Sparks of Varying Intensities. *Proc. R. Soc. London. Ser. A, Contain. Pap. a Math. Phys. Character* **1927**, *114* (768), 442–449.
- (102) Heaston, R. J. INVESTIGATION OF METHANE AND METHANE-STEAM REACTIONS IN AN ARGON ARC PLASMA; The Ohio State University: 1964.
- (103) Clump, C. W.; Kwasnoski, D.; MacRae, D. R.; Douglas Thompson, C. A Study of High-Temperature Methane Reforming. *Ind. Eng. Chem. Process Des. Dev.* **1975**, *14* (4), 433–441.
- (104) Larkin, D. W.; Caldwell, T. A.; Lobban, L. L.; Mallinson, R. G. Oxygen Pathways and Carbon Dioxide Utilization in Methane Partial Oxidation in Ambient Temperature Electric Discharges. *Energy Fuels* **1998**, *12* (4), 740–744.
- (105) Liu, C.; Marafee, A.; Mallinson, R.; Lobban, L. Methane Conversion to Higher Hydrocarbons in a Corona Discharge over Metal Oxide Catalysts with OH Groups. *Appl. Catal. A Gen.* **1997**, *164* (1–2), 21–33.
- (106) Liu, C.; Marafee, A.; Hill, B.; Xu, G.; Mallinson, R.; Lobban, L. Oxidative Coupling of Methane with Ac and Dc Corona Discharges. *Ind. Eng. Chem. Res.* **1996**, *35* (10), 3295–3301.
- (107) Geng, F.; Haribal, V. P.; Hicks, J. C. Non-Thermal Plasma-Assisted Steam Methane Reforming for Electrically-Driven Hydrogen Production. *Appl. Catal. A Gen.* **2022**, *647*, No. 118903.
- (108) Wang, Y.; Wang, N.; Harding, J.; Chen, G.; Tu, X. Chapter 14 - Plasma Technology for Syngas Production. In *Advances in Synthesis Gas: Methods, Technologies and Applications*; Elsevier: 2023; Vol. 1, pp 327–359. DOI: [10.1016/B978-0-323-91871-8.00014-3](https://doi.org/10.1016/B978-0-323-91871-8.00014-3).
- (109) Eliasson, B.; Liu, C. J.; Kogelschatz, U. Direct Conversion of Methane and Carbon Dioxide to Higher Hydrocarbons Using Catalytic Dielectric-Barrier Discharges with Zeolites. *Ind. Eng. Chem. Res.* **2000**, *39* (5), 1221–1227.
- (110) Gallon, H. J.; Tu, X.; Whitehead, J. C. Effects of Reactor Packing Materials on H₂ Production by CO₂ Reforming of CH₄ in a Dielectric Barrier Discharge. *Plasma Process. Polym.* **2012**, *9* (1), 90–97.
- (111) Zhang, K.; Kogelschatz, U.; Eliasson, B. Conversion of Greenhouse Gases to Synthesis Gas and Higher Hydrocarbons. *Energy Fuels* **2001**, *15* (2), 395–402.
- (112) Zhang, K.; Eliasson, B.; Kogelschatz, U. Direct Conversion of Greenhouse Gases to Synthesis Gas and C₄ Hydrocarbons over Zeolite HY Promoted by a Dielectric-Barrier Discharge. *Ind. Eng. Chem. Res.* **2002**, *41* (6), 1462–1468.
- (113) Jiang, T.; Li, Y.; Liu, C.; Xu, G.; Eliasson, B.; Xue, B. Plasma Methane Conversion Using Dielectric-Barrier Discharges with Zeolite A. *Catal. Today* **2002**, *72* (3–4), 229–235.
- (114) Mei, D.; Ashford, B.; He, Y. L.; Tu, X. Plasma-Catalytic Reforming of Biogas over Supported Ni Catalysts in a Dielectric Barrier Discharge Reactor: Effect of Catalyst Supports. *Plasma Process. Polym.* **2017**, *14* (6), No. 1600076.
- (115) Zeng, Y.; Zhu, X.; Mei, D.; Ashford, B.; Tu, X. Plasma-Catalytic Dry Reforming of Methane over γ-Al₂O₃ Supported Metal Catalysts. *Catal. Today* **2015**, *256* (P1), 80–87.
- (116) Mei, D.; Shen, X.; Liu, S.; Zhou, R.; Yuan, X.; Rao, Z.; Sun, Y.; Fang, Z.; Du, X.; Zhou, Y.; Tu, X. Plasma-Catalytic Reforming of Biogas into Syngas over Ni-Based Bimetallic Catalysts. *Chem. Eng. J.* **2023**, *462*, No. 142044.
- (117) Tu, X.; Whitehead, J. C. Plasma Dry Reforming of Methane in an Atmospheric Pressure AC Gliding Arc Discharge: Co-Generation of Syngas and Carbon Nanomaterials. *Int. J. Hydrogen Energy* **2014**, *39* (18), 9658–9669.
- (118) Chung, W. C.; Pan, K. L.; Lee, H. M.; Chang, M. B. Dry Reforming of Methane with Dielectric Barrier Discharge and Ferroelectric Packed-Bed Reactors. *Energy Fuels* **2014**, *28* (12), 7621–7631.
- (119) Kim, S. S.; Jorat, M.; Voecks, G.; Kuthi, A.; Surampudi, S.; Kent, R. L. Hydrogen from Steam Methane Reforming by Catalytic Nonthermal Plasma Using a Dielectric Barrier Discharge Reactor. *AIChE J.* **2020**, *66* (4), 1–10.
- (120) George, A.; Shen, B.; Craven, M.; Wang, Y.; Kang, D.; Wu, C.; Tu, X. A Review of Non-Thermal Plasma Technology: A Novel Solution for CO₂ Conversion and Utilization. *Renew. Sustain. Energy Rev.* **2021**, *135*, No. 109702.
- (121) Mei, D.; Tu, X. Conversion of CO₂ in a Cylindrical Dielectric Barrier Discharge Reactor: Effects of Plasma Processing Parameters and Reactor Design. *J. CO₂ Util.* **2017**, *19*, 68–78.

- (122) Snoeckx, R.; Zeng, Y. X.; Tu, X.; Bogaerts, A. Plasma-Based Dry Reforming: Improving the Conversion and Energy Efficiency in a Dielectric Barrier Discharge. *RSC Adv.* **2015**, *5* (38), 29799–29808.
- (123) Kim, J.; Go, D. B.; Hicks, J. C. Synergistic Effects of Plasma-Catalyst Interactions for CH₄ Activation. *Phys. Chem. Chem. Phys.* **2017**, *19* (20), 13010–13021.
- (124) Tu, X.; Whitehead, J. C. Plasma-Catalytic Dry Reforming of Methane in an Atmospheric Dielectric Barrier Discharge: Understanding the Synergistic Effect at Low Temperature. *Appl. Catal. B Environ.* **2012**, *125*, 439–448.
- (125) Nguyen, H. H.; Nasonova, A.; Nah, I. W.; Kim, K. S. Analysis on CO₂ Reforming of CH₄ by Corona Discharge Process for Various Process Variables. *J. Ind. Eng. Chem.* **2015**, *32*, 58–62.
- (126) Lu, N.; Sun, D.; Xia, Y.; Shang, K.; Wang, B.; Jiang, N.; Li, J.; Wu, Y. Dry Reforming of CH₄–CO₂ in AC Rotating Gliding Arc Discharge: Effect of Electrode Structure and Gas Parameters. *Int. J. Hydrogen Energy* **2018**, *43* (29), 13098–13109.
- (127) Xia, Y.; Lu, N.; Wang, B.; Li, J.; Shang, K.; Jiang, N.; Wu, Y. Dry Reforming of CO₂–CH₄ Assisted by High-Frequency AC Gliding Arc Discharge: Electrical Characteristics and the Effects of Different Parameters. *Int. J. Hydrogen Energy* **2017**, *42* (36), 22776–22785.
- (128) Akande, O.; Lee, B. J.; Okolie, J. A.; Museba, H. N. Hydrogen-Rich Syngas Generation through Microwave Plasma Reforming of Greenhouse Gases. *Int. J. Hydrogen Energy* **2023**, *48* (89), 34649–34658.
- (129) Rahmati, H.; Ghorbanzadeh, A. Parallel Electrodes Gliding Plasma: Working Principles and Application in Dry Reforming of Methane. *Energy* **2021**, *230*, No. 120753.
- (130) Vakili, R.; Gholami, R.; Stere, C. E.; Chansai, S.; Chen, H.; Holmes, S. M.; Jiao, Y.; Hardacre, C.; Fan, X. Plasma-Assisted Catalytic Dry Reforming of Methane (DRM) over Metal-Organic Frameworks (MOFs)-Based Catalysts. *Appl. Catal. B Environ.* **2020**, *260*, No. 118195.
- (131) Wang, Y. F.; Tsai, C. H.; Chang, W. Y.; Kuo, Y. M. Methane Steam Reforming for Producing Hydrogen in an Atmospheric-Pressure Microwave Plasma Reactor. *Int. J. Hydrogen Energy* **2010**, *35* (1), 135–140.
- (132) Czylkowski, D.; Hrycak, B.; Jasiński, M.; Dors, M.; Mizeraczyk, J. Microwave Plasma-Based Method of Hydrogen Production via Combined Steam Reforming of Methane. *Energy* **2016**, *113* (2016), 653–661.
- (133) Maqueo, P. D. G.; Coulombe, S.; Bergthorson, J. M. Energy Efficiency of a Nanosecond Repetitively Pulsed Discharge for Methane Reforming. *J. Phys. D. Appl. Phys.* **2019**, *52* (27), No. 274002.
- (134) Martin-del-Campo, J.; Coulombe, S.; Kopyscinski, J. Influence of Operating Parameters on Plasma-Assisted Dry Reforming of Methane in a Rotating Gliding Arc Reactor. *Plasma Chem. Plasma Process.* **2020**, *40* (4), 857–881.
- (135) LI, J.; XU, B.; WANG, W.; XIE, J.; YIN, X.; WU, C.; XIAO, J. Experimental Study on Dry Reforming of Methane by a Plasma Catalytic Hybrid System. *J. Fuel Chem. Technol.* **2021**, *49* (8), 1161–1172.
- (136) Wang, Q.; Zhu, T.; Li, Z.; Zhu, X.; Liu, J.; Sun, B. Plasma Activation of Methane for Hydrogen in Microwave Liquid Discharge by Auxiliary Gases: A Way to Realize Efficient Utilization of Resources. *Fuel* **2022**, *330* (July), No. 125673.
- (137) Kok, D. H. K.; Ibrahim, R. K. R.; Toemen, S.; Bakar, M. B. The Catalytic Efficiency of Ru/Mn/Ce-Al₂O₃ in the Reduction of HCN in Dry Methane Reforming with CO₂ Assisted by Non-Thermal Plasma. *J. Phys. Conf. Ser.* **2023**, *2432* (1), No. 012011.
- (138) Kraus, M.; Eliasson, B.; Kogelschatz, U.; Wokaun, A. CO₂ Reforming of Methane by the Combination of Dielectric-Barrier Discharges and Catalysis. *Phys. Chem. Chem. Phys.* **2001**, *3* (3), 294–300.
- (139) Liu, C.-J.; Xue, B.; Eliasson, B.; He, F.; Li, Y.; Xu, G.-H. Methane Conversion to Higher Hydrocarbons in the Presence of Carbon Dioxide Using Dielectric-Barrier Discharge Plasmas. *Plasma Chem. Plasma Process.* **2001**, *21* (3), 301–310.
- (140) Zeng, Y. X.; Wang, L.; Wu, C. F.; Wang, J. Q.; Shen, B. X.; Tu, X. Low Temperature Reforming of Biogas over K-, Mg- and Ce-Promoted Ni/Al₂O₃ Catalysts for the Production of Hydrogen Rich Syngas: Understanding the Plasma-Catalytic Synergy. *Appl. Catal. B Environ.* **2018**, *224*, 469–478.
- (141) Ray, D.; Reddy, P. M. K.; Subrahmanyam, C. Ni-Mn/γ-Al₂O₃ Assisted Plasma Dry Reforming of Methane. *Catal. Today* **2018**, *309*, 212–218.
- (142) Wang, Q.; Cheng, Y.; Jin, Y. Dry Reforming of Methane in an Atmospheric Pressure Plasma Fluidized Bed with Ni/γ-Al₂O₃ Catalyst. *Catal. Today* **2009**, *148* (3–4), 275–282.
- (143) Zhou, L. M.; Xue, B.; Kogelschatz, U.; Eliasson, B. Nonequilibrium Plasma Reforming of Greenhouse Gases to Synthesis Gas. *Energy Fuels* **1998**, *12* (6), 1191–1199.
- (144) Vakili, R.; Gholami, R.; Stere, C. E.; Chansai, S.; Chen, H.; Holmes, S. M.; Jiao, Y.; Hardacre, C.; Fan, X. Plasma-Assisted Catalytic Dry Reforming of Methane (DRM) over Metal-Organic Frameworks (MOFs)-Based Catalysts. *Appl. Catal. B Environ.* **2020**, *260*, No. 118195.
- (145) Li, M. W.; Tian, Y. L.; Xu, G. H. Characteristics of Carbon Dioxide Reforming of Methane via Alternating Current (AC) Corona Plasma Reactions. *Energy Fuels* **2007**, *21* (4), 2335–2339.
- (146) Zheng, X.; Tan, S.; Dong, L.; Li, S.; Chen, H. LaNiO₃@SiO₂ Core-Shell Nano-Particles for the Dry Reforming of CH₄ in the Dielectric Barrier Discharge Plasma. *Int. J. Hydrogen Energy* **2014**, *39* (22), 11360–11367.
- (147) Krawczyk, K.; Młotek, M.; Ulejczyk, B.; Schmidt-Sałowski, K. Methane Conversion with Carbon Dioxide in Plasma-Catalytic System. *Fuel* **2014**, *117*, 608–617.
- (148) Kameshima, S.; Tamura, K.; Mizukami, R.; Yamazaki, T.; Nozaki, T. Parametric Analysis of Plasma-Assisted Pulsed Dry Methane Reforming over Ni/Al₂O₃ Catalyst. *Plasma Process. Polym.* **2017**, *14* (6), 1–7.
- (149) Kameshima, S.; Mizukami, R.; Yamazaki, T.; Prananto, L. A.; Nozaki, T. Interfacial Reactions between DBD and Porous Catalyst in Dry Methane Reforming. *J. Phys. D. Appl. Phys.* **2018**, *51* (11), No. 114006.
- (150) Gallon, H. J.; Tu, X.; Whitehead, J. C. Effects of Reactor Packing Materials on H₂ Production by CO₂ Reforming of CH₄ in a Dielectric Barrier Discharge. *Plasma Process. Polym.* **2012**, *9* (1), 90–97.
- (151) Ray, D.; Manoj Kumar Reddy, P.; Subrahmanyam, C. Glass Beads Packed DBD-Plasma Assisted Dry Reforming of Methane. *Top. Catal.* **2017**, *60* (12–14), 869–878.
- (152) Wang, Q.; Yan, B. H.; Jin, Y.; Cheng, Y. Investigation of Dry Reforming of Methane in a Dielectric Barrier Discharge Reactor. *Plasma Chem. Plasma Process.* **2009**, *29* (3), 217–228.
- (153) Chen, X.; Sheng, Z.; Murata, S.; Zen, S.; Kim, H. H.; Nozaki, T. CH₄ Dry Reforming in Fluidized-Bed Plasma Reactor Enabling Enhanced Plasma-Catalyst Coupling. *J. CO₂ Util.* **2021**, *S4* (June), No. 101771.
- (154) Zhu, F.; Zhang, H.; Yan, X.; Yan, J.; Ni, M.; Li, X.; Tu, X. Plasma-Catalytic Reforming of CO₂-Rich Biogas over Ni/γ-Al₂O₃ Catalysts in a Rotating Gliding Arc Reactor. *Fuel* **2017**, *199*, 430–437.
- (155) Dinh, D. K.; Trenchev, G.; Lee, D. H.; Bogaerts, A. Arc Plasma Reactor Modification for Enhancing Performance of Dry Reforming of Methane. *J. CO₂ Util.* **2020**, *42*, No. 101352.
- (156) Kwon, H.; Kim, T.; Song, S. Dry Reforming of Methane in a Rotating Gliding Arc Plasma: Improving Efficiency and Syngas Cost by Quenching Product Gas. *J. CO₂ Util.* **2023**, *70*, No. 102448.
- (157) Cleiren, E.; Heijkers, S.; Ramakers, M.; Bogaerts, A. Dry Reforming of Methane in a Gliding Arc Plasmatron: Towards a Better Understanding of the Plasma Chemistry. *ChemSusChem* **2017**, *10* (20), 4025–4036.
- (158) Jasiński, M.; Czylkowski, D.; Hrycak, B.; Dors, M.; Mizeraczyk, J. Atmospheric Pressure Microwave Plasma Source for

- Hydrogen Production. *Int. J. Hydrogen Energy* **2013**, *38* (26), 11473–11483.
- (159) Nozaki, T.; Muto, N.; Kado, S.; Okazaki, K. Dissociation of vibrationally excited Methane on Ni Catalyst: Part 1. Application to Methane Steam Reforming. *Catal. Today* **2004**, *89* (1–2), 57–65.
- (160) Zhu, X.; Liu, X.; Lian, H. Y.; Liu, J. L.; Li, X. S. Plasma Catalytic Steam Methane Reforming for Distributed Hydrogen Production. *Catal. Today* **2019**, *337* (May), 69–75.
- (161) Hrycak, B.; Mizeraczyk, J.; Czylkowski, D.; Dors, M.; Budnarowska, M.; Jasiński, M. Hydrogen Production by the Steam Reforming of Synthetic Biogas in Atmospheric-Pressure Microwave (915 MHz) Plasma. *Sci. Rep.* **2023**, *13* (1), 1–15.
- (162) Nozaki, T.; Hattori, A.; Okazaki, K. Partial Oxidation of Methane Using a Microscale Non-Equilibrium Plasma Reactor. *Catal. Today* **2004**, *98* (4), 607–616.
- (163) Zhang, X.; Cha, M. S. Partial Oxidation of Methane in a Temperature-Controlled Dielectric Barrier Discharge Reactor. *Proc. Combust. Inst.* **2015**, *35* (3), 3447–3454.
- (164) Shareei, M.; Taghvaei, H.; Azimi, A.; Shahbazi, A.; Mirzaei, M. Catalytic DBD Plasma Reactor for Low Temperature Partial Oxidation of Methane: Maximization of Synthesis Gas and Minimization of CO₂. *Int. J. Hydrogen Energy* **2019**, *44* (60), 31873–31883.
- (165) Chawdhury, P.; Ray, D.; Subrahmanyam, C. Single Step Conversion of Methane to Methanol Assisted by Nonthermal Plasma. *Fuel Process. Technol.* **2018**, *179* (March), 32–41.
- (166) Indarto, A.; Yang, D. R.; Palgunadi, J.; Choi, J. W.; Lee, H.; Song, H. K. Partial Oxidation of Methane with Cu-Zn-Al Catalyst in a Dielectric Barrier Discharge. *Chem. Eng. Process. Process Intensif.* **2008**, *47* (5), 780–786.
- (167) Jo, S.; Lee, D. H.; Song, Y. H. Effect of Gas Temperature on Partial Oxidation of Methane in Plasma Reforming. *Int. J. Hydrogen Energy* **2013**, *38* (31), 13643–13648.
- (168) Chao, Y.; Huang, C. T.; Lee, H. M.; Chang, M. B. Hydrogen Production via Partial Oxidation of Methane with Plasma-Assisted Catalysis. *Int. J. Hydrogen Energy* **2008**, *33* (2), 664–671.
- (169) Maqueo, P. D. G.; Maier, M.; Evans, M. D. G.; Coulombe, S.; Bergthorson, J. M. Regimes of an Atmospheric Pressure Nanosecond Repetitively Pulsed Discharge for Methane Partial Oxidation. *J. Phys. D. Appl. Phys.* **2018**, *51* (13), No. 134005.
- (170) Liu, C. J.; Mallinson, R.; Lobban, L. Nonoxidative Methane Conversion to Acetylene over Zeolite in a Low Temperature Plasma. *J. Catal.* **1998**, *179* (1), 326–334.
- (171) Yang, Y. Direct Non-Oxidative Methane Conversion by Non-Thermal Plasma: Experimental Study. *Plasma Chem. Plasma Process.* **2003**, *23* (2), 283–296.
- (172) Indarto, A. Hydrogen Production from Methane in a Dielectric Barrier Discharge Using Oxide Zinc and Chromium as Catalyst. *J. Chinese Inst. Chem. Eng.* **2008**, *39* (1), 23–28.
- (173) Rueangjitt, N.; Sreethawong, T.; Chavadej, S.; Sekiguchi, H. Plasma-Catalytic Reforming of Methane in AC Microsized Gliding Arc Discharge: Effects of Input Power, Reactor Thickness, and Catalyst Existence. *Chem. Eng. J.* **2009**, *155* (3), 874–880.
- (174) Hu, S.; Wang, B.; Lv, Y.; Yan, W. Conversion of Methane to C₂ Hydrocarbons and Hydrogen Using a Gliding Arc Reactor. *Plasma Sci. Technol.* **2013**, *15* (6), 555–561.
- (175) Ghanbari, M.; Binazadeh, M.; Zafarnak, S.; Taghvaei, H.; Rahimpour, M. R. Hydrogen Production via Catalytic Pulsed Plasma Conversion of Methane: Effect of Ni-K₂O/Al₂O₃ Loading, Applied Voltage, and Argon Flow Rate. *Int. J. Hydrogen Energy* **2020**, *45* (27), 13899–13910.
- (176) Kasinathan, P.; Park, S.; Choi, W. C.; Hwang, Y. K.; Chang, J. S.; Park, Y. K. Plasma-Enhanced Methane Direct Conversion over Particle-Size Adjusted MO_x/Al₂O₃ (M = Ti and Mg) Catalysts. *Plasma Chem. Plasma Process.* **2014**, *34* (6), 1317–1330.
- (177) Li, X.-S.; Shi, C.; Wang, K.-J.; Zhang, X.-L.; Xu, Y.; Zhu, A.-M. High Yield of Aromatics from CH₄ in a Plasma-Followed-by-Catalyst(PFC) Reactor. *AIChE J.* **2006**, *52* (9), 3321–3324.
- (178) Yi, Y.; Wang, X.; Jafarzadeh, A.; Wang, L.; Liu, P.; He, B.; Yan, J.; Zhang, R.; Zhang, H.; Liu, X.; Guo, H.; Neyts, E. C.; Bogaerts, A. Plasma-Catalytic Ammonia Reforming of Methane over Cu-Based Catalysts for the Production of HCN and H₂ at Reduced Temperature. *ACS Catal.* **2021**, *11* (3), 1765–1773.
- (179) Khalifeh, O.; Taghvaei, H.; Mosallanejad, A.; Rahimpour, M. R.; Shariati, A. Extra Pure Hydrogen Production through Methane Decomposition Using Nanosecond Pulsed Plasma and Pt-Re Catalyst. *Chem. Eng. J.* **2016**, *294*, 132–145.
- (180) Cho, D. L.; Kim, H. N.; Lee, M.; Cho, E. Production of Pure Hydrogen from Methane by Low Temperature Plasma Processing. *Korean J. Chem. Eng.* **2015**, *32* (12), 2519–2523.
- (181) Khoja, A. H.; Azad, A. K.; Saleem, F.; Khan, B. A.; Naqvi, S. R.; Mehran, M. T.; Amin, N. A. S. Hydrogen Production from Methane Cracking in Dielectric Barrier Discharge Catalytic Plasma Reactor Using a Nanocatalyst. *Energies* **2020**, *13* (22), 5921.
- (182) Rahimpour, M. R.; Jahanmiri, A.; Mohamadzadeh Shirazi, M.; Hooshmand, N.; Taghvaei, H. Combination of Non-Thermal Plasma and Heterogeneous Catalysis for Methane and Hexadecane Co-Cracking: Effect of Voltage and Catalyst Configuration. *Chem. Eng. J.* **2013**, *219*, 245–253.
- (183) Wang, K.; Li, X.; Zhu, A. A Green Process for High-Concentration Ethylene and Hydrogen Production from Methane in a Plasma-Followed-by-Catalyst Reactor. *Plasma Sci. Technol.* **2011**, *13* (1), 77–81.
- (184) García-Moncada, N.; van Rooij, G.; Cents, T.; Lefferts, L. Catalyst-Assisted DBD Plasma for Coupling of Methane: Minimizing Carbon-Deposits by Structured Reactors. *Catal. Today* **2021**, *369*, 210–220.
- (185) El-Shafie, M.; Kambara, S.; Hayakawa, Y. Alumina Particle Size Effect on H₂ Production from Ammonia Decomposition by DBD Plasma. *Energy Reports* **2020**, *6*, 25–30.
- (186) Chen, G.; Qu, J.; Cheah, P.; Cao, D.; Zhao, Y.; Xiang, Y. Size-Dependent Activity of Iron Nanoparticles in Both Thermal and Plasma Driven Catalytic Ammonia Decomposition. *Ind. Eng. Chem. Res.* **2022**, *61* (31), 11436–11443.
- (187) Wang, L.; Zhao, Y.; Liu, C.; Gong, W.; Guo, H. Plasma Driven Ammonia Decomposition on a Fe-Catalyst: Eliminating Surface Nitrogen Poisoning. *Chem. Commun.* **2013**, *49* (36), 3787–3789.
- (188) Wang, L.; Yi, Y.; Guo, Y.; Zhao, Y.; Zhang, J.; Guo, H. Synergy of DBD Plasma and Fe-Based Catalyst in NH₃ Decomposition: Plasma Enhancing Adsorption Step. *Plasma Process. Polym.* **2017**, *14* (6), No. 1600111.
- (189) Wang, L.; Yi, Y. H.; Guo, H. C.; Du, X. M.; Zhu, B.; Zhu, Y. M. Highly Dispersed Co Nanoparticles Prepared by an Improved Method for Plasma-Driven NH₃ Decomposition to Produce H₂. *Catalysts* **2019**, *9* (2), 107.
- (190) Wang, L.; Yi, Y.; Zhao, Y.; Zhang, R.; Zhang, J.; Guo, H. NH₃ Decomposition for H₂ Generation: Effects of Cheap Metals and Supports on Plasma-Catalyst Synergy. *ACS Catal.* **2015**, *5* (7), 4167–4174.
- (191) Yi, Y.; Wang, L.; Guo, Y.; Sun, S.; Guo, H. Plasma-Assisted Ammonia Decomposition over Fe-Ni Alloy Catalysts for CO_x-Free Hydrogen. *AIChE J.* **2019**, *65* (2), 691–701.
- (192) Gao, Y.; Hu, E.; Yi, Y.; Yin, G.; Huang, Z. Plasma-Assisted Low Temperature Ammonia Decomposition on 3d Transition Metal (Fe, Co and Ni) Doped CeO₂ Catalysts: Synergetic Effect of Morphology and Co-Doping. *Fuel Process. Technol.* **2023**, *244*, No. 107695.
- (193) Yu, X.; Hu, K.; Zhang, H.; He, G.; Xia, Y.; Deng, M.; Shi, Y.; Yang, C.; Mao, X.; Wang, Z. Plasma-Catalytic Ammonia Decomposition for Carbon-Free Hydrogen Production Using Low Pressure-Synthesized Mo₂N Catalyst. *Plasma Chem. Plasma Process.* **2023**, *43* (1), 183–197.
- (194) Zhao, Y.; Wang, L.; Zhang, J.; Gong, W.; Guo, H. Decomposition of Ammonia by Atmospheric Pressure AC Discharge: Catalytic Effect of the Electrodes. *Catal. Today* **2013**, *211*, 72–77.
- (195) Akiyama, M.; Aihara, K.; Sawaguchi, T.; Matsukata, M.; Iwamoto, M. Ammonia Decomposition to Clean Hydrogen Using

- Non-Thermal Atmospheric-Pressure Plasma. *Int. J. Hydrogen Energy* **2018**, *43* (31), 14493–14497.
- (196) Maslova, V.; Fourré, E.; Veryasov, G.; Nesterenko, N.; Grishin, A.; Louste, C.; Nassar, M.; Guignard, N.; Arri, S.; Batiot-Dupeyrat, C. Ammonia Decomposition in Electric Field over Ce-Based Materials. *ChemCatChem*. **2023**, *15* (4), No. e202201626.
- (197) Navascués, P.; Obrero-Pérez, J. M.; Cotrino, J.; González-Elipe, A. R.; Gómez-Ramírez, A. Unraveling Discharge and Surface Mechanisms in Plasma-Assisted Ammonia Reactions. *ACS Sustain. Chem. Eng.* **2020**, *8* (39), 14855–14866.
- (198) Lin, Q. F.; Jiang, Y. M.; Liu, C. Z.; Chen, L. W.; Zhang, W. J.; Ding, J.; Li, J. G. Instantaneous Hydrogen Production from Ammonia by Non-Thermal Arc Plasma Combining with Catalyst. *Energy Reports* **2021**, *7*, 4064–4070.
- (199) Khoja, A. H.; Tahir, M.; Amin, N. A. S. Recent Developments in Non-Thermal Catalytic DBD Plasma Reactor for Dry Reforming of Methane. *Energy Convers. Manag.* **2019**, *183*, 529–560.
- (200) Li, Y.; Xu, G.; Liu, C.; Eliasson, B.; Xue, B. Co-Generation of Syngas and Higher Hydrocarbons from CO₂ and CH₄ Using Dielectric-Barrier Discharge: Effect of Electrode Materials. *Energy Fuels* **2001**, *15* (2), 299–302.
- (201) Wang, W.; Kim, H. H.; Van Laer, K.; Bogaerts, A. Streamer Propagation in a Packed Bed Plasma Reactor for Plasma Catalysis Applications. *Chem. Eng. J.* **2018**, *334*, 2467–2479.
- (202) Sheng, Z.; Kameshima, S.; Sakata, K.; Nozaki, T. Plasma-Enabled Dry Methane Reforming, Chapter 3. *Plasma Chemistry and Gas Conversion* **2018**, 1.
- (203) Kim, H.-H.; Teramoto, Y.; Ogata, A. National. Time-Resolved Imaging of Positive Pulsed Corona-Induced Surface Streamers on TiO₂ and γ-Al₂O₃-Supported Ag Catalysts. *J. Phys. D. Appl. Phys.* **2016**, *49* (45), No. 415204.
- (204) Bogaerts, A.; Tu, X.; Rooij, G. Van. Plasma-Based CO₂ Conversion. In *Carbon Dioxide Utilisation; Transformations*; De Gruyter: 2019; pp 585–634. DOI: [10.1515/9783110665147-028](https://doi.org/10.1515/9783110665147-028).
- (205) Khoja, A. H.; Tahir, M.; Amin, N. A. S. Dry Reforming of Methane Using Different Dielectric Materials and DBD Plasma Reactor Configurations. *Energy Convers. Manag.* **2017**, *144*, 262–274.
- (206) Uytdenhouwen, Y.; Hereijgers, J.; Breugelmans, T.; Cool, P.; Bogaerts, A. How Gas Flow Design Can Influence the Performance of a DBD Plasma Reactor for Dry Reforming of Methane. *Chem. Eng. J.* **2021**, *405*, No. 126618.
- (207) Nozaki, T.; Chen, X.; Kim, D. Y.; Zhan, C. Combination of DBD and Catalysts for CH₄ and CO₂ Conversion: Basics and Applications. *Plasma Chem. Plasma Process.* **2023**, *43*, 1385.
- (208) Chen, X.; Kim, H. H.; Nozaki, T. Plasma Catalytic Technology for CH₄ and CO₂ Conversion: A Review Highlighting Fluidized-Bed Plasma Reactor. *Plasma Process. Polym.* **2024**, *21*, No. e2200207.
- (209) Jasiński, M.; Czyłkowski, D.; Hrycak, B.; Dors, M.; Mizeraczyk, J. Atmospheric Pressure Microwave Plasma Source for Hydrogen Production. *Int. J. Hydrogen Energy* **2013**, *38* (26), 11473–11483.
- (210) Rahim, I.; Nomura, S.; Mukasa, S.; Toyota, H. Decomposition of Methane Hydrate for Hydrogen Production Using Microwave and Radio Frequency In-Liquid Plasma Methods. *Appl. Therm. Eng.* **2015**, *90*, 120–126.
- (211) Pan, J.; Liu, Y.; Zhang, S.; Hu, X.; Liu, Y.; Shao, T. Deep Learning-Assisted Pulsed Discharge Plasma Catalysis Modeling. *Energy Convers. Manag.* **2023**, *277*, No. 116620.
- (212) Chen, X.; Zhang, S.; Li, S.; Zhang, C.; Pan, J.; Murphy, A. B.; Shao, T. Temperature-Independent, Nonoxidative Methane Conversion in Nanosecond Repetitively Pulsed DBD Plasma. *Sustain. Energy Fuels* **2021**, *5* (3), 787–800.
- (213) Maitre, P. A.; Bieniek, M. S.; Kechagiopoulos, P. N. Plasma-Enhanced Catalysis for the Upgrading of Methane: A Review of Modelling and Simulation Methods. *React. Chem. Eng.* **2020**, *5* (5), 814–837.
- (214) Xia, Y.; Lu, N.; Li, J.; Jiang, N.; Shang, K.; Wu, Y. Combined Steam and CO₂ Reforming of CH₄ for Syngas Production in a Gliding Arc Discharge Plasma. *J. CO₂ Util.* **2020**, *37*, 248–259.
- (215) Starik, A. M.; Kuleshov, P. S.; Loukhovitski, B. I.; Titova, N. S. Theoretical Study of Partial Oxidation of Methane by Non-Equilibrium Oxygen Plasma to Produce Hydrogen Rich Syngas. *Int. J. Hydrogen Energy* **2015**, *40* (32), 9872–9884.
- (216) Zhou, J.; Zhou, J.; Xu, Y.; Yan, B.; Yu, X. Control of Methane Plasma Oxidative Pathways by Altering the Contribution of Oxygen Species. *Fuel* **2021**, *284*, No. 118944.
- (217) Hrabovsky, M.; Hlina, M.; Kopecky, V.; Maslani, A.; Krenek, P.; Serov, A.; Hurba, O. Steam Plasma Methane Reforming for Hydrogen Production. *Plasma Chem. Plasma Process.* **2018**, *38* (4), 743–758.
- (218) Wang, B.; Cheng, Y.; Wang, C.; Zou, J. Steam Reforming of Methane in a Gliding Arc Discharge Reactor to Produce Hydrogen and Its Chemical Kinetics Study. *Chem. Eng. Sci.* **2022**, *253* (S0), No. 117560.
- (219) Loenders, B.; Engelmann, Y.; Bogaerts, A. Plasma-Catalytic Partial Oxidation of Methane on Pt(111): A Microkinetic Study on the Role of Different Plasma Species. *J. Phys. Chem. C* **2021**, *125* (5), 2966–2983.
- (220) Sun, J.; Chen, Q.; Yang, X.; Koel, B. E. Effects of Non-Equilibrium Excitation on Methane Oxidation in a Low-Temperature RF Discharge. *J. Phys. D. Appl. Phys.* **2020**, *53* (6), No. 064001.
- (221) Snoeckx, R.; Aerts, R.; Tu, X.; Bogaerts, A. Plasma-Based Dry Reforming: A Computational Study Ranging from the Nanoseconds to Seconds Time Scale. *J. Phys. Chem. C* **2013**, *117* (10), 4957–4970.
- (222) Pan, J.; Chen, T.; Gao, Y.; Liu, Y.; Zhang, S.; Liu, Y.; Shao, T. Numerical Modeling and Mechanism Investigation of Nanosecond-Pulsed DBD Plasma-Catalytic CH₄ Dry Reforming. *J. Phys. D. Appl. Phys.* **2022**, *55* (3), No. 035202.
- (223) Bogaerts, A.; Kozak, T.; van Laer, K.; Snoeckx, R. Plasma-Based Conversion of CO₂: Current Status and Future Challenges. *Faraday Discuss.* **2015**, *183*, 217–232.
- (224) Kozák, T.; Bogaerts, A. Splitting of CO₂ by Vibrational Excitation in Non-Equilibrium Plasmas: A Reaction Kinetics Model. *Plasma Sources Sci. Technol.* **2014**, *23* (4), No. 045004.
- (225) Zhu, M.; Zhong, A.; Dai, D.; Wang, Q.; Shao, T.; Ostrikov, K. Surface-Induced Gas-Phase Redistribution Effects in Plasma-Catalytic Dry Reforming of Methane: Numerical Investigation by Fluid Modeling. *J. Phys. D. Appl. Phys.* **2022**, *55* (35), No. 355201.
- (226) Sheng, Z.; Kamemshima, S.; Yao, S.; Nozaki, T. Oxidation Behavior of Ni/Al₂O₃ Catalyst in Nonthermal Plasma-Enabled Catalysis. *J. Phys. D. Appl. Phys.* **2018**, *51* (44), No. 445205.
- (227) Zhang, S.; Li, Y.; Knoll, A.; Oehrlein, G. S. Mechanistic Aspects of Plasma-Enhanced Catalytic Methane Decomposition by Time-Resolved Operando Diffuse Reflectance Infrared Fourier Transform Spectroscopy. *J. Phys. D. Appl. Phys.* **2020**, *53* (21), No. 215201.
- (228) Li, Y.; Hinshelwood, M.; Oehrlein, G. S. Investigation of Ni Catalyst Activation during Plasma-Assisted Methane Oxidation. *J. Phys. D. Appl. Phys.* **2022**, *55* (15), No. 155202.
- (229) Sheng, Z.; Kim, H. H.; Yao, S.; Nozaki, T. Plasma-Chemical Promotion of Catalysis for CH₄ Dry Reforming: Unveiling Plasma-Enabled Reaction Mechanisms. *Phys. Chem. Chem. Phys.* **2020**, *22* (34), 19349–19358.
- (230) Zhang, S.; Oehrlein, G. S. From Thermal Catalysis to Plasma Catalysis: A Review of Surface Processes and Their Characterizations. *J. Phys. D. Appl. Phys.* **2021**, *54* (21), No. 213001.
- (231) Xu, Y.; Bao, X.; Lin, L. Direct Conversion of Methane under Nonoxidative Conditions. *J. Catal.* **2003**, *216* (1–2), 386–395.
- (232) Anderson, A. B.; Maloney, J. J. Activation of Methane on Iron, Nickel, and Platinum Surfaces: A Molecular Orbital Study. *J. Phys. Chem.* **1988**, *92* (3), 809–812.
- (233) Anderson, R. P.; Fincke, J. R.; Taylor, C. E. Conversion of Natural Gas to Liquids via Acetylene as an Intermediate. *Fuel* **2002**, *81* (7), 909–925.

- (234) Ertl, G.; Knözinger, H.; Schüth, F.; Weitkamp, J. *Handbook of Heterogeneous Catalysis*; Wiley-VCH: 2008.
- (235) Buff, H.; Hofmann, A. W. XXV.-Decomposition of Gaseous Compounds by Electrical Incandescence. *J. Chem. Soc. London* **1860**, *12* (2), 273–289.
- (236) Gladisch, H. How Huels Makes Acetylene by DC Arc. *Hydrocarb. Process. Pet. Refin.* **1962**, *41* (6), 159–164.
- (237) Wan, J. K. S. Microwave Induced Catalytic Conversion of Methane to Ethylene and Hydrogen. US Patent No. 4,574,038, 1986.
- (238) Huang, J. H.; Suib, S. L. Methane Dimerization via Microwave Plasmas. *Res. Chem. Intermed.* **1994**, *20* (1), 133–139.
- (239) Pollington, S. D.; Ioffe, M. S.; Westergaard, M.; Wan, J. K. S. A High-Power X-Band Pulsed Microwave Induced Catalytic Decomposition of Methane with Integral Acoustic Measurements. *Res. Chem. Intermed.* **1995**, *21* (1), 59–68.
- (240) Wan, J.; Tse, M.; Husby, H.; Depew, M. High-Power Pulsed Microwave Catalytic Processes: Decomposition of Methane. *J. Microw. Power Electromagn. Energy* **1990**, *25* (1), 32–38.
- (241) Marún, C.; et al. Catalytic Oligomerization of Methane via Microwave Heating. *J. Phys. Chem. A* **1999**, *103* (22), 4332–4340.
- (242) Yang, Y. Direct Non-Oxidative Methane Conversion by Non-Thermal Plasma: Modeling Study. *Plasma Chem. Plasma Process.* **2003**, *23* (2), 327–346.
- (243) Wang, L.; Tao, L.; Xie, M.; Xu, G.; Huang, J.; Xu, Y. Dehydrogenation and Aromatization of Methane under Non-Oxidizing Conditions. *Catal. Lett.* **1993**, *21* (1–2), 35–41.
- (244) Heintze, M.; Magureanu, M. Methane Conversion into Aromatics in a Direct Plasma-Catalytic Process. *J. Catal.* **2002**, *206* (1), 91–97.
- (245) Park, S.; Lee, M.; Bae, J.; Hong, D. Y.; Park, Y. K.; Hwang, Y. K.; Jeong, M. G.; Kim, Y. D. Plasma-Assisted Non-Oxidative Conversion of Methane over Mo/HZSM-5 Catalyst in DBD Reactor. *Top. Catal.* **2017**, *60* (9–11), 735–742.
- (246) Van, J.; Chen, G.; Xiang, Y. Dual-Bed Plasma/Catalytic Synergy for Methane Transformation into Aromatics. *Ind. Eng. Chem. Res.* **2023**, *62* (6), 2516–2524.
- (247) Vuitton, V.; Yelle, R. V.; McEwan, M. J. Ion Chemistry and N-Containing Molecules in Titan's Upper Atmosphere. *Icarus* **2007**, *191* (2), 722–742.
- (248) Bai, M.; Zhang, Z.; Bai, M.; Bai, X.; Gao, H. Synthesis of Ammonia Using CH₄/N₂ Plasmas Based on Micro-Gap Discharge under Environmentally Friendly Condition. *Plasma Chem. Plasma Process.* **2008**, *28* (4), 405–414.
- (249) Mingdong, B.; Xiying, B.; Zhitao, Z.; Mindi, B. Synthesis of Ammonia in a Strong Electric Field Discharge at Ambient Pressure. *Plasma Chem. Plasma Process.* **2000**, *20* (4), 511–520.
- (250) Poirier, D.; Hale, D.; Barboun, P.; Hicks, J. Toward Sustainable Production of N-Containing Products Via Non Thermal Plasma-Enhanced Conversion of Natural Gas Resources. *J. Environ. Chem. Eng.* **2024**, *12* (2), No. 111970.
- (251) Clarke, R. J.; Hicks, J. C. Self-Organization and Nitrogen Incorporation in Diamond-Like Carbon Microstructures Synthesized by Nonthermal Plasma. *J. Phys. Chem. C* **2023**, *127* (31), 15239–15245.
- (252) Chen, G.; Tu, X.; Homm, G.; Weidenkaff, A. Plasma Pyrolysis for a Sustainable Hydrogen Economy. *Nat. Rev. Mater.* **2022**, *7* (5), 333–334.
- (253) Raja, R. B.; Sarathi, R.; Vinu, R. Selective Production of Hydrogen and Solid Carbon via Methane Pyrolysis Using a Swirl-Induced Point–Plane Non-Thermal Plasma Reactor. *Energy Fuels* **2022**, *36* (2), 826–836.
- (254) Akintola, I.; Rivera-Castro, G.; Yang, J.; Sechrist, J.; Hicks, J. C.; Veloso, F.; Go, D. B. Temperature Inhibition of Plasma-Driven Methane Conversion in DBD Systems. *Plasma Chem. Plasma Process.* **2023**, *43*, 1999–2016.
- (255) Rivera-castro, G. J.; Scotto, A.; Cho, Y.; Hicks, J. C. Plasma-Catalyst Synergy in the One-Pot Nonthermal Plasma-Assisted Synthesis of Aromatics from Methane. *Ind. Eng. Chem. Res.* **2023**, *62* (44), 18394–18402.
- (256) Bazelyan, E. M.; Raizer, Y. P. *Spark Discharge*; CRC Press: 1997.
- (257) Kogelschatz, U. Dielectric-Barrier Discharges: Their History, Discharge Physics, and Industrial Applications. *Plasma Chem. Plasma Process.* **2003**, *23* (1), 1–46.
- (258) Scapinello, M.; Delikontantis, E.; Stefanidis, G. D. The Panorama of Plasma-Assisted Non-Oxidative Methane Reforming. *Chem. Eng. Process. Process Intensif.* **2017**, *117* (April), 120–140.
- (259) Nagazoe, H.; Kobayashi, M.; Yamaguchi, T.; Kimuro, H.; Onoe, K. Characteristics of Methane Conversion under Combined Reactions of Solid Catalyst with Microwave Plasma. *J. Chem. Eng. Jpn.* **2006**, *39* (3), 314–320.
- (260) Julian, I.; Ramirez, H.; Hueso, J. L.; Mallada, R.; Santamaría, J. Non-Oxidative Methane Conversion in Microwave-Assisted Structured Reactors. *Chem. Eng. J.* **2019**, *377*, No. 119764.
- (261) Fridman, A.; Nester, S.; Kennedy, L. A.; Saveliev, A.; Mutaf-Yardimci, O. Gliding Arc Discharge. *Prog. Energy Combust. Sci.* **1999**, *25* (2), 211–231.
- (262) Lee, H.; Sekiguchi, H. Plasma-Catalytic Hybrid System Using Spouted Bed with a Gliding Arc Discharge: CH₄ Reforming as a Model Reaction. *J. Phys. D. Appl. Phys.* **2011**, *44* (27), No. 274008.
- (263) De Bie, C.; Verheyde, B.; Martens, T.; Van Dijk, J.; Paulussen, S.; Bogaerts, A. Fluid Modeling of the Conversion of Methane into Higher Hydrocarbons in an Atmospheric Pressure Dielectric Barrier Discharge. *Plasma Process. Polym.* **2011**, *8* (11), 1033–1058.
- (264) Somers, W.; Bogaerts, A.; Van Duin, A. C. T.; Neyts, E. C. Plasma Species Interacting with Nickel Surfaces: Toward an Atomic Scale Understanding of Plasma-Catalysis. *J. Phys. Chem. C* **2012**, *116* (39), 20958–20965.
- (265) Somers, W.; Bogaerts, A.; Van Duin, A. C. T.; Huygh, S.; Bal, K. M.; Neyts, E. C. Temperature Influence on the Reactivity of Plasma Species on a Nickel Catalyst Surface: An Atomic Scale Study. *Catal. Today* **2013**, *211*, 131–136.
- (266) Spiess, F. J.; Suib, S. L.; Irie, K.; Hayashi, Y.; Matsumoto, H. Metal Effect and Flow Rate Effect in the Hydrogen Production from Methane. *Catal. Today* **2004**, *89* (1–2), 35–45.
- (267) Engelmann, Y.; Mehta, P.; Neyts, E. C.; Schneider, W. F.; Bogaerts, A. Predicted Influence of Plasma Activation on Non-oxidative Coupling of Methane on Transition Metal Catalysts. *ACS Sustain. Chem. Eng.* **2020**, *8* (15), 6043–6054.
- (268) Klerke, A.; Christensen, C. H.; Nørskov, J. K.; Vegge, T. Ammonia for Hydrogen Storage: Challenges and Opportunities. *J. Mater. Chem.* **2008**, *18* (20), 2304–2310.
- (269) Mlotek, M.; Perron, M.; Krawczyk, K. Ammonia Decomposition in a Gliding Discharge Plasma. *Energy Technol.* **2021**, *9* (12), 1–6.
- (270) Sun, S.; Jiang, Q.; Zhao, D.; Cao, T.; Sha, H.; Zhang, C.; Song, H.; Da, Z. Ammonia as Hydrogen Carrier: Advances in Ammonia Decomposition Catalysts for Promising Hydrogen Production. *Renew. Sustain. Energy Rev.* **2022**, *169*, No. 112918.
- (271) Barboun, P. M.; Hicks, J. C. Unconventional Catalytic Approaches to Ammonia Synthesis. *Annu. Rev. Chem. Biomol. Eng.* **2020**, *11*, 503–521.
- (272) Sousa, J.; Waiblinger, W.; Friedrich, K. A. Techno-Economic Study of an Electrolysis-Based Green Ammonia Production Plant. *Ind. Eng. Chem. Res.* **2022**, *61* (39), 14515–14530.
- (273) Lee, B.; Winter, L. R.; Lee, H.; Lim, D.; Lim, H.; Elimelech, M. Pathways to a Green Ammonia Future. *ACS Energy Lett.* **2022**, *7*, 3032–3038.
- (274) Chehade, G.; Dincer, I. Progress in Green Ammonia Production as Potential Carbon-Free Fuel. *Fuel* **2021**, *299*, No. 120845.
- (275) Barboun, P.; Mehta, P.; Herrera, F. A.; Go, D. B.; Schneider, W. F.; Hicks, J. C. Distinguishing Plasma Contributions to Catalyst Performance in Plasma-Assisted Ammonia Synthesis. *ACS Sustain. Chem. Eng.* **2019**, *7* (9), 8621–8630.
- (276) Barboun, P. M.; Otor, H. O.; Ma, H.; Goswami, A.; Schneider, W. F.; Hicks, J. C. Plasma-Catalyst Reactivity Control of Surface Nitrogen Species through Plasma-Temperature-Programmed Hydro-

- genation to Ammonia. *ACS Sustain. Chem. Eng.* **2022**, *10* (48), 15741–15748.
- (277) Rouwenhorst, K. H. R.; Engelmann, Y.; Van 'T Veer, K.; Postma, R. S.; Bogaerts, A.; Lefferts, L. Plasma-Driven Catalysis: Green Ammonia Synthesis with Intermittent Electricity. *Green Chem.* **2020**, *22* (19), 6258–6287.
- (278) Hollevoet, L.; Jardali, F.; Gorbanev, Y.; Creel, J.; Bogaerts, A.; Martens, J. A. Towards Green Ammonia Synthesis through Plasma-Driven Nitrogen Oxidation and Catalytic Reduction. *Angew. Chem.* **2020**, *132* (52), 24033–24037.
- (279) Arnaiz del Pozo, C.; Cloete, S. Techno-Economic Assessment of Blue and Green Ammonia as Energy Carriers in a Low-Carbon Future. *Energy Convers. Manag.* **2022**, *255*, No. 115312.
- (280) Andersen, J. A.; Christensen, J. M.; Østberg, M.; Bogaerts, A.; Jensen, A. D. Plasma-Catalytic Ammonia Decomposition Using a Packed-Bed Dielectric Barrier Discharge Reactor. *Int. J. Hydrogen Energy* **2022**, *47* (75), 32081–32091.
- (281) Nehra, V.; Kumar, A.; Dwivedi, H. K. Atmospheric Non-Thermal Plasma Sources. *Int. J. Eng.* **2008**, *2* (1), 53–68.
- (282) Conrads, H.; Schmidt, M. Plasma Generation and Plasma Sources. *Plasma Sources Sci. Technol.* **2000**, *9* (4), 441–454.
- (283) Devins, J. C.; Burton, M. Formation of Hydrazine in Electric Discharge Decomposition of Ammonia. *J. Am. Chem. Soc.* **1954**, *76* (10), 2618–2626.
- (284) Freeman, M. P.; Skrivan, J. F. Rate Studies of the Decomposition of Ammonia and Methane in a Plasma Jet. *AIChE J.* **1962**, *8* (4), 450–454.
- (285) d'Agostino, R.; Cramarossa, F.; De Benedictis, S.; Ferraro, G. Kinetic and Spectroscopic Analysis of NH₃ Decomposition under R.F. Plasma at Moderate Pressures. *Plasma Chem. Plasma Process.* **1981**, *1* (1), 19–35.
- (286) Soucy, G.; Jurewicz, J. W.; Boulos, M. I. Parametric Study of the Decomposition of NH₃ for an Induction Plasma Reactor Design. *Plasma Chem. Plasma Process.* **1995**, *15* (4), 693–710.
- (287) Arkhipenko, V. I.; Kirillov, a a; Simonchik, L. V.; Zgirouski, S. M.; Safronau, Y. a. Hydrogen Generation in Self-Sustained Normal DC Atmospheric Pressure Glow Discharge in Helium-Ammonia Mixture. *Int. Symp. plasma Chem. Bochum, Ger.* **2009**, 27–31.
- (288) Mehta, P.; Barboun, P.; Herrera, F. A.; Kim, J.; Rumbach, P.; Go, D. B.; Hicks, J. C.; Schneider, W. F. Overcoming Ammonia Synthesis Scaling Relations with Plasma-Enabled Catalysis. *Nat. Catal.* **2018**, *1* (4), 269–275.
- (289) Van Laer, K.; Bogaerts, A. Influence of Gap Size and Dielectric Constant of the Packing Material on the Plasma Behaviour in a Packed Bed DBD Reactor: A Fluid Modelling Study. *Plasma Process. Polym.* **2017**, *14* (4–5), No. 1600129.
- (290) Van Laer, K.; Bogaerts, A. How Bead Size and Dielectric Constant Affect the Plasma Behaviour in a Packed Bed Plasma Reactor: A Modelling Study. *Plasma Sources Sci. Technol.* **2017**, *26* (8), No. 085007.
- (291) Zhao, Y.; Wang, L.; Zhang, J.; Guo, H. Enhancing the Ammonia to Hydrogen (ATH) Energy Efficiency of Alternating Current Arc Discharge. *Int. J. Hydrogen Energy* **2014**, *39* (15), 7655–7663.
- (292) Kim, J.; Go, D. B.; Hicks, J. C. Synergistic Effects of Plasma-Catalyst Interactions for CH₄ Activation. *Phys. Chem. Chem. Phys.* **2017**, *19* (20), 13010–13021.
- (293) Moszczyńska, J.; Liu, X.; Wiśniewski, M. Non-Thermal Ammonia Decomposition for Hydrogen Production over Carbon Films under Low-Temperature Plasma—In-Situ FTIR Studies. *Int. J. Mol. Sci.* **2022**, *23* (17), 9638.
- (294) Gorky, F.; Lucero, J. M.; Crawford, J. M.; Blake, B. A.; Guthrie, S. R.; Carreon, M. A.; Carreon, M. L. Insights on Cold Plasma Ammonia Synthesis and Decomposition Using Alkaline Earth Metal-Based Perovskites. *Catal. Sci. Technol.* **2021**, *11* (15), 5109–5118.
- (295) Abdel-kader, M. E.; Gaber, W. H.; Ebrahim, F. A.; Abd Al-Halim, M. A. Characterization of the Electrical Breakdown for DC Discharge in Ar-He Gas Mixture. *Vacuum* **2019**, *169* (May), No. 108922.
- (296) Liu, J.; Zhu, X.; Hu, X.; Zhang, F.; Tu, X. Plasma-Assisted Ammonia Synthesis in a Packed-Bed Dielectric Barrier Discharge Reactor: Effect of Argon Addition. *Vacuum* **2022**, *197*, No. 110786.
- (297) Li, S.; van Raak, T.; Gallucci, F. Investigating the Operation Parameters for Ammonia Synthesis in Dielectric Barrier Discharge Reactors. *J. Phys. D. Appl. Phys.* **2020**, *53* (1), No. 014008.
- (298) Bai, C.; Li, S.; Chen, T.; Chen, X.; Meng, W.; Pan, J. Methane-Air Plasma-Assisted Ignition Excited by Nanosecond Repetitively Pulsed Discharge: Numerical Modeling and Effect of Inert Gas. *ACS Omega* **2021**, *6* (37), 24156–24165.
- (299) Fateev, A.; Leipold, F.; Kusano, Y.; Stenum, B.; Tsakadze, E.; Bindslev, H. Plasma Chemistry in an Atmospheric Pressure Ar/NH₃ Dielectric Barrier Discharge. *Plasma Process. Polym.* **2005**, *2* (3), 193–200.
- (300) Inoue, Y.; Hayakawa, Y.; Takeyama, A.; Miura, T.; Kambara, S. Hydrogen Production by Ammonia Decomposition Using Pulsed Plasma. *Int. Symp. Electrohydrodynamics(ISEHD)* **2014**, 2–5.
- (301) Lim, K. H.; Yue, Y.; Bella, N.; Gao, X.; Zhang, T.; Hu, F.; Das, S.; Kawi, S. Sustainable Hydrogen and Ammonia Technologies with Nonthermal Plasma Catalysis: Mechanistic Insights and Technoeconomic Analysis. *ACS Sustain. Chem. Eng.* **2023**, *11* (13), 4903–4933.
- (302) Barboun, P. M.; Daemen, L. L.; Waitt, C.; Wu, Z.; Schneider, W. F.; Hicks, J. C. Inelastic Neutron Scattering Observation of Plasma-Promoted Nitrogen Reduction Intermediates on Ni/γ-Al₂O₃. *ACS Energy Lett.* **2021**, *6* (6), 2048–2053.
- (303) Bayer, B. N.; Bruggeman, P. J.; Bhan, A. Species, Pathways, and Timescales for NH₃ Formation by Low-Temperature Atmospheric Pressure Plasma Catalysis. *ACS Catal.* **2023**, *13* (4), 2619–2630.
- (304) He, Z.; Yang, M.; Wang, X.; Zhao, Z.; Duan, A. Effect of the Transition Metal Oxide Supports on Hydrogen Production from Bio-Ethanol Reforming. *Catal. Today* **2012**, *194* (1), 2–8.
- (305) Frusteri, F.; Bonura, G. Hydrogen Production by Reforming of Bio-Alcohols. In *Compendium of Hydrogen Energy*; Elsevier: 2015; pp 109–136. DOI: [10.1016/B978-1-78242-361-4.00005-4](https://doi.org/10.1016/B978-1-78242-361-4.00005-4).
- (306) Nielsen, M.; Kammer, A.; Cozzula, D.; Junge, H.; Gladiali, S.; Beller, M. Efficient Hydrogen Production from Alcohols under Mild Reaction Conditions. *Angew. Chem.* **2011**, *123* (41), 9767–9771.
- (307) Trincado, M.; Banerjee, D.; Grützmacher, H. Molecular Catalysts for Hydrogen Production from Alcohols. *Energy Environ. Sci.* **2014**, *7* (8), 2464–2503.
- (308) Morton, D.; Cole-Hamilton, D. J.; Utuk, I. D.; Paneque-Sosa, M.; Lopez-Poveda, M. Hydrogen Production from Ethanol Catalysed by Group 8 Metal Complexes. *J. Chem. Soc. Dalt. Trans.* **1989**, No. 3, 489–495.
- (309) Ranjekar, A. M.; Yadav, G. D. Steam Reforming of Methanol for Hydrogen Production: A Critical Analysis of Catalysis, Processes, and Scope. *Ind. Eng. Chem. Res.* **2021**, *60* (1), 89–113.
- (310) Kubacka, A.; Fernández-García, M.; Martínez-Arias, A. Catalytic Hydrogen Production through WGS or Steam Reforming of Alcohols over Cu, Ni and Co Catalysts. *Appl. Catal. A Gen.* **2016**, *S18*, 2–17.
- (311) Liu, S.; Zhang, K.; Fang, L.; Li, Y. Thermodynamic Analysis of Hydrogen Production from Oxidative Steam Reforming of Ethanol. *Energy Fuels* **2008**, *22* (2), 1365–1370.
- (312) Zhu, X.; Hoang, T.; Lobban, L. L.; Mallinson, R. G. Low CO Content Hydrogen Production from Bio-Ethanol Using a Combined Plasma Reforming-Catalytic Water Gas Shift Reactor. *Appl. Catal. B Environ.* **2010**, *94* (3–4), 311–317.
- (313) Du, C.; Huang, D.; Mo, J.; Ma, D.; Wang, Q.; Mo, Z.; Ma, S. Renewable Hydrogen from Ethanol by a Miniaturized Nonthermal Arc Plasma-Catalytic Reforming System. *Int. J. Hydrogen Energy* **2014**, *39* (17), 9057–9069.
- (314) Du, C.; Ma, D.; Wu, J.; Lin, Y.; Xiao, W.; Ruan, J.; Huang, D. Plasma-Catalysis Reforming for H₂ Production from Ethanol. *Int. J. Hydrogen Energy* **2015**, *40* (45), 15398–15410.

- (315) Ulejczyk, B.; Nogal, Ł.; Młotek, M.; Krawczyk, K. Efficient Plasma Technology for the Production of Green Hydrogen from Ethanol and Water. *Energies* **2022**, *15* (8), 2777.
- (316) Ulejczyk, B.; Jóźwik, P.; Nogal, Ł.; Młotek, M.; Krawczyk, K. Efficient Conversion of Ethanol to Hydrogen in a Hybrid Plasma-Catalytic Reactor. *Energies* **2022**, *15* (9), 3050.
- (317) Ulejczyk, B.; Nogal, Ł.; Młotek, M.; Falkowski, P.; Krawczyk, K. Hydrogen Production from Ethanol Using a Special Multi-Segment Plasma-Catalytic Reactor. *J. Energy Inst.* **2021**, *95*, 179–186.
- (318) Ulejczyk, B.; Nogal, Ł.; Jóźwik, P.; Młotek, M.; Krawczyk, K. Plasma-Catalytic Process of Hydrogen Production from Mixture of Methanol and Water. *Catalysts* **2021**, *11* (7), 864.
- (319) Lian, H. Y.; Liu, J. L.; Li, X. S.; Zhu, X.; Weber, A. Z.; Zhu, A. M. Plasma Chain Catalytic Reforming of Methanol for On-Board Hydrogen Production. *Chem. Eng. J.* **2019**, *369*, 245–252.
- (320) Lepage, T.; Kammoun, M.; Schmetz, Q.; Richel, A. Biomass-to-Hydrogen: A Review of Main Routes Production, Processes Evaluation and Techno-Economical Assessment. *Biomass and Bioenergy* **2021**, *144*, No. 105920.
- (321) Fahmy, T. Y. A.; Fahmy, Y.; Mobarak, F.; El-Sakhawy, M.; Abou-Zeid, R. E. Biomass Pyrolysis: Past, Present, and Future. *Environ. Dev. Sustain.* **2020**, *22* (1), 17–32.
- (322) Demirbaş, A.; Arin, G. An Overview of Biomass Pyrolysis. *Energy Sources* **2002**, *24* (5), 471–482.
- (323) Ni, M.; Leung, D. Y. C.; Leung, M. K. H.; Sumathy, K. An Overview of Hydrogen Production from Biomass. *Fuel Process. Technol.* **2006**, *87* (5), 461–472.
- (324) Kawi, S.; Ashok, J.; Dewangan, N.; Pati, S.; Junmei, C. Recent Advances in Catalyst Technology for Biomass Tar Model Reforming: Thermal, Plasma and Membrane Reactors. *Waste and Biomass Valorization* **2022**, *13* (1), 1–30.
- (325) Xu, B.; Xie, J.; Wang, N.; Huang, Y.; Liu, H.; Yin, X.; Wu, C.; Tu, X. Plasma-Enabled Catalytic Steam Reforming of Toluene as a Biomass Tar Surrogate: Understanding the Synergistic Effect of Plasma Catalysis. *Chem. Eng. J.* **2023**, *464* (March), No. 142696.
- (326) Xu, B.; Wang, N.; Xie, J.; Song, Y.; Huang, Y.; Yang, W.; Yin, X.; Wu, C. Removal of Toluene as a Biomass Tar Surrogate by Combining Catalysis with Nonthermal Plasma: Understanding the Processing Stability of Plasma Catalysis. *Catal. Sci. Technol.* **2020**, *10* (20), 6953–6969.
- (327) Elhambakhsh, A.; Van Duc Long, N.; Lamichhane, P.; Hessel, V. Recent Progress and Future Directions in Plasma-Assisted Biomass Conversion to Hydrogen. *Renew. Energy* **2023**, *218* (June), No. 119307.
- (328) Saleem, F.; Rehman, A.; Abbas, A.; Hussain Khoja, A.; Ahmad, F.; Liu, L.; Zhang, K.; Harvey, A. A Comparison of the Decomposition of Biomass Gasification Tar Compound in CO, CO₂, H₂ and N₂ Carrier Gases Using Non-Thermal Plasma. *J. Energy Inst.* **2021**, *97*, 161–168.
- (329) Gomez-Rueda, Y.; Zaini, I. N.; Yang, W.; Helsen, L. Thermal Tar Cracking Enhanced by Cold Plasma – A Study of Naphthalene as Tar Surrogate. *Energy Convers. Manag.* **2020**, *208*, No. 112540.
- (330) Gao, N.; Milandile, M. H.; Quan, C.; Rundong, L. Critical Assessment of Plasma Tar Reforming during Biomass Gasification: A Review on Advancement in Plasma Technology. *J. Hazard. Mater.* **2022**, *421*, No. 126764.
- (331) Blanquet, E.; Nahil, M. A.; Williams, P. T. Enhanced Hydrogen-Rich Gas Production from Waste Biomass Using Pyrolysis with Non-Thermal Plasma-Catalysis. *Catal. Today* **2019**, *337*, 216–224.
- (332) Blanquet, E.; Williams, P. T. Biomass Pyrolysis Coupled with Non-Thermal Plasma/Catalysis for Hydrogen Production: Influence of Biomass Components and Catalyst Properties. *J. Anal. Appl. Pyrolysis* **2021**, *159* (July), No. 105325.
- (333) Zeng, Y.; Chen, G.; Wang, J.; Zhou, R.; Sun, Y.; Weidenkaff, A.; Shen, B.; Tu, X. Plasma-Catalytic Biogas Reforming for Hydrogen Production over K-Promoted Ni/Al₂O₃ Catalysts: Effect of K-Loading. *J. Energy Inst.* **2022**, *104* (June), 12–21.
- (334) Zeng, Y.; Chen, G.; Bai, Q.; Wang, L.; Wu, R.; Tu, X. Biogas Reforming for Hydrogen-Rich Syngas Production over a Ni-K/Al₂O₃ Catalyst Using a Temperature-Controlled Plasma Reactor. *Int. J. Hydrogen Energy* **2023**, *48* (16), 6192–6203.
- (335) Wang, W.; Ma, Y.; Chen, G.; Quan, C.; Yanik, J.; Gao, N.; Tu, X. Enhanced Hydrogen Production Using a Tandem Biomass Pyrolysis and Plasma Reforming Process. *Fuel Process. Technol.* **2022**, *234* (June), No. 107333.
- (336) Xu, Z.; Gao, N.; Ma, Y.; Wang, W.; Quan, C.; Tu, X.; Miskolczi, N. Biomass Volatiles Reforming by Integrated Pyrolysis and Plasma-Catalysis System for H₂ Production: Understanding Roles of Temperature and Catalyst. *Energy Convers. Manag.* **2023**, *288* (May), No. 117159.
- (337) Ashok, J.; Kawi, S. Low-Temperature Biomass Tar Model Reforming over Perovskite Materials with DBD Plasma: Role of Surface Oxygen Mobility. *Energy Convers. Manag.* **2021**, *248*, No. 114802.
- (338) Mei, D.; Liu, S.; Wang, Y.; Yang, H.; Bo, Z.; Tu, X. Enhanced Reforming of Mixed Biomass Tar Model Compounds Using a Hybrid Gliding Arc Plasma Catalytic Process. *Catal. Today* **2019**, *337*, 225–233.
- (339) Mei, D.; Liu, S.; Yanik, J.; Lopez, G.; Olazar, M.; Fang, Z.; Tu, X. Plasma-Catalytic Reforming of Naphthalene and Toluene as Biomass Tar over Honeycomb Catalysts in a Gliding Arc Reactor. *ACS Sustain. Chem. Eng.* **2022**, *10* (27), 8958–8969.
- (340) Zhang, H.; Xu, R.; Jia, Z.; Zheng, J.; Wan, J.; Wang, K.; Lan, B.; Yan, J.; Li, X. Destruction of Biomass Tar Model Compound in a Rotating Gliding Arc Plasma Catalytic System: Contribution of Typical Transition Metals in Ni-Based Bimetallic Catalyst. *Fuel* **2022**, *323*, No. 124385.
- (341) Xu, R.; Kong, X.; Zhang, H.; Ruya, P. M.; Li, X. Destruction of Gasification Tar over Ni Catalysts in a Modified Rotating Gliding Arc Plasma Reactor: Effect of Catalyst Position and Nickel Loading. *Fuel* **2021**, *289*, No. 119742.
- (342) Mei, D.; Zhang, P.; Liu, S.; Ding, L.; Ma, Y.; Zhou, R.; Gu, H.; Fang, Z.; Cullen, P. J.; Tu, X. Highly Efficient Reforming of Toluene to Syngas in a Gliding Arc Plasma Reactor. *J. Energy Inst.* **2021**, *98* (April), 131–143.
- (343) Midilli, A.; Kucuk, H.; Haciosmanoglu, M.; Akbulut, U.; Dincer, I. A Review on Converting Plastic Wastes into Clean Hydrogen via Gasification for Better Sustainability. *Int. J. Energy Res.* **2022**, *46* (4), 4001–4032.
- (344) Aminu, I.; Nahil, M. A.; Williams, P. T. Hydrogen from Waste Plastics by Two-Stage Pyrolysis/Low-Temperature Plasma Catalytic Processing. *Energy Fuels* **2020**, *34* (9), 11679–11689.
- (345) Aminu, I.; Nahil, M. A.; Williams, P. T. Hydrogen Production by Pyrolysis-Nonthermal Plasma/Catalytic Reforming of Waste Plastic over Different Catalyst Support Materials. *Energy Fuels* **2022**, *36* (7), 3788–3801.
- (346) Xiao, H.; Harding, J.; Lei, S.; Chen, W.; Xia, S.; Cai, N.; Chen, X.; Hu, J.; Chen, Y.; Wang, X.; Tu, X.; Yang, H.; Chen, H. Hydrogen and Aromatics Recovery through Plasma-Catalytic Pyrolysis of Waste Polypropylene. *J. Clean. Prod.* **2022**, *350*, No. 131467.
- (347) Nguyen, H. M.; Carreon, M. L. Non-Thermal Plasma-Assisted Deconstruction of High-Density Polyethylene to Hydrogen and Light Hydrocarbons over Hollow ZSM-5 Microspheres. *ACS Sustain. Chem. Eng.* **2022**, *10* (29), 9480–9491.
- (348) Xiao, H.; Li, S.; Shi, Z.; Cui, C.; Xia, S.; Chen, Y.; Zhou, Z.; Tu, X.; Chen, X.; Yang, H.; Chen, H. Plasma-Catalytic Pyrolysis of Polypropylene for Hydrogen and Carbon Nanotubes: Understanding the Influence of Plasma on Volatiles. *Appl. Energy* **2023**, *351* (June), No. 121848.
- (349) Nozaki, T.; Okazaki, K. Non-Thermal Plasma Catalysis of Methane: Principles, Energy Efficiency, and Applications. *Catal. Today* **2013**, *211*, 29–38.
- (350) Kabashima, H.; Einaga, H.; Futamura, S. Hydrogen Generation from Water, Methane, and Methanol with Nonthermal Plasma. *IEEE Trans. Ind. Appl.* **2003**, *39* (2), 340–345.

- (351) Tiwari, S.; Caiola, A.; Bai, X.; Lalsare, A.; Hu, J. Microwave Plasma-Enhanced and Microwave Heated Chemical Reactions. *Plasma Chem. Plasma Process.* **2020**, *40* (1), 1–23.
- (352) Bogaerts, A.; Neyts, E. C. Plasma Technology: An Emerging Technology for Energy Storage. *ACS Energy Lett.* **2018**, *3* (4), 1013–1027.
- (353) Adamovich, I.; Agarwal, S.; Ahedo, E.; Alves, L. L.; Baalrud, S.; Babaeva, N.; Bogaerts, A.; Bourdon, A.; Bruggeman, P. J.; Canal, C.; Choi, E. H.; Coulombe, S.; Donkó, Z.; Graves, D. B.; Hamaguchi, S.; Hegemann, D.; Hori, M.; Kim, H. H.; Kroesen, G. M. W.; Kushner, M. J.; Laricchiuta, A.; Li, X.; Magin, T. E.; Mededovic Thagard, S.; Miller, V.; Murphy, A. B.; Oehrlein, G. S.; Puac, N.; Sankaran, R. M.; Samukawa, S.; Shiratani, M.; Šimek, M.; Tarasenko, N.; Terashima, K.; Thomas, E.; Trieschmann, J.; Tsikata, S.; Turner, M. M.; Van Der Walt, I. J.; Van De Sanden, M. C. M.; Von Woedtke, T. The 2022 Plasma Roadmap: Low Temperature Plasma Science and Technology. *J. Phys. D. Appl. Phys.* **2022**, *55* (37), No. 373001.
- (354) Rabinovich, A.; Nirenberg, G.; Kocagoz, S.; Surace, M.; Sales, C.; Fridman, A. Scaling Up of Non-Thermal Gliding Arc Plasma Systems for Industrial Applications. *Plasma Chem. Plasma Process.* **2022**, *42* (1), 35–50.
- (355) Bromberg, L.; Cohn, D. R.; Rabinovich, A.; O'Brien, C.; Hochgreb, S. Plasma Reforming of Methane. *Energy Fuels* **1998**, *12* (1), 11–18.
- (356) Martini, L. M.; Coller, G.; Schiavon, M.; Cernuto, A.; Ragazzi, M.; Dilecce, G.; Tosi, P. Non-Thermal Plasma in Waste Composting Facilities: From a Laboratory-Scale Experiment to a Scaled-up Economic Model. *J. Clean. Prod.* **2019**, *230*, 230–240.
- (357) Ueckerdt, F.; Brecha, R.; Luderer, G. Analyzing Major Challenges of Wind and Solar Variability in Power Systems. *Renew. Energy* **2015**, *81*, 1–10.
- (358) Rouwenhorst, K. H. R.; Jardali, F.; Bogaerts, A.; Lefferts, L. From the Birkeland-Eyde Process towards Energy-Efficient Plasma-Based NO_x Xsynthesis: A Techno-Economic Analysis. *Energy Environ. Sci.* **2021**, *14* (5), 2520–2534.
- (359) DOE Announces Goal to Cut Solar Costs by More than Half by 2030. Department of Energy: <https://www.energy.gov/articles/doe-announces-goal-cut-solar-costs-more-half-2030> (accessed 2021-03-25).
- (360) Bespalko, S.; Mizeraczyk, J. Overview of the Hydrogen Production by Plasma-Driven Solution Electrolysis. *Energies* **2022**, *15* (20), 7508.
- (361) Bruggeman, P. J.; Frontier, R. R.; Kortshagen, U. R.; Kushner, M. J.; Linic, S.; Schatz, G. C.; Andaraarachchi, H.; Exarhos, S.; Jones, L. O.; Mueller, C. M.; Rich, C. C.; Xu, C.; Yue, Y.; Zhang, Y. Plasma-Driven Solution Electrolysis. *J. Appl. Phys.* **2021**, *129* (20), No. 200902.